

Donor-Acceptor Conjugated Polymers for Application in Organic Electronic Devices

Dissertation zur Erlangung des
naturwissenschaftlichen Doktorgrades
der Julius-Maximilians-Universität Würzburg

vorgelegt von
Dörte Reitzenstein
aus Heidelberg

Würzburg 2010

Eingereicht am: _____

bei der Fakultät für Chemie und Pharmazie

1. Gutachter: _____

2. Gutachter: _____

der Dissertation

1. Prüfer: _____

2. Prüfer: _____

3. Prüfer: _____

des öffentlichen Promotionskolloquiums

Tag des öffentlichen Promotionskolloquiums: _____

Doktorurkunde ausgehändigt am: _____

Die vorliegende Arbeit wurde in der Zeit von Februar 2006 bis November 2010 am
Institut für Organische Chemie der Universität Würzburg angefertigt.

Mein besonderer Dank gilt

Herrn Prof. Dr. Christoph Lambert

für die Vergabe des vielseitigen Themas, die intensive Betreuung und Förderung und
das mit vielen Anregungen und Diskussionen verbundene Interesse an dieser Arbeit.

Contents

1	Introduction	1
1.1	OFET Devices - Assembly, Working Principle and Organic Materials.....	2
1.2	OLED Devices - Assembly, Working Principle and Organic Materials.....	14
1.3	OPV Cells - Assembly, Working Principle and Organic Materials.....	18
2	Polycarbazoles	26
2.1	Introduction and Aim of the Project.....	26
2.2	Synthesis.....	28
2.3	Absorption and Fluorescence Spectroscopy	32
2.4	Cyclic Voltammetry.....	39
2.5	Single Layer OLED.....	45
2.6	Conclusions.....	46
3	Low Band Gap Donor-Acceptor Conjugated Polymer	48
3.1	Introduction and Aim of the Project.....	48
3.2	Synthesis.....	51
3.3	Absorption Spectroscopy.....	55
3.4	Cyclic Voltammetry.....	58
3.5	Spectroelectrochemistry	61
3.6	Transient Absorption Spectroscopy.....	63
3.7	Field-Effect Transistors.....	68
3.8	Solar Cells	71
3.9	Conclusions.....	74
4	Summary	76
5	Experimental Section.....	78
5.1	Apparatus and Methods	78
5.2	Syntheses.....	85
5.2.1	Materials	85
5.2.2	Synthesis of Polycarbazoles.....	86
5.2.3	Synthesis of the Low Band Gap Polymer	96
6	References	109
7	Appendix	119
7.1	Formeltafel.....	119

7.1.1	Polycarbazoles.....	119
7.1.2	Low Band Gap Polymer	120
7.2	Zusammenfassung	121
7.3	Danksagung	123

Abbreviations

AFM	atomic force microscopy
BC/BG	bottom contact/bottom gate
BC/TG	bottom contact/top gate
BHJ	bulk heterojunction
CIE	Commission Internationale de l'Éclairage
CT	charge transfer
CV	cyclic voltammogram
D-A	donor-acceptor
DSC	differential scanning calorimetry
eq./eqs.	equation/equations
EQE	external quantum efficiency
ET	electron transfer
Fc/Fc ⁺	ferrocene/ferrocenium
GPC	gel permeation chromatography
HMDS	hexamethyldisilazane
IR	infrared
ITO	indium tin oxide
IV-CT	intervalence charge transfer
MALDI-TOF	matrix assisted laser desorption/ionization time-of-flight
NIR	near-infrared
OFET	organic field-effect transistor
OLED	organic light emitting diode
OPVs	organic photovoltaic devices
OTS	octadecyltrichlorosilane
[60]PCBM	[6,6]-phenyl C ₆₁ butyric acid methylester
[70]PCBM	[6,6]-phenyl C ₇₁ butyric acid methylester
PCE	power conversion efficiency
PCTM	perchlorotriphenylmethane
PDI	polydispersity index
PE	petrol ether
PEDOT:PSS	polyethylenedioxythiophene:poly(styrene sulfonic acid)
P3HT	poly(3-hexylthiophene)

PMMA	polymethylmethacrylate
PPcB	polypropylene-co-1-butene
PVA	polyvinylalcohol
rpm	revolutions per minute
r. t.	room temperature
TBAP	tetrabutylammonium perchlorate
TBAPF ₆	tetrabutylammonium hexafluorophosphate
TC/BG	top contact/bottom gate

1 Introduction

Conjugated organic polymers exhibit a great variety of technologically relevant properties as for example absorption and emission of light or electrical¹⁻⁴ and photoconductivity⁵, thus making them useful materials for the application in electronic devices such as organic field-effect transistors (OFETs)⁶⁻⁹, organic light emitting diodes (OLEDs)¹⁰⁻¹² and organic photovoltaic devices (OPVs)¹³⁻¹⁶. Organic polymers typically offer the advantage that they are light-weight and flexible materials which can be processed from solution by spin coating or inkjet printing¹⁷⁻¹⁸ at room temperature.¹⁹ This makes them promising for the production at low cost and for large-area employments and opens up a new field of applications as for example in packaging and advertising or in active matrix displays.²⁰ Usually it is distinguished between organic electronics based on small molecules and those based on polymers. In general small molecules can be vacuum deposited which causes on the one hand higher costs and rules large-area applications out but on the other hand results in better device performance. In contrast solution processing of both small molecules and polymers is cheaper on the expense of device performance. Thus it depends on the particular application whether small molecules or polymers are preferred.

In this work novel donor (D) - acceptor (A) conjugated polymers were to be synthesized for use in OFETs, OLEDs and OPVs. Donor and acceptor moieties were chosen in regard to their hole and electron transporting properties, respectively. Moreover by selection of appropriate donor and acceptor entities the HOMO and LUMO levels and thus the band gap (= energy difference between HOMO and LUMO) can be controlled. The knowledge of HOMO and LUMO levels of an organic material is important for optimized charge injection into or charge extraction out of the organic layer. The band gap on the other hand determines the absorption edge which affects among other parameters the amount of harvested light. Since charge transport in organic materials occurs via charge hopping between neighbouring orbitals conjugated polymers are preferred for these applications.

In order to enable a better understanding why some organic materials/devices perform well and others don't a deeper insight into assembly, working principle and

applied organic materials for OFETs (chapter 1.1), OLEDs (chapter 1.2) and OPVs (chapter 1.3) will be given in the following three sections.

1.1 OFET Devices - Assembly, Working Principle and Organic Materials

Field-effect transistors are the basic elements of integrated circuits and, thus, technologically important as evident by manifold applications: OFET driven bendable active matrix displays have already been realized by various research groups.²¹⁻²³ Several industrial companies have recently joined forces to develop optimized RFID tags based on printable organic electronics for large-scale production.²⁴ Another such project ("Polytos") aims at the development of sensor printed boards.²⁵ An even more ambitious goal is the realization of so-called smart objects which combine several organic electronic components like sensors, batteries, displays or switches.²⁶ From a scientific point of view the investigation of such devices can contribute to a better understanding of charge transport in organic semiconductors and the factors that influence it.

Assembly and Working Principle

OFETs consist of a gate electrode, an insulating gate dielectric, source and drain contacts which enclose the channel of length L and width W and a semiconducting organic layer (Figure 1). The metal (gate electrode)-insulator-semiconductor (MIS) configuration is basically a capacitor. When a voltage V_g is applied to the gate electrode an electric field is generated normal to the semiconductor layer and charge carriers accumulate at the semiconductor/insulator interface within the channel. When at the same time a voltage V_d is applied to the drain electrode (the source electrode is grounded, $V_s = 0$) the charge carriers can be transported across the channel. The conductivity σ of the semiconductor is proportional to the charge carrier mobility μ and the free charge carrier concentration n , $\sigma = en\mu$ (e = unit electronic charge), with n being proportional to the capacitance C_i of the insulator and the magnitude of the applied electric field.²⁰ The conductivity of the semiconductor can

then be modulated by the application of different electric fields. This is called the field-effect.

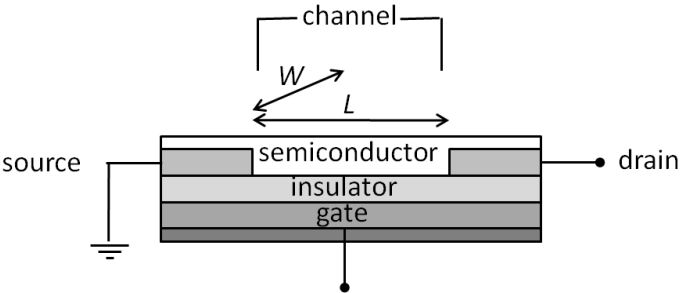


Figure 1. Assembly of an OFET device. W : width, L : length.

I/V Characteristics

The output characteristic of an OFET is shown in Figure 2.

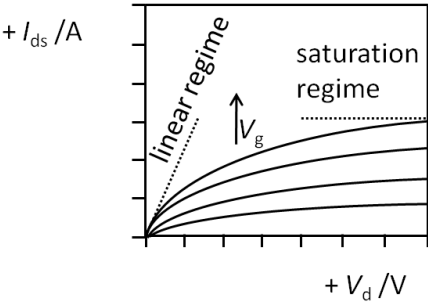


Figure 2. Output characteristic of an OFET device. I_{ds} : source-drain current, V_g : gate voltage, V_d : drain voltage.

The source-drain current I_{ds} is plotted versus the drain voltage V_d at different gate voltages V_g . At low drain voltage, $V_d \ll V_g$, I_{ds} is proportional to V_d (linear regime) which can be described by eq. 1 assuming that the charge carrier mobility μ is independent of V_g . W is the channel width, L is the channel length, μ_{lin} is the mobility in the linear regime, C_i is the capacitance of the gate dielectric per unit area and V_{th} is the threshold voltage (see below). μ_{lin} can then be calculated from a plot of $I_{ds,lin}$ versus V_g at constant V_d (transfer plot) according to eq. 2. When $V_d \geq (V_g - V_{th})$ the

source-drain current is saturated, that is I_{ds} is not further increased by increasing V_d . The saturation regime is described by eq. 3 derived from eq. 1 by substitution of V_d by $(V_g - V_{th})$. Assuming μ_{sat} to be independent of V_g , μ_{sat} is calculated from the plot of the square root of $I_{ds,sat}$ versus V_g according to eq. 4. Extrapolation of the linear slope to zero yields V_{th} . The gate voltage dependent saturation mobility can be calculated according to eq. 5.

$$I_{ds,lin} = \frac{W}{L} \mu_{lin} C_i \left((V_g - V_{th}) - \frac{V_d}{2} \right) V_d \quad V_d \ll V_g \quad (1)$$

$$\mu_{lin} = \frac{\partial I_{ds,lin}}{\partial V_g} \times \frac{L}{WC_i V_d} \quad (2)$$

$$I_{ds,sat} = \frac{W}{2L} \mu_{sat} C_i (V_g - V_{th})^2 \quad V_d \geq (V_g - V_{th}) \quad (3)$$

$$\sqrt{\mu_{sat}} = \frac{\partial \sqrt{I_{ds}}}{\partial V_g} \times \sqrt{\frac{2L}{WC_i}} \quad (4)$$

$$\mu_{sat}(V_g) = \frac{\partial I_{ds}}{\partial V_g} \times \frac{L}{WC_i (V_g - V_{th})} \quad (5)$$

The performance of an OFET device is characterized by V_{th} , the ratio I_{on}/I_{off} and by μ .⁸ V_{th} determines the value of the gate voltage V_g above which a source-drain current I_{ds} can flow. This is because a part of the induced charges will be trapped and it is only when the trap states are filled that further induced charges will be mobile. So the effective gate voltage is $(V_g - V_{th})$. Thus the power consumption is increased with increasing V_{th} . However, V_{th} can be diminished by enhancement of the gate capacitance. The ratio I_{on}/I_{off} should be high (10^6 - 10^8)²⁷ in order to obtain a clear distinction between the states "0" and "1" in electronic circuits.¹⁹ I_{on} is the source-drain current in the saturation regime at a normal (maximum) gate voltage which reflects the magnitude of the charge carrier mobility. It is affected by charge injection barriers and by C_i and V_{th} .⁸ I_{off} is the leakage current at $V_g = 0$ which is caused by alternative conduction pathways or by the bulk conductivity of the semiconductor due to unintentional doping²⁸⁻³⁰. Finally, μ is the most important parameter in an OFET device and should be as high as possible in order to decrease power consumption. Transport behaviour is influenced by the device geometry, charge injection barriers and specifically by the gate dielectric and the morphology of the semiconductor layer as outlined below.

Device Configuration

In Figure 3 three different device structures in reference to the position of the gate and source/drain electrodes relative to the semiconductor layer are depicted.

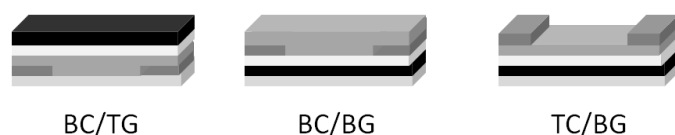


Figure 3. OFET device configurations. Left: bottom contact/top gate (BC/TG); middle: bottom contact/bottom gate (BC/BG); right: top contact/bottom gate (TC/BG); (—) gate; (—) contacts; (—) semiconductor; (—) substrate; (—) dielectric.

In the bottom contact/top gate (BC/TG) configuration the source/drain electrodes are directly deposited onto the surface of the substrate followed by the semiconductor layer and the insulator layer and finally by the gate electrode on top of the device. In the top contact/bottom gate (TC/BG) configuration the layers are arranged vice versa and in the bottom contact/bottom gate (BC/BG) configuration the semiconductor layer is deposited lastly. The type of configuration influences on the one hand the morphology of the semiconductor layer (deposition on top of the source/drain contacts/substrate surface/insulator surface) and on the other hand the charge injection into the semiconductor:⁸ In the BC/BG structure electrons are injected directly into the channel through the small electrode area that faces the channel, whereas in the other two arrangements electrons are also injected through the electrode area that overlaps with the gate electrode (staggered configuration). In the latter case more electrons can be injected thus reducing the contact resistance.³¹ In the TC/BG assembly evaporation of the metal contacts on top of the semiconductor layer can lead to metal atom diffusion into the semiconductor which affects electron injection.³² All these factors can lead to different device performances for the same semiconductor in different device architectures.

Source/Drain Electrodes

The selection of the source/drain electrode material depends primarily on its work function which should be as close as possible to the HOMO (hole transport) or LUMO

(electron transport) or to both energy levels (ambipolar transport, see below) in order to reduce charge injection barriers. However, the work function is not a definite value but varies for different surface atomic geometries of the same electrode material.³³ Moreover upon semiconductor deposition Fermi level pinning can further change the work function.³⁴ Another difficulty arises from the low environmental stability of low work function metals. Frequently used electrode materials are Au (-5.2 eV), Ag (-4.9 eV), Cu (-4.7 eV), Al (-4.0 eV), and Ca (-2.8 eV),³⁵⁻³⁶ whereas for all-printed devices doped conducting polymers like polyethylenedioxythiophene:poly(styrene sulfonic acid) (PEDOT:PSS)³⁷⁻³⁹ and polyaniline (PANI)⁴⁰⁻⁴² are used.

Gate Dielectrics

A huge impact on the device characteristics is observed by the type of insulator. In many cases SiO₂ (insulator) on top of a silicon wafer (gate) is used due to its ready availability at high purity, usefulness as substrate, compatibility with subsequent processing steps and its reasonably high dielectric constant $\epsilon = 3.9$.²⁰ The dielectric constant is related to the capacitance by $C_i = \epsilon\epsilon_0 A/d$ (ϵ_0 is the permittivity in vacuum, A is the contact area and d is the dielectric layer thickness).²⁰ Thus a thin insulator layer of high ϵ results in a high amount of induced charges at the semiconductor/insulator interface thereby enhancing the conductivity of the semiconductor. However, if SiO₂ was used electron trapping at the SiO₂/semiconductor interface was observed for several semiconductor polymers.⁴³ This could be reduced by treatment of the SiO₂ surface with alkyltrichlorosilanes or hexamethyldisilazane (HMDS) or by the introduction of a hydroxyl free organic buffer dielectric, which shields the semiconductor from free hydroxyl groups at the surface. Another group⁴⁴ observed higher mobilities for polytriarylaminines with insulators of low ϵ (polypropylene-co-1-butene (PPcB), polypropylene (PP)) than with insulators of higher ϵ (polyvinylphenol (PVP), polyvinylalcohol (PVA), polymethylmethacrylate (PMMA)) which was explained by additional energetic disorder induced by the high ϵ insulator at the interface.

Morphology

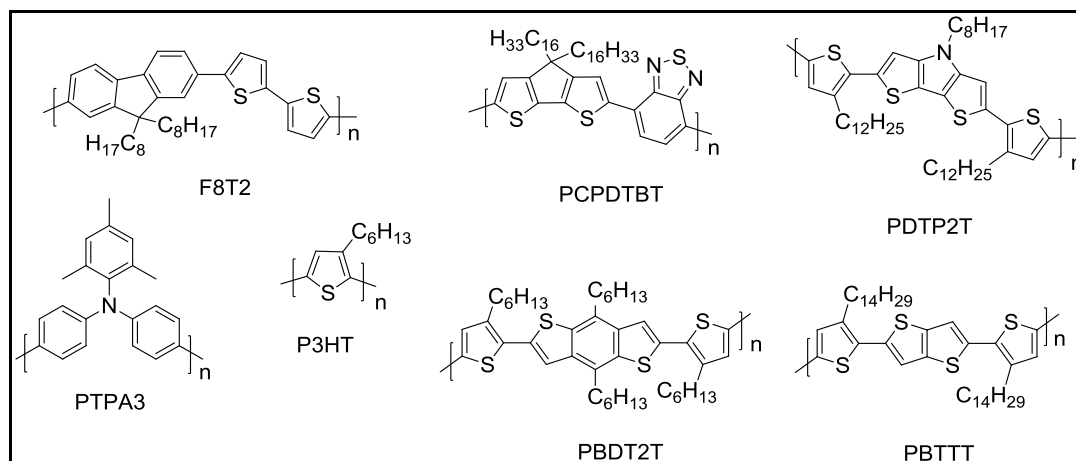
The morphology of the semiconductor layer is the most important factor that affects mobilities. Thus the highest mobilities (up to $20 \text{ cm}^2 \text{ V}^{-1} \text{ s}^{-1}$ in rubrene⁴⁵⁻⁴⁶) among organic semiconductors were achieved in single crystals due to the absence of grain boundaries and trap states in these highly pure materials.⁸ However, single crystals are not suitable for the application in large-area devices or for processing by printing techniques thus being delimited to more fundamental studies. The particular arrangement of semiconductor polymers in a thin film is strongly influenced by the surface of the underlying substrate (substrate, source/drain electrodes, dielectric)³⁴, the deposition technique (e.g. vacuum deposition, spin coating, drop casting, printing)⁴⁷ and the precise polymer structure (planarity, side chains, molecular shape and dimensions)⁴⁸. For example, for spin coated thin films of highly regioregular (>91 %) poly(3-hexylthiophene) (P3HT) of high molecular weight high hole mobilities of $0.05\text{-}0.1 \text{ cm}^2 \text{ V}^{-1} \text{ s}^{-1}$ were obtained.⁴⁹ In contrast for less regioregular (81 %) P3HT of low molecular weight mobilities of only $2 \times 10^{-4} \text{ cm}^2 \text{ V}^{-1} \text{ s}^{-1}$ in spin coated thin films were achieved. However for the latter sample an almost equally high value (ca. $0.07 \text{ cm}^2 \text{ V}^{-1} \text{ s}^{-1}$) was obtained from films formed by slow casting from a dilute solution.⁴⁹ The higher hole mobilities are caused by a better interchain transport along coplanar arranged polymer backbones oriented perpendicular to the substrate surface as compared to the arrangement of the backbones parallel to the substrate surface. For poly(*p*-phenylene vinylene)s also a strong influence of the substitution pattern and the nature of the side chain as well as of the film processing conditions on the charge carrier mobilities was observed.⁵⁰⁻⁵¹

p-Channel OFETs

In Chart 1 hole transporting polymer semiconductors used in OFET devices are depicted. P3HT is among the best investigated materials with which hole mobilities up to $0.2 \text{ cm}^2 \text{ V}^{-1} \text{ s}^{-1}$ are now achievable.⁵²⁻⁵³ Best results were obtained for highly regioregular⁴⁹ P3HT of high molecular weight⁵⁴⁻⁵⁶ when deposited from chloroform solutions⁵⁷. One drawback is the high HOMO level of P3HT (-4.9 eV)⁴³ making it unstable towards oxygen. A lowering of the HOMO level can be obtained by a

reduction of the delocalization along the backbone by for example incorporation of fused rings into the thiophene polymer chain.

Chart 1



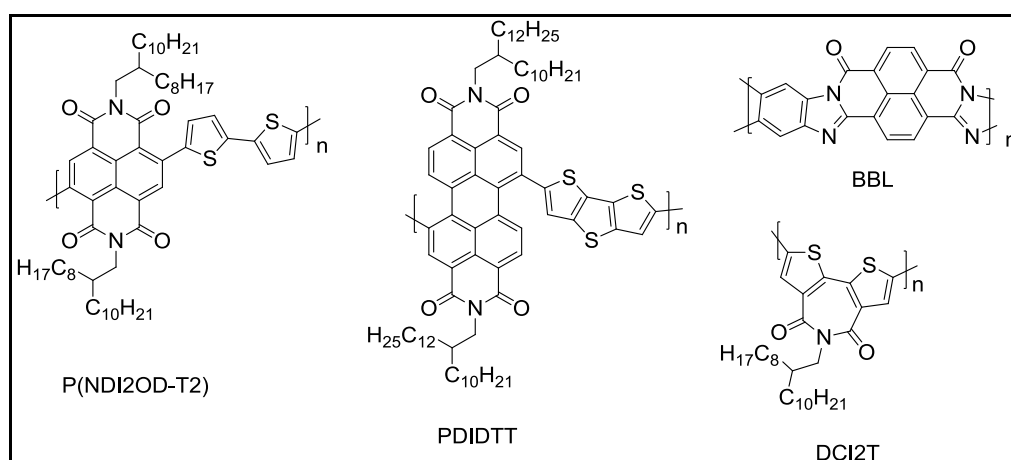
This has been realized for PBDT2T⁵⁸ (Chart 1) giving saturation mobilities of 0.15-0.25 cm² V⁻¹ s⁻¹ when measured in ambient conditions with only minor device degradation upon standing at 20 % relative humidity. Another such example is PBTTT⁵⁹ giving the highest reported hole mobility among polymer based OFETs so far with a maximum saturation mobility of 0.72 cm² V⁻¹ s⁻¹ in nitrogen atmosphere thus reaching the mobility of amorphous silicon thin-film transistors (0.5-1 cm² V⁻¹ s⁻¹)²⁷. Other high mobility semiconductors are PCPDTBT ($\mu_{\text{sat,max}} = 0.17 \text{ cm}^2 \text{ V}^{-1} \text{ s}^{-1}$ in nitrogen atmosphere)⁶⁰ and PDTP2T ($\mu_{\text{sat,max}} = 0.21 \text{ cm}^2 \text{ V}^{-1} \text{ s}^{-1}$ measured under argon)⁶¹. Interestingly, in contrast to the highly ordered lamellar structures observed for P3HT, PBDT2T and PBTTT rather disordered structures were found for PCPDTBT and PDTP2T which suggests that the lamellar structure is not the exclusive structure to gain high mobilities. Nevertheless a flat, planar backbone with small interbackbone distances seems to be important for efficient charge transport. Thus, polytrialylamines, e.g. PTPA3, show lower hole mobilities up to 0.01 cm² V⁻¹ s⁻¹.⁶² However, they form stable amorphous films and the OFET performance is impressively stable upon storage and operation in air.⁴⁴ Moreover, a printed, flexible OFET device using PTPA3 showed also good device performance.⁶³ Another class of hole transporting polymers are copolymers comprising fluorene and thiophene, as for example F8T2 with $\mu_{\text{sat,max}} = 0.02 \text{ cm}^2 \text{ V}^{-1} \text{ s}^{-1}$ obtained in layers of parallel aligned polymer chains in printed devices³⁹. The low lying HOMO of F8T2 (-5.5 eV) gives

improved operating stability compared to printed P3HT devices, whereas the high contact resistance in F8T2 devices hampers charge injection into the channel.

n-Channel OFETs

In contrast to p-channel transistors there are only a few examples of well performing polymer n-channel transistors (Chart 2). This is due to the high LUMO (ca. 3 eV) of most organic semiconductors which requires low work function metal contacts (Ca, Mg) in order to minimize charge injection barriers. However, these metals as well as the organic radical anions formed upon electron injection are environmentally unstable⁶⁴. Another reason for the few examples of efficient electron transport is that electron transport is highly affected by the gate dielectric: OH groups at the surface can effectively trap electrons (see above). In contrast, high electron affinity semiconductors are less sensitive to electron traps⁶⁵ and ambient conditions. Thus, DCI2T(LUMO ~ -3.5 eV)⁶⁶ and PDIDTT(LUMO ~ -3.9 eV)⁶⁷ gave $\mu_{\text{sat,max}} = 0.01 \text{ cm}^2 \text{ V}^{-1} \text{ s}^{-1}$ obtained in vacuum on HMDS treated SiO₂ and under nitrogen atmosphere on OTS (octadecyltrichlorosilane) treated SiO₂, respectively (Chart 2). A higher mobility $\mu_{\text{max,lin}} = 0.1 \text{ cm}^2 \text{ V}^{-1} \text{ s}^{-1}$ measured in air (!) on HMDS treated SiO₂ was obtained with BBL (LUMO < -4 eV).⁶⁸ Currently the best n-channel performance was obtained with P(NDI2OD-T2) with maximum values of $0.85 \text{ cm}^2 \text{ V}^{-1} \text{ s}^{-1}$ measured in air (LUMO ~ -4 eV) on a polyolefin-polyacrylate dielectric.⁴⁷ Interestingly, films of P(NDI2OD-T2) are rather amorphous in contrast to DCI2T and BBL.

Chart 2



It has long been thought that different organic materials are needed for the construction of organic p- and n-channel transistors. However, a few years ago it has been demonstrated that organic semiconductors are inherently ambipolar^{43,69}, that is they can be switched between pure hole, pure electron and ambipolar transport by altering the voltage offsets between gate, source and drain electrodes provided that electrode material, gate dielectric and device geometry are suitable.⁸ One striking example is pentacene – one of the highest mobility p-channel organic semiconductors, which reaches hole mobilities up to $5 \text{ cm}^2 \text{ V}^{-1} \text{ s}^{-1}$ in sublimed thin films³²: When PVA was used as the gate dielectric and gold electrodes placed on top of the pentacene film ambipolar transport with hole and electron mobilities of 0.3 and $0.04 \text{ cm}^2 \text{ V}^{-1} \text{ s}^{-1}$ were achieved.⁷⁰

In Figure 4 an ambipolar output characteristic is shown. In contrast to the unipolar transistor (Figure 2), the ambipolar transistor is not in the off-state when the voltage polarity of gate and drain electrode is inverted with respect to the source ($V_s = 0$). In fact just the same processes occur with the opposite carrier type (compare first and third quadrant). Furthermore the output characteristic differs from a unipolar transistor, which can be explained as follows: If we assume a high positive gate voltage $V_g > V_{th}(\text{electron})$ and a small positive drain voltage $V_d \ll V_g$ only electrons are accumulated in the channel and the output characteristic is similar to the linear regime of the unipolar transistor (see the curves with $V_g > 40 \text{ V}$, Figure 4). If V_g is reduced such that $V_g - V_{th}(\text{electron}) < V_d$ a reverse electrical field between V_g and V_d is generated compared to the fields between source and gate and source and drain, respectively. Thus a depletion region is formed near the drain electrode, which causes the saturation of the source-drain current similar to the saturation regime of the unipolar transistor. Further reduction of V_g such that $V_g - V_d < V_{th}(\text{hole})$ (note, that $V_{th}(\text{hole})$ is negative) causes holes to be injected by the drain electrode. This yields a p/n junction in the channel and thus a diode characteristic (see the curves with $V_g \leq 40 \text{ V}$) typical of the ambipolar transport mode. The same explanations can also be applied to negative V_g and V_d (hole accumulation mode).

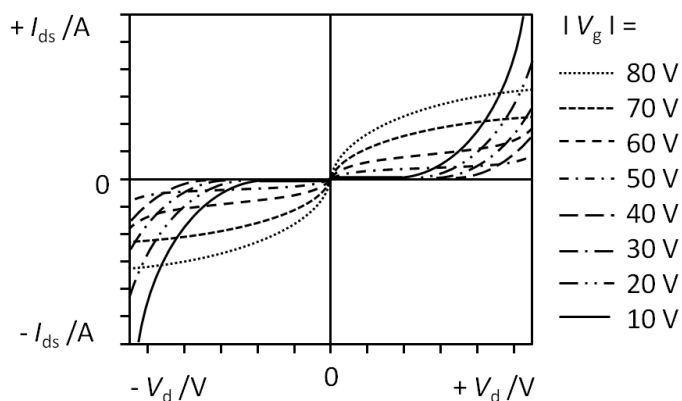


Figure 4. Output characteristic of an ambipolar OFET device. I_{ds} : source-drain current, V_d : drain voltage, V_g : gate voltage.

The transfer plots (I_{ds} vs. V_g at constant V_d) depicted in Figure 5 show characteristic v-shaped curves: When a high positive gate voltage is applied only electrons are present in the channel (right arm), whereas at low positive V_g also holes are present in the channel (left arm, ambipolar regime). According to the relation $V_g - V_d < V_{th}(\text{hole})$ for hole injection by the drain electrode the minima of the v-shaped curves shift to higher V_g values with increasing V_d . The same interpretations hold for negative values of V_g and V_d (left part of Figure 5). Mobilities are calculated in the unipolar regime from eqs. 2, 4 and 5.

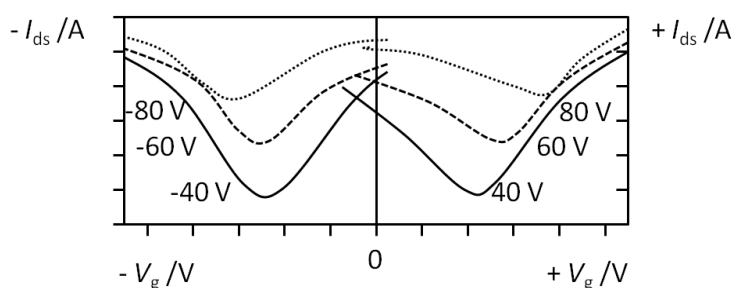


Figure 5. Transfer plots of an ambipolar OFET device for different drain voltage values V_d denoted next to the curves. I_{ds} : source-drain current, V_g : gate voltage.

Ambipolar OFETs - Organic Materials

One obstacle for obtaining efficient ambipolar transport is to match both HOMO and LUMO level to the work function of the charge carrier injecting source and drain electrodes. Since most organic semiconductors have band gaps of 2-3 eV for at least

one carrier type a high injection barrier is to be expected hampering balanced hole and electron transport. There have been several strategies to overcome this problem.

In bilayer devices a p-channel and an n-channel semiconductor layer are deposited on top of each other and transport of holes and electrons, respectively, occurs in separate layers⁷¹. This yields high balanced hole and electron transport in vacuum deposited small molecule bilayer OFETs.⁷² However, this device structure is difficult to realize by solution processing of different organic semiconductors since orthogonal solvents have to be used in order to prevent mixing of the layers and no reports using this strategy for polymers exist. Liu and Sirringhaus prepared ambipolar bilayer OFETs by a more complex method depositing the two polymer semiconductors initially on different substrates before attaching them to each other.⁷³ They observed ambipolar transport but with a clear deviation from ideal transport characteristics due to carrier transfer across the bilayer interface.

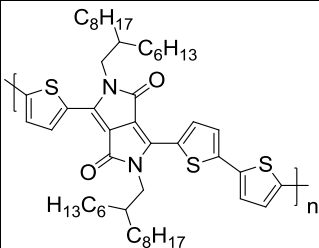
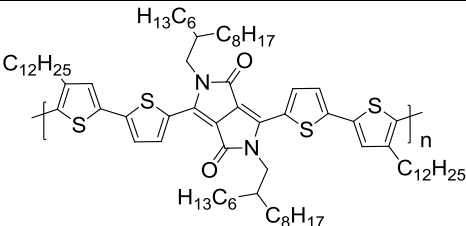
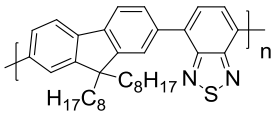
Another approach is the use of blends of p- and n-channel semiconductors, which requires an interpenetrating network of the two components. A blend of regioregular P3HT (Chart 1) and P(NDI2OD-T2) (Chart 2), the best performing p- and n-channel polymers so far, resulted in balanced hole and electron mobilities of $2-4 \times 10^{-3} \text{ cm}^2 \text{ V}^{-1} \text{ s}^{-1}$ being significantly lower than the mobilities of the single polymers.⁷⁴ Higher mobilities in blend devices have yet not been achieved.

A third possibility to overcome energy level mismatch is to use different metals for source and drain contacts, which can be deposited by subsequent angled evaporation.⁷⁵⁻⁷⁶ However, in case of the wide band gap polymer F8T2 (Chart 1) with HOMO and LUMO levels at -5.6 eV and -3.2 eV, respectively, no significant improvement was observable when Ca (-2.8 eV) and Au (-5.2 eV) contacts were used instead of ITO (-4.8 eV) contacts for source and drain electrodes.^{43,77} This indicates that the main obstacle for this material is not the HOMO/LUMO alignment with the work function of the source/drain electrodes.

The use of single layer devices with an appropriate gate dielectric and adequate, equal source and drain contacts is the most straightforward device architecture and recently high balanced hole and electron mobilities of $0.01-0.1 \text{ cm}^2 \text{ V}^{-1} \text{ s}^{-1}$ were obtained when PDPP3T⁷⁸, BBTDPP1⁷⁹ and F8BT⁸⁰⁻⁸¹ were used as semiconductors (Chart 3). Interestingly, a polymer, which differs from PDPP3T only by the absence of

one thiophene moiety in the repeating unit, exhibited rather low hole and electron mobilities in the order of $10^{-4} \text{ cm}^2 \text{ V}^{-1} \text{ s}^{-1}$, probably due to the different processing procedure of the device.⁸² The high mobilities of F8BT (up to $0.01 \text{ cm}^2 \text{ V}^{-1} \text{ s}^{-1}$) resulted from an improved device structure: The TG/BC geometry is in particular suitable for a wide band gap polymer in order to compensate for the high injection barriers by exploiting the larger injection area. Moreover by using a dielectric of low ϵ like polystyrene the mobilities could be enhanced by an order of magnitude compared to those obtained with PMMA.

Chart 3

		
PDPP3T	BBT DPP1	F8BT
LUMO: -3.6 eV HOMO: -5.2 eV	LUMO: -4.0 eV HOMO: -5.5 eV	LUMO: -3.3 eV HOMO: -5.9 eV
<u>device:</u> geometry: BG/BC dielectric: HMDS treated SiO ₂ source/drain: Au measurement: in vacuum	<u>device:</u> geometry: BG/TC dielectric: OTS treated SiO ₂ source/drain: Ba/Al measurement: under nitrogen	<u>device:</u> geometry: TG/BC dielectric: polystyrene source/drain: Au measurement: under nitrogen

One of the exiting features about ambipolar OFET devices is that light can be emitted from the channels upon recombination of holes and electrons, which can be controlled by the voltage supplied to gate and drain electrode.⁷⁶

In summary ambipolar OFET devices offer on the one hand the possibility to investigate charge transport of both holes and electrons in the same device and on the other hand they can be implemented in complementary-like inverters and other flexible integrated electronic circuits.

1.2 OLED Devices - Assembly, Working Principle and Organic Materials

The OLED technology is already present in small displays, e.g. in mobile phones, MP3-players, digital cameras and watches, and even an OLED TV produced by Sony is already available.⁸³ The advantages over the common LCD technology are manifold: background illumination is no longer necessary which saves energy; the contrast is higher and colours are brilliant; the viewing angle is almost unlimited; the response time is much faster (1×10^3) and the displays are extremely flat (3 mm for the OLED TV XEL-1 by Sony).⁸³ Moreover lifetimes of many OLED displays are now comparable or better than those of LCD displays: Many of them exceed 50000 h.⁸⁴ In the field of lighting applications the Novalad AG recently presented a white light device with a power efficiency of 30 lm W^{-1} at an initial luminance of 1000 cd m^{-2} and a lifetime exceeding 50000 h.⁸⁵ On the laboratory scale a power efficiency of 90 lm W^{-1} (34 % external quantum efficiency (EQE)) at 1000 cd m^{-2} for a device of 6.7 mm^2 was achieved.⁸⁶ Philips soon will enter the market with the first commercially available OLED white light source to be driven with 230 V power supply voltage.⁸⁷ It has a power efficiency of 25 lm W^{-1} and a brightness of 3000 cd m^{-2} with a lifetime of 10000 h.⁸⁸ The lit area is $119 \text{ mm} \times 37 \text{ mm}$. In the future even more revolutionary display and lighting applications will be feasible as for example completely flexible TVs or mobile phones one can coil up or wall paper, partitions and windows that illuminate rooms and are transparent in the off-state.

Assembly and Working Principle

The working principles of OLEDs and OPVs are opposed to each other: OLEDs convert electrical energy into light energy whereas with OPVs it is the other way around. In the most simple case the organic layer is embedded between two electrodes of different work function, one of which having to be transparent for the output/input of light. For this purpose ITO coated glass substrates are frequently used. As counter electrode aluminium is used mostly. At the electrode surfaces holes and electrons are injected into (OLEDs) or extracted out (OPVs) of the organic layer. Upon electron/hole recombination energy can be dissipated by the emission of photons (OLEDs), whereas in OPV devices photons are absorbed to create excited

electron-hole pairs which can separate to give free charge carriers that can be collected at the electrodes (Figure 6).

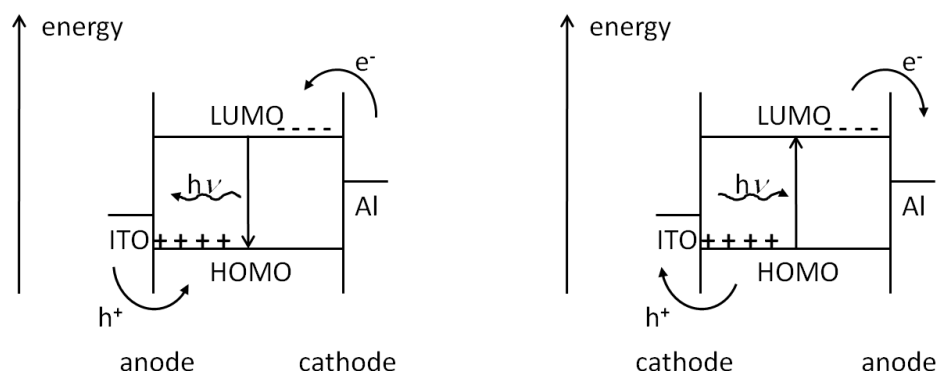


Figure 6. Working principles of OLED (left) and OPV devices (right).

Generation of Light

There are four processes to be considered during the operation of an OLED: Charge injection into the organic layer, charge transport, electron/hole recombination and emissive decay.⁸⁹

For efficient charge injection the HOMO and LUMO energy levels of the organic layer need to be close to the metals' work functions as already pointed out for OFET devices. Additional charge injection layers can be introduced to adapt the different energy levels. A commonly used hole injection layer is p-doped PEDOT:PSS.⁹⁰⁻⁹⁴ If Al is used as cathode material electron injection can be enhanced by the additional deposition of a LiF layer between Al and the organic layer.⁹⁵

Charge transport in organic materials is slow compared to that in metallic conductors, because it takes place via a hopping process of charges between neighbouring orbitals instead of movement within a conduction band.⁸ Therefore additional hole transport (carbazole⁹⁶⁻⁹⁸ and triphenylamine derivatives⁹⁹⁻¹⁰³) and electron transport layers [(tris(8-hydroxyquinoline) aluminium (=Alq₃)^{99,104-106}, 1,3,5-tris(*N*-phenylbenzimidazole-2-yl)benzene (=TPBI)⁹⁴, 2,(4-biphenyl)-5-(4-tert-butylphenyl-1,3,4-oxadiazole (=Bu-PBD)¹⁰⁷⁻¹⁰⁸, 5,5'-bis(dimesitylboryl)-2,2'-bithiophene (=BMB-2T)¹⁰⁹⁻¹¹⁰] are introduced, which in case of Alq₃ and BMB-2T may

also serve as emissive layer¹¹¹⁻¹¹³. In order to avoid charge trapping at defect sites the organic layer should be of high purity.

High efficiencies require a balanced charge transport. However, often holes are more efficiently transported in organic semiconductors than electrons (see OFET devices) which results in holes reaching the cathode without recombination with electrons. This is prevented in a two- or multilayer device, in which holes concentrate at layer boundaries because of energy differences which in turn amplify the electric field in the electron transport layer and, thus, charge transport becomes more balanced.⁹⁹

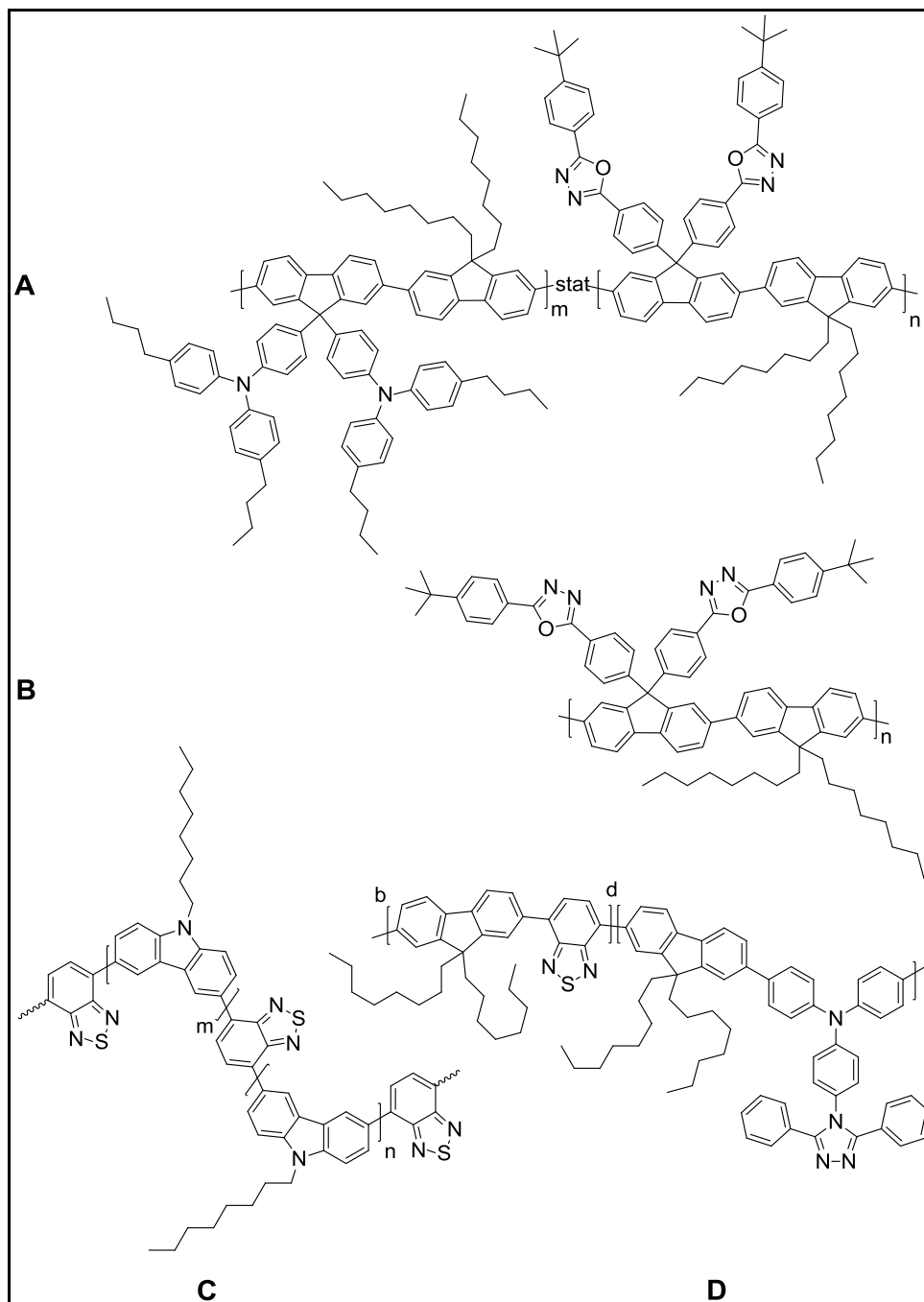
Finally, a highly emissive organic material is needed, which favourably emits a pure, saturated colour, that is, the CIE coordinates should lie as close as possible to the outer curved boundary of the gamut.

Organic Materials

Until now small organic molecules are mostly used as the light emitting material since they are still superior to polymers concerning the quality of the resulting images and the long-term stability.¹¹⁴ In contrast, the application of polymers reduces costs and allows for the construction of large-area devices. Therefore better performing polymers are still needed. The reason for the superior performance of small molecules is that they can be vacuum deposited which allows for the facile construction of multi-layer devices. Thus, every single layer can be optimized independently. Moreover vacuum deposition usually yields very pure layers. Since polymers are typically deposited from solution, orthogonal solvents would have to be used for the deposition of consecutive layers in order to avoid dissolution of the underlying layer which, however, limits the choice of applicable polymers. Hence, the challenge for the construction of OLEDs based on polymers is to synthesize polymers which combine all the different requirements, i.e. close match of HOMO and LUMO levels with the metals' work functions, balanced and fast hole and electron transport, highly efficient emission and long-term stability. This can be achieved by the synthesis of D - A conjugated polymers, in which the donor acts as the hole transport layer and the acceptor acts as the electron transport layer and in which at the same time one of these moieties strongly emits in the desired

wavelength region. A range of such D- A conjugated polymers were prepared and tested in OLED devices for their electroluminescent efficiencies in the past decade.^{90,92,94,115-119} A few of them are shown in Chart 4.

Chart 4



Shu et al.¹¹⁹ demonstrated that the performance of a double¹-layer OLED device with the configuration ITO/PEDOT:PSS/polymer/Ca/Ag could be more than doubled if polymer **A** is used instead of polymer **B**. The former gives a maximum brightness of 4080 cd m⁻² at 12 V ($\eta_{\text{ext}} = 1.21 \%$). This is obviously due to the introduced triarylamine moieties which adjust the HOMO level of the polymer to the Fermi level of the modified ITO electrode and improve hole transport. Likewise Yuan et al.⁹⁴ presented with a polymer similar to **A** incorporated in a triple-layer device a much better performing OLED in comparison to the same device made from pure poly(9,9-dioctylfluorene). This again corroborates the importance of the hole (triarylamine) and electron (oxadiazole) transport moieties in addition to the strongly emitting polyfluorene backbone. The device ITO/PEDOT:PSS/polymer **C**/Ba/Al⁹¹ using carbazole as donor and benzothiadiazole as acceptor moiety gave an external quantum efficiency of 0.48 % and the device ITO/PEDOT:PSS/polymer **D**/Ca/Ag¹¹⁵ containing a triarylamine donor group, benzothiadiazole and 1,2,4-triazole acceptor groups and fluorene as the emitting moiety showed a brightness of 696 cd m⁻². All of these devices had a rather low turn-on voltage of about 5 V due to the improved hole and electron injection.

1.3 OPV Cells - Assembly, Working Principle and Organic Materials

OPV devices have not been brought onto the market up to now with one exception: Konarka Technologies offers thin (0.5 mm \pm 0.05 mm), light (~940 g m⁻²) and flexible plastic solar cells for charging batteries of portable electronics. In July 2010 a new OPV cell power conversion efficiency (PCE) record of 8.13 % was reported.¹²⁰ The company that produced the cell¹²⁰ hopes to reach 10 % efficiency by the end of 2011. Nevertheless, OPV cells won't replace silicon based solar cells due to lower efficiencies and less stability, but will likely be used for new applications in portable digital electronic devices or in textiles due to inherent flexibility, light weight and low production costs.

¹ PEDOT:PSS does not cause any problems in device fabrication since it is spin coated from an aqueous solution thus not being dissolved during spin coating of the polymer layer from an organic solvent. It modifies the work function of the ITO electrode, improves hole injection and smoothes the ITO surface.

Assembly and Working Principle

The basic working principle of OPV cells is opposed to that of OLED devices and is explained at the beginning of chapter 1.2. The common assembly of polymer solar cells is the following¹²¹: A PEDOT:PSS layer is spin coated onto an ITO coated glass substrate, which smoothes the ITO surface and improves hole extraction. On top a solution of a donor and an acceptor compound is spin coated. Finally a LiF/Al layer is deposited under high vacuum as counter electrode. This type of organic solar cell is called bulk heterojunction (BHJ) solar cell, referring to the interfaces formed between the donor and the acceptor within the blend.¹²²⁻¹²³ In order to obtain free charge carriers, charge transfer from the donor to the acceptor and subsequent charge separation is necessary which can only take place in close proximity (10-20 nm) to the D-A interfaces. Therefore a large interfacial area is required. Well-known donor polymers are MDMO-PPV (poly[2-methoxy-5-(3', 7'-dimethyloctyloxy)-1,4-phenylenevinylene]) and P3HT.¹²⁴ As acceptor the fullerenes [6,6]-phenyl C₆₁ butyric acid methylester ([60]PCBM) and its higher homologue [70]PCBM have turned out to perform best. This is due to ultrafast photoinduced charge transfer being observed in several polymer/[60]PCBM systems in the sub-picosecond timescale.¹²⁵ Moreover C₆₀ shows an electron mobility of up to 1 cm² V⁻¹ s⁻¹⁷⁰ and [60]PCBM has a LUMO level close to the Fermi level of the Al electrode (both ~ -4.3 eV)^{13,126-127}. In contrast to [60]PCBM, [70]PCBM has a considerably higher absorption coefficient thus contributing significantly to the photocurrent in the visible region.¹²⁸

I/V Characteristics

From the output characteristic of a solar cell (Figure 7) J_{SC} , FF and V_{OC} are obtained, from which the power conversion efficiency (PCE) values are calculated according to eqs. 6 and 7:¹²⁹

$$PCE = (J_{SC} \times FF \times V_{OC}) / I_p \quad (6)$$

$$FF = (J_{mpp} \times V_{mpp}) / (J_{SC} \times V_{OC}) \quad (7)$$

J_{SC} is the short-circuit current density, which is measured upon electroconductive connection of the electrodes under illumination, FF is the fill-factor defined by eq. 7, V_{OC} is the open-circuit voltage (the voltage the cell delivers under illumination in absence of a current flow) and I_p is the power density of the sunlight. I_p is standardized as 100 mA cm^{-2} under AM1.5 illumination, which corresponds to the solar irradiance at the surface of the earth with the sun 45° above the horizon. This definition makes results comparable. J_{mpp} and V_{mpp} are the current density and the voltage at the maximum power point as depicted in Figure 7.

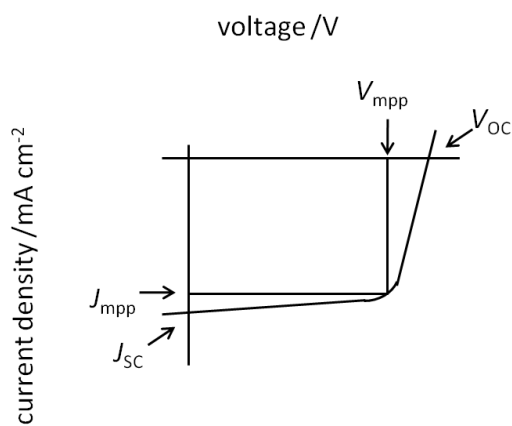


Figure 7. Output characteristic and cell parameters.

It is obvious from eq. 6 that high PCEs result from high values of J_{SC} , FF and V_{OC} . V_{OC} is limited by the energy difference between the HOMO of the donor and the LUMO of the acceptor according to eq. 8,

$$V_{OC} = (1/e)(|E^{\text{Donor HOMO}}| - |E^{\text{PCBM LUMO}}|) - 0.3 \text{ V} \quad (8)$$

where e is the elementary charge and 0.3 V is an empirical factor.¹³⁰ J_{SC} is influenced by the efficiency of charge generation in general (see below) and in particular by the amount of absorbed photons:¹²⁹ Devices containing [70]PCBM as acceptor material exhibited enlarged J_{SC} values compared to those with [60]PCBM due to enhanced absorption of [70]PCBM in the visible region.^{16,126} The fill-factor is predominantly dependent on the intrinsic conductivity of the active layer¹²⁹ and on a balanced charge transport¹²¹.

Generation of Free Charge Carriers

The important processes in an organic solar cell are:^{121,131}

- 1) Absorption of a photon.
- 2) Diffusion of the exciton to the D-A interface.
- 3) Charge transfer from the donor to the acceptor.
- 4) Charge separation of the coulomb-bound $[D^{*+}A^{*-}]^*$ state.
- 5) Charge transport of holes and electrons through donor and acceptor phase, respectively.
- 6) Charge extraction at the respective electrodes interfaces.

By light absorption an electron is promoted from the HOMO into the LUMO which leaves a hole in the HOMO. Thus an excited coulomb-bound electron-hole pair, a so-called exciton, is formed. The exciton should reach the D-A interface within the lifetime of the exciton before relaxation occurs. This refers to an exciton diffusion length of ca. 10-20 nm. For efficient charge transfer from the donor to the acceptor the LUMO of the acceptor ought to be at least 0.3 eV below the LUMO of the donor in order to overcome the exciton binding energy.¹²⁴ This energy offset also slows down back electron transfer. After charge transfer charge separation from the coulomb-bound $[D^{*+}A^{*-}]^*$ state is achieved thermally and by the electric field built up by the difference of the work functions of the electrodes.¹²¹ Additionally it is promoted by a reasonably high dielectric constant of the organic layer.¹³² Note, however, that charge separation is a reversible step reducing the overall amount of free charge carriers. In order to suppress charge recombination and to enhance the current output charge carrier mobilities should be sufficiently high ($> 10^{-3} \text{ cm}^2 \text{ V}^{-1} \text{ s}^{-1}$)¹²⁴ and balanced. Finally, as already mentioned HOMO and LUMO levels of the blend must match the work functions of the electrode materials (ITO/PEDOT:PSS $\sim -5.0 \text{ eV}$ ¹²⁹, Al $\sim -4.3 \text{ eV}$ ¹²⁷).

Absorption of Light and Energy Levels

Absorption of light over a broad range of the solar spectrum, i.e. a good overlap of the polymer's absorption spectrum with the solar spectrum, is also important to achieve high efficiencies. Unfortunately, most of the organic polymers only absorb below 650 nm (band gap 1.9 eV), which means that only 22.4 % of the photons emitted by the sun between 280 and 4000 nm can be harvested at most and the theoretically available maximum current density thus only amounts to 14.3 mA cm^{-2} .¹⁴ Extending the absorption edge to 800 nm, which corresponds to an optical band gap of $E_g^{\text{opt}} = 1.55 \text{ eV}$, would increase the amount of harvestable photons to 37.3 % and the maximum current density to 23.8 mA cm^{-2} . However, the band gap cannot be diminished infinitely, since the HOMO and LUMO levels of the polymer have to be adjusted to HOMO and LUMO of the acceptor (PCBM) and to the electrode levels. Moreover the energy difference between the HOMO of the donor and the LUMO of the acceptor determines the open circuit voltage, V_{oc} (eq. 8), which should be as high as possible.

These requirements suggest a minimum band gap of about 1.2 eV and a LUMO energy level of $\geq -4.0 \text{ eV}$, if PCBM (LUMO -4.3 eV) is used as the acceptor, in order to ensure efficient charge transfer onto the PCBM molecule (Figure 8).¹³ However note that band gaps and HOMO/LUMO values determined from absorption edges and cyclic voltammetric measurements are often rather imprecise.

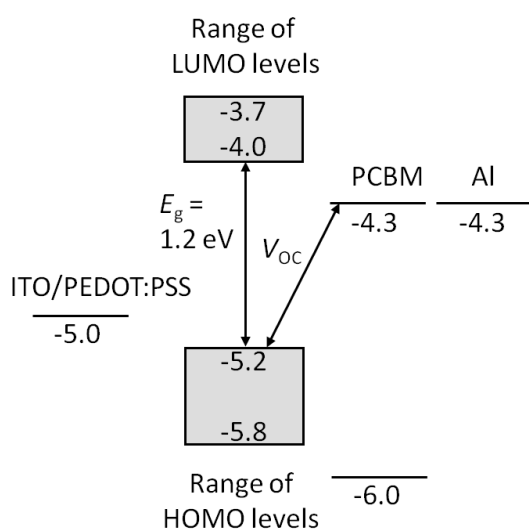


Figure 8. Adjustment of energy levels in BHJ solar cells.

Low band gaps (< 1.9 eV) can be achieved by different strategies.^{14,129,133} One is the synthesis of D-A conjugated polymers¹³⁴⁻¹³⁵: Donor moieties raise the HOMO level and acceptor moieties lower the LUMO level of the polymer by orbital mixing of the respective HOMO and LUMO orbitals of donor and acceptor. This effect can be further increased by enhancement of donor and acceptor strength via the introduction of electron donating and electron withdrawing substituents. Moreover the alternation between donor and acceptor moieties induces a more delocalized electronic structure due to the contribution of the $D^+=A^-$ resonance structure (= quinoid structure), which also decreases the band gap. Another strategy is to design planar, rigid polymer backbones with hindered rotation in order to get extended π -conjugation. However, such polymers are often less soluble. A further possibility is to enforce a quinoid structure in the polymer backbone, which has been shown to reduce the band gap of polyisothianaphthene by 1 eV compared to the aromatic structure of polythiophene.¹³⁶⁻¹³⁸ Above all the band gap can be reduced by intermolecular interactions in the solid state.

Organic Materials

During the past decade a huge amount of novel low band gap polymers with suitable HOMO and LUMO levels have been synthesized and applied in BHJ cells.^{13,16,126-127,139-148} However, most of these devices gave rather low PCEs compared to the state of the art device ITO/PEDOT:PSS/(P3HT/[60]PCBM)/LiF/Al, which reproducibly gives PCEs of around 5 %¹⁴⁹⁻¹⁵¹, even though the band gap of P3HT is about 1.9 eV. This is caused by several factors:¹²¹ Charge transfer and charge transport are strongly dependent on the morphology of the active layer. For efficient charge transfer the mean domain size of donor and acceptor phases should not exceed the exciton diffusion length. Moreover, both phases need to be highly ordered and the two phases have to form a bicontinuous network in order to obtain efficient charge transport towards the electrodes. The formation of such a nanoscale phase separated bicontinuous network requires good solubility and miscibility of donor and acceptor in the same solvent so as to avoid the formation of clusters. Furthermore, it depends on the ratio of donor and acceptor, their intermolecular interaction, molecular weight and purity of the polymer, the type of solvent and the

solvent evaporation rate. All these aforementioned parameters determine a preliminary order in the active layer. Thermal annealing can further improve the morphology: P3HT starts to crystallize and [60]PCBM diffuses through the layer, which finally can give the optimized morphology. All of these fabrication parameters have been evaluated for the P3HT/[60]PCBM system by many research groups resulting in numerous publications.^{149-150,152-156} Since every single donor/acceptor system is unique, the morphology has to be optimized for each system individually, which has not been done for most of the new D-A low band gap polymers. Another reason for the observed low PCEs of solar cells comprising these new polymers is their low intrinsic charge carrier mobility.^{142,148} In fact many of the low band gap polymers strongly absorb in the long wavelength range but at the same time absorption between 300 and 500 nm is rather weak.^{127,142,147}

However, some of the novel low band gap donor polymers exhibit promising PCEs in BHJ cells being even superior to the P3HT cell as can be inferred from Table 1. The structures of the applied polymers are depicted in Chart 5.

Table 1. Results of BHJ solar cells made from low band gap donor polymers A-D.^{16,126,141,145}

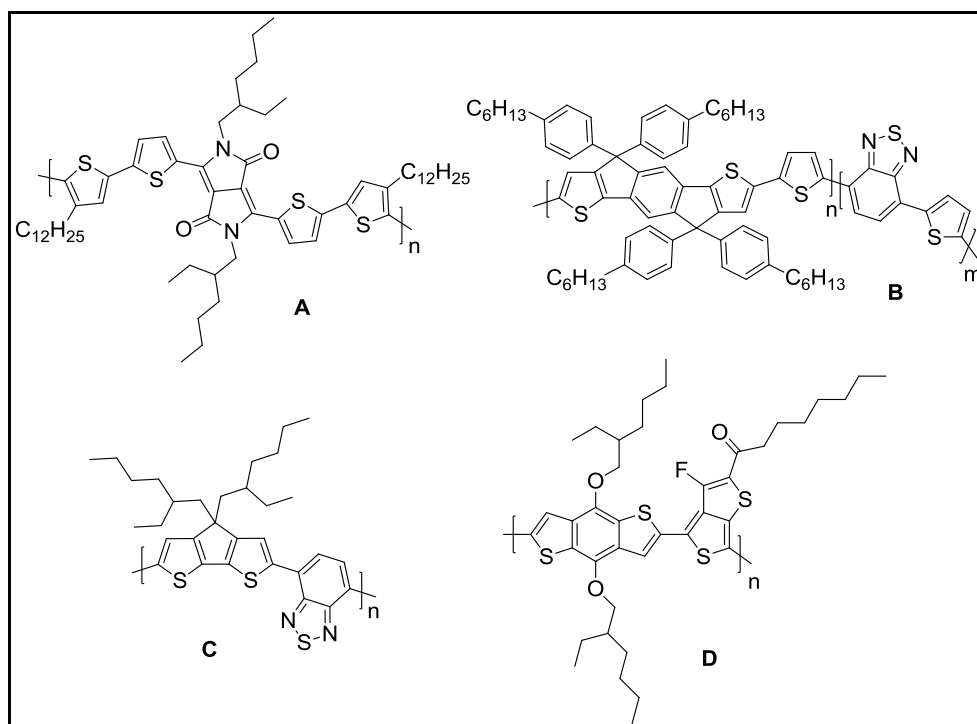
	\bar{M}_w /kDa	E_g^{opt} /eV ^a	HOMO /eV ^b	LUMO /eV ^b	J_{SC} /mA cm ⁻²	FF	V_{OC} /V	PCE /%
A/[70]PCBM	67	1.4	-5.1	-3.4	11.3	0.58	0.61	4.0
B/[70]PCBM	38.6	1.7	-5.43	-3.66	10.1	0.53	0.8	4.3
C/[70]PCBM	-	1.46	-5.3	-3.57	16.2	0.55	0.62	5.5
D/[70]PCBM	-	~1.61	-5.22	-3.45	15.2	0.67	0.76	7.4

^a measured in thin films; ^b from cyclic voltammetric measurements

All of these polymers consist of electron-rich and electron-poor units with optical band gaps E_g^{opt} between 1.4 and 1.7 eV, with appropriate HOMO and LUMO levels and with high weight-average molecular weights \bar{M}_w (where specified), which is important for obtaining a good morphology. The reasons for the good device performances are however rather difficult to elucidate in most cases, since the device performance is governed by an interplay of several factors. For the device made from

polymer **A** the morphology was optimized by testing different solvents for spin coating which had a dramatic effect on the device performance.¹⁶ Polymer **B** exhibits a sufficiently high absorption coefficient in thin films of $> 1 \times 10^5 \text{ cm}^{-1}$ between 450 and 650 nm and a reasonable high hole mobility of $3.4 \times 10^{-3} \text{ cm}^2 \text{ V}^{-1} \text{ s}^{-1}$ as evaluated from measurements on OFET devices.¹²⁶ In a BHJ device the maximum EQE observed was 55 % at 470 nm.¹²⁶ The EQE is a measure of the overall conversion of incident photons to extracted electrons at certain wavelengths. About the same peak value is achieved for a device comprising polymer **C**. Here the device performance was improved through altering the BHJ morphology by spin-coating the active layer from a solution containing not only polymer **C** and [70]PCBM but also 1,8-octanedithiole.¹⁴⁵ The best device performance was obtained using polymer **D**, which gave a maximum EQE of 69 % at 630 nm and an internal quantum efficiency IQE (absorbed photons to extracted electrons) of 90 % between 400 and 700 nm confirming the efficient overall photoconversion process.¹⁴¹

Chart 5

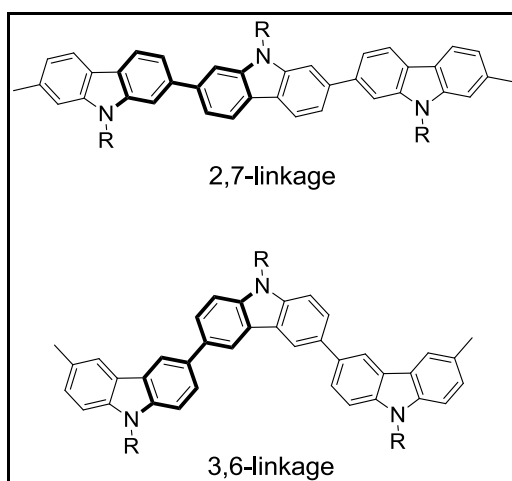


2 Polycarbazoles

2.1 Introduction and Aim of the Project

Owing to their promising electrical and photophysical properties¹⁵⁷ polycarbazoles are interesting candidates for applications in optoelectronic devices such as OPVs¹³, OFETs¹⁵⁸ and OLEDs^{107-108,159-160}. Polycarbazoles are strong blue emitters with high fluorescence quantum yields¹⁶¹⁻¹⁶² and they are excellent hole transport materials with high thermal stability¹⁶³ and glass forming properties¹⁶¹. Moreover, depending on the substitution and connection pattern (3,6- vs. 2,7-linkage, Chart 6) they can closely match the hole injection energy of ITO electrodes.¹⁶⁴⁻¹⁶⁶ The 2,7-linked polycarbazoles are often favoured to 3,6-linked polycarbazoles because of their higher fluorescence quantum yields in solution and their extended conjugation over several monomer units.^{163,166}

Chart 6

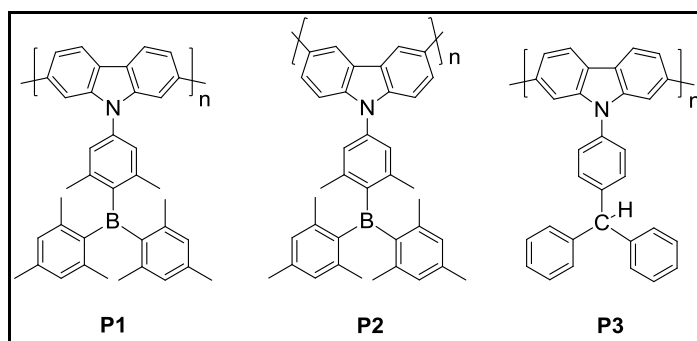


This extended conjugation in poly-2,7-carbazoles results from the rigid poly-*para*-phenylene motif which is bridged by nitrogen atoms in contrast to the more flexible 1,4-diaminobiphenyl structure of poly-3,6-carbazoles which may be conceived as nitrogen connected benzidines. However, the preparation of 3,6-disubstituted carbazoles is much easier than that of their 2,7-analogues and 3,6-polymers are more soluble than 2,7-polymers due to greater flexibility of the polymer backbone. Moreover, 3,6-polycarbazoles show higher in situ conductivities than their 2,7-analogues.¹⁶⁷

OLEDs have been fabricated from both 2,7¹⁰⁷- and 3,6-linked^{108,159} polycarbazoles. However, compared to the devices made from D-A conjugated polymers mentioned above these were rather low performing OLED devices. As an acceptor moiety in D-A compounds triarylboranes have been successfully used in small molecule OLEDs in the past decade.^{104,106,112-113,168} They have been shown to be applicable as electron transport layer¹¹⁰, hole blocking layer⁹⁹ and light emitting layer with colours ranging from blue, over green, yellow to orange depending on the donor and the bridge^{109,169}. Even white light-emitting devices have been fabricated from triarylborane containing molecules.⁹³

The aim of this project was to synthesize a 2,7- and a 3,6-linked polycarbazole with a triarylborane moiety attached to the nitrogen atom of the carbazole (**P1** and **P2**, Chart 7) and to investigate and compare their spectroscopic and electrochemical properties as well as their suitability for the application in an OLED device. As a reference molecule 2,7-linked polycarbazole **P3** (Chart 7) containing a triarylmethane moiety instead of the triarylborane acceptor was to be synthesized.

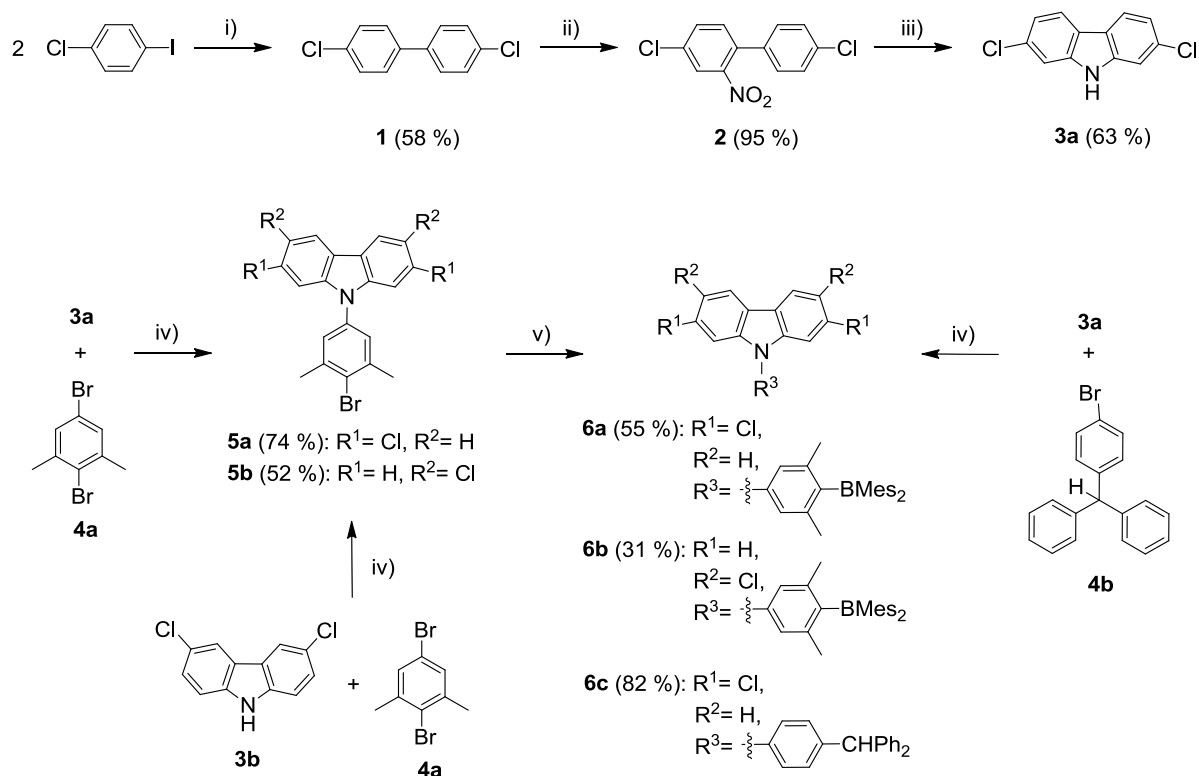
Chart 7



2.2 Synthesis

The synthetic approach to monomers **6a-c** is outlined in Scheme 1a. Leclerc et al. published an efficient two-step synthesis of 2,7-dichlorocarbazole **3a**.¹⁷⁰ However, the starting material they used – 4-chlorophenylboronic acid and 1-bromo-4-chloro-2-nitrobenzene – is rather expensive. Therefore, **3a** was prepared in three steps starting with cheap and commercially available 1-chloro-4-iodobenzene.

Scheme 1a. Synthesis of the monomers 6a-c.

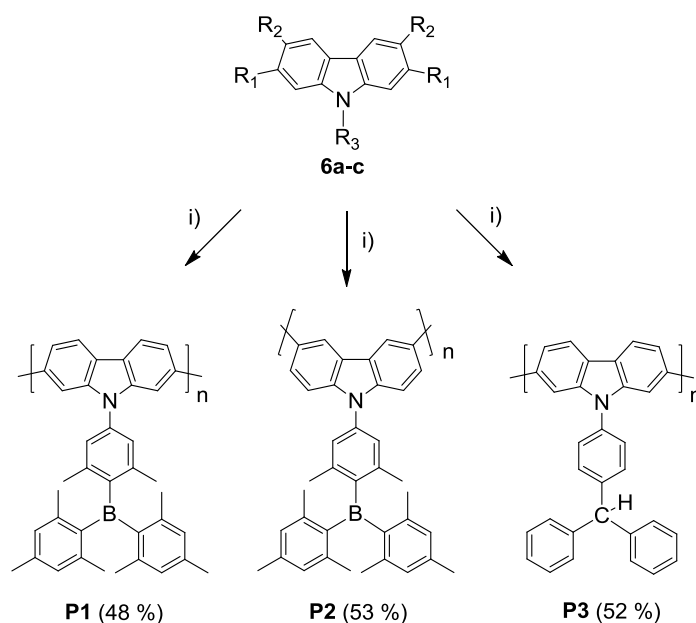


i) Cu, 230-250 °C, 3 h; ii) HNO₃, CH₃COOH, 110 °C, 1 h; iii) P(OEt)₃, 170 °C, 16 h; iv) CuI, K₃PO₄, *trans*-1,2-cyclohexanediamine, 1,4-dioxane, 110 °C, 72 h (19 h for **5b**); v) 1. *tert*-butyllithium, diethylether, -68 °C, 3 h 2. dimesitylboron fluoride (FBMes₂), diethylether, -68 °C -> r. t. over night

The first step was an Ullmann coupling reaction¹⁷¹ to give 4,4'-dichlorobiphenyl **1**¹⁷² in moderate yield, which was then nitrated to afford **2**¹⁷³ in 95 % yield. Finally, a Cadogan ring closure,¹⁷⁴ as it was also used by Leclerc *et al.*¹⁷⁰, gave **3a** in 63 % yield. The 2,7- and 3,6-dichlorocarbazole **3a** and **3b**¹⁷⁵ were then *N*-arylated by 1,4-dibromo-3,5-dimethylbenzene **4a**¹⁷⁶⁻¹⁷⁸ catalyzed by CuI to afford **5a** and **5b**,

respectively.¹⁷⁹ The same reaction was applied for the attachment of 1-bromo-4-(diphenylmethyl)benzene **4b**¹⁸⁰ to the carbazole-nitrogen of **3a** to give the monomer **6c**. In case of **5b** the reaction time was only 19 h in contrast to 72 h for **5a** and **6c** which might have been the reason for the lower yield of **5b**. Finally, reaction of dimethylboronfluoride with the aryllithium derivatives of **5a** and **5b** afforded the monomers **6a** and **6b**, respectively.¹⁷⁹ Polymerization of the monomers **6a-c** was achieved by standard Yamamoto coupling reaction¹⁸¹ with an in situ generated zerovalent nickel complex as catalyst to give **P1**, **P2** and **P3** in acceptable yields (Scheme 1b).¹⁷⁰

Scheme 1b. Polymerization of the monomers 6a-c to give P1-P3.



i) Zn powder, NiCl₂, 2,2'-bipyridyl, PPh₃, *N,N*-dimethylacetamide, 70 °C, 3 d

The 2,7-linked polymers **P1** and **P3** are only slightly soluble in chloroform, dichloromethane and THF, whereas the 3,6-linked polymer **P2** is more soluble in these solvents due to its more flexible polymer backbone.

Gel permeation chromatography (GPC) vs. polystyrene standards performed in THF at 35 °C indicated an average molecular weight \bar{M}_w of 2300 Da ($\bar{M}_n = 2100$ Da, PDI = 1.1) for **P1**, $\bar{M}_w = 6000$ Da ($\bar{M}_n = 4900$ Da, PDI = 1.2) for **P2** and $\bar{M}_w = 1900$ Da ($\bar{M}_n = 1700$ Da, PDI = 1.1) for **P3** corresponding to a degree of polymerization of $\bar{X}_w = 4, 12$ and 5, respectively (Table 2).

Table 2. GPC measurements in THF at 35 °C.

	\bar{M}_w /Da	\bar{M}_n /Da	PDI	\bar{X}_w
P1	2300 (4000) ^a	2100 (2300) ^a	1.1 (1.8) ^a	4 (8) ^a
P2	6000	4900	1.2	12
P3	1900	1700	1.1	5

^a numbers in brackets correspond to a measurement in 1,2,4-trichlorobenzene at 135 °C performed by S. Seiwald from the group of Prof. K. Müllen, MPI für Polymerforschung, Mainz

The higher \bar{M}_w of **P2** compared to the \bar{M}_w 's of the 2,7-linked polymers **P1** and **P3** can possibly be attributed to the better solubility of **P2** thus allowing the polymerization reaction to continue even for chains of higher molar mass. Moreover, it is not possible to obtain a clear solution of **P1** and **P3** in THF, that is, chains of higher molar mass might be removed by filtration before injection into the GPC-columns. This explanation is substantiated by an additional GPC measurement of **P1** in 1,2,4-trichlorobenzene at 135 °C which gave an \bar{M}_w of 4000 Da with a higher PDI of 1.8. In the latter solvent **P1** is more soluble so that chains of higher molar mass are also injected into the GPC-columns which consequently leads to a broader molecular weight distribution. Leclerc *et al.*¹⁶¹ reported an \bar{M}_n value of 2600 Da (PDI = 1.9) for poly[*N*-(2-ethylhexyl)-2,7-carbazole] measured in THF which corresponds to about 9 repeating units. This polymer was obtained by polymerization of *N*-(2-ethylhexyl)-2,7-dichlorocarbazole via standard Yamamoto coupling with Ni(1,5-cyclooctadiene)₂ as catalyst. The same reaction method was used by Fu and Bo¹⁸² for the polymerization of *N*-octyl-2,7-dibromocarbazole to obtain an \bar{M}_n value of 6400 Da. Even higher \bar{M}_n values were obtained for poly[*N*-(9'-heptadecanyl)-2,7-carbazole], $\bar{M}_n = 27000$ Da,¹⁸³ and for poly[*N*-(2-decyltetradecyl)-2,7-carbazole], $\bar{M}_n = 39100$ Da,¹⁸⁴ using the standard Yamamoto coupling reaction. This shows that high molecular weight 2,7-linked polycarbazoles can be obtained depending on the substituent at the nitrogen atom and the exact reaction conditions. For 3,6-linked polyalkylcarbazoles a high molecular weight synthesis based on the standard Yamamoto coupling reaction was developed to yield poly[*N*-(3,7-dimethyloctyl)-3,6-carbazole] with $\bar{M}_w = 120$ kDa using a reverse order of adding reagents.¹⁸⁵ In order to enhance the \bar{M}_w 's of **P1-P3** one would need to optimize the reaction conditions: For example, higher dilution could

avoid possible aggregation and precipitation of the resultant polymer chains.¹⁸⁶ However, dilute solutions of 3,6-dichlorocarbazole could promote formation of macrocycles.¹⁸⁷ Lowering the reaction temperature could avoid decomposition of the Ni(II)aryl complex which otherwise would result in termination of the polymerization process.¹⁸⁸ However, solubility decreases with decreasing temperature, too. Maybe one also has to raise the NiCl₂ : monomer ratio for small scale reactions (< 1 mmol of monomer) or use Ni(1,5-cyclooctadiene)₂ instead of generating the active Ni(0) species in situ from NiCl₂ and Zn, since Ni(1,5-cyclooctadiene)₂ is mainly used for this type of polymerization reactions in the literature. Using the dibromo instead of the dichloro monomers would certainly give better results. To this end one has to modify the synthesis of the monomers, which would include more synthetic steps, which in turn is unfavourable for industrial applications. Because optimization of the polymerization reaction was not the main goal, none of the above mentioned possibilities was pursued to increase the \bar{M}_w 's of the polymers **P1-P3**.

MALDI-TOF spectra revealed that not all polymer chains are terminated by hydrogen atoms. Chains of **P1** are mainly terminated by hydrogen atoms. However, there are additional small mass peaks which can be assigned to chains terminated at one end by one chlorine atom. For **P2** only hydrogen-terminated chains are found. **P3** consists of a mixture of chains terminated by one or two chlorine atoms and chains without chlorine atoms. These findings can be an indication of the type of polymerization mechanism taking place here: If the monomer reacts via an intermolecular catalyst-transfer condensation polymerization (CTCP) mechanism both ends of the chains should be terminated either by hydrogen or by chlorine atoms. If they react via an intramolecular CTCP mechanism one end should be terminated by a chlorine atom and the other end by a hydrogen atom. Therefore one can conclude that the polymerization of **P1** and **P2** proceeds mainly via the intermolecular mechanism whereas the polymerization of **P3** proceeds via inter- and intramolecular CTCP mechanisms. On the first sight, this is in contrast to the very narrow molecular weight distribution (PDI = 1.1 for **P1** and **P3** and 1.2 for **P2**) observed for the polymers, since the intermolecular CTCP mechanism is expected to result in a broader molecular weight distribution as opposed to the intramolecular mechanism.¹⁸⁸ However, as stated above, chains of higher molecular weight might

be removed by filtration before injection into the GPC-columns and thus the real molecular weight distribution might be broader at least for **P1** and **P3**.

NMR spectra of the polymers were recorded in chloroform and in THF. Although in the literature discrete doublets and singlets are found for carbazole protons of high molecular weight polycarbazoles only broad signals were observed for **P1-P3**. This is due to the short polymer chains investigated in the present work which leads to different chemical shifts for each monomer unit and, thus, to a distribution of overlapping signals. Due to their low solubility ^{13}C NMR spectra of **P1** and **P3** could not be recorded.

2.3 Absorption and Fluorescence Spectroscopy

Absorption Spectra

Absorption and emission spectra of **P1-P3** in solution and solid state are displayed in Figures 9a and 9b, respectively. Absorption maxima are listed in Tables 3 (solution) and 5 (solid state).

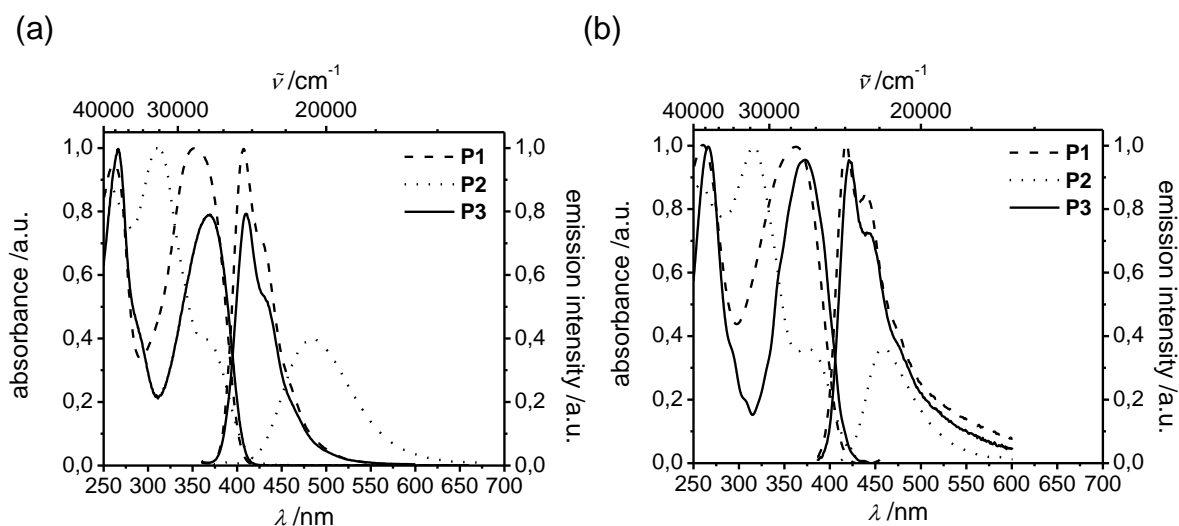


Figure 9. Absorption spectra (normalized) and emission spectra (normalized to the intensity of the lowest energy absorption band) of dichloromethane solutions of **P1-3** (a) and of thin films spin coated from dichloromethane solutions onto quartz plates (b).

The absorption spectra of 2,7-linked polymers **P1** and **P3** measured in dichloromethane are similar to each other (Figure 9a) and to other 2,7-linked *N*-alkyl- and *N*-arylcarbazole polymers.^{162-164,183} This fact nicely demonstrates that the *N*-substituents only weakly interact with the polymer backbone. Nevertheless, the absorption band of the triarylborane moiety cannot be seen, since its molar extinction coefficient ϵ is too small: The absorption maximum of dimesityl(2,6-dimethylphenyl)borane dissolved in dichloromethane is at $\lambda = 327$ nm (spectrum not displayed) with $\epsilon = 13300 \text{ M}^{-1}\text{cm}^{-1}$. The molar extinction coefficient of **P1** dissolved in dichloromethane is ca. $19100 \text{ M}^{-1}\text{cm}^{-1}$ at $\lambda = 327$ nm. Overlaying both spectra shows that the absorption band of the triarylborane compound is completely covered by the band of **P1**. The absorption edge of triphenylmethane is situated at 280 nm.¹⁸⁹ Absorption spectra were also recorded of solutions of **P1** and **P3** in cyclohexane, *tert*-butyl-methylether, ethylacetate, 1,4-dioxane and THF. Only minor variations of the shape of the absorption bands with the solvent were observed, which can be explained by the fact that different solvents dissolve different weight fractions of the polymers (the solutions had to be filtered before measurement due to the low solubility in these solvents). This interpretation is supported by the work by Iraqi et al.¹⁶³ and by the fact, that there is no systematic solvatochromism vs. any solvent polarity function.

Much in contrast, the absorption spectrum of 3,6-linked polymer **P2** in dichloromethane deviates from those of the pentamer and polymer of 3,6-linked *N*-alkyl-carbazole¹⁵⁸ because it shows an additional low energy band at 365 nm in dichloromethane arising from a charge transfer (CT) from the carbazole donor to the triarylborane acceptor. This process causes a reversal of the dipole moment. Thus, a pronounced negative solvatochromism is observed in the absorption spectra (Figure 10a) and a positive solvatochromism is found in the emission spectra of **P2** (Figure 10b). This phenomenon has already been discussed for the monomer analogue of **P2**.¹⁷⁹

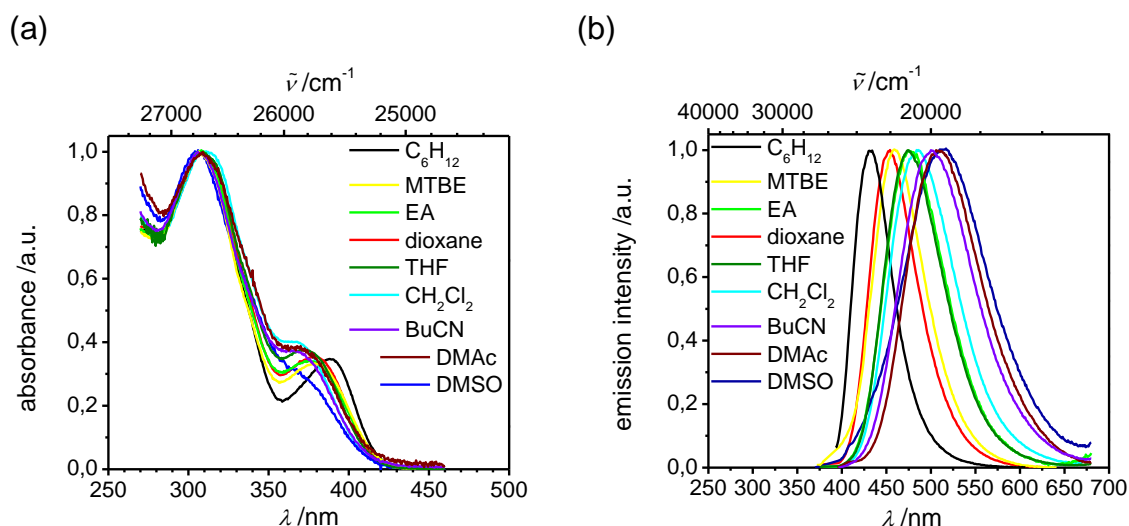


Figure 10. Normalized absorption spectra (a) and normalized emission spectra (b) of **P2** in different solvents. MTBE: *tert*-butyl-methylether; EA: ethylacetate; BuCN: butyronitrile; DMAc: *N,N*-dimethylacetamide.

Emission Spectra

Absorption and emission maxima λ_{abs} and λ_{em} , Stokes shifts, fluorescence quantum yields Φ_f , lifetimes τ , and rate constants k_f and k_{nr} measured in dichloromethane are listed in Table 3.

Table 3. Absorption and emission maxima λ_{abs} and λ_{em} , Stokes shifts, fluorescence quantum yields Φ_f , lifetimes τ and rate constants k_f and k_{nr} measured in dichloromethane.

	$\lambda_{\text{abs}} / \text{nm}$	$\lambda_{\text{em}} / \text{nm}$	Stokes shift / cm^{-1}	Φ_f	τ / ns	$k_f / 10^8 \text{ s}^{-1}$	$k_{\text{nr}} / 10^8 \text{ s}^{-1}$
P1	261, 353	407	3800	0.80	0.96	8.3	2.1
P2	257, 310, 365	484	6700	0.54	8.5	0.64	0.54
P3	267, 369	410	2800	0.85	0.77	11	1.9

Emission spectra of **P1** and **P3** are very similar concerning λ_{em} (407 and 410 nm in dichloromethane) and the shape of the emission bands (Figure 9a). They are also very similar to other 2,7-linked *N*-alkyl and *N*-aryl-carbazole polymers reported in the literature.^{162,161,163} The Stokes shifts are somewhat higher in energy than that of

already known 2,7-polycarbazoles (poly[*N*-(2-ethylhexyl)-2,7-carbazole]: 2300 cm⁻¹)¹⁹⁰ with that of **P1** being also higher than that of **P3** (3800 cm⁻¹ vs. 2800 cm⁻¹). In going from cyclohexane to dichloromethane both polymers show small solvatochromic shifts of about 400 cm⁻¹ (**P1**) and 700 cm⁻¹ (**P3**). Therefore, fluorescence quantum yields Φ_f and lifetimes τ were measured in dichloromethane only. Rate constants k_f and k_{nr} are calculated according to eqs. 11 and 12, which can be derived from combination of eqs. 9 and 10.

$$\tau = \frac{1}{k_f + k_{nr}} \quad (9)$$

$$\phi_f = \frac{k_f}{k_f + k_{nr}} \quad (10)$$

$$k_f = \frac{\phi_f}{\tau} \quad (11)$$

$$k_{nr} = \frac{1 - \phi_f}{\tau} \quad (12)$$

The k_f and k_{nr} values of **P1** are about half of those of poly[*N*-octyl-2,7-carbazole] ($k_f = 17 \times 10^8 \text{ s}^{-1}$; $k_{nr} = 4.3 \times 10^8 \text{ s}^{-1}$, $\tau = 0.48 \text{ ns}$, $\Phi_f = 0.80$) while the lifetime is doubled and the quantum yield is the same.¹⁹⁰ The Φ_f , τ , k_f and k_{nr} values of **P3** are similar to the corresponding values of **P1** (Table 3). All these similarities of **P1** and **P3** and other 2,7-linked polycarbazoles and the lack of solvatochromic fluorescence of **P1** clearly show that the triarylborane substituent does not influence the fluorescence properties in this type of polymer. Thus, one can conclude that fluorescence in **P1** and **P3** emanates from the polymer backbone.

Unlike **P1** and **P3**, **P2** shows strong solvatochromic fluorescence arising from a low lying CT state. The energy shift between the emission maxima in cyclohexane and DMSO is 3800 cm⁻¹. In Table 4 results of time resolved fluorescence measurements of **P2** are listed for solvents of increasing polarity.

Table 4. Emission maxima λ_{em} , Stokes shifts, fluorescence quantum yields Φ_f , lifetimes τ and rate constants k_f and k_{nr} of P2 measured in different solvents.

solvent	λ_{em} /nm	Stokes shift /cm ⁻¹	Φ_f	τ /ns	k_f /10 ⁸ s ⁻¹	k_{nr} /10 ⁸ s ⁻¹
cyclohexane	432	2700	0.37	3.2	1.2	2.0
MTBE	459	4700	0.48	5.3	0.91	0.98
ethylacetate	475	5900	0.44	6.4	0.69	0.88
1,4-dioxane	453	4500	0.62	5.3	1.2	0.72
THF	475	5900	0.54	7.3	0.74	0.63
dichloromethane	484	6700	0.54	8.5	0.64	0.54
butyronitrile	501	7500	0.40	9.9	0.40	0.61
DMAc	509	7800	0.51	13	0.39	0.38
DMSO	514	8100	0.75	–	–	–

MTBE: *tert*-butyl-methylether; DMAc: *N,N*-dimethylacetamide

Except for the values obtained in 1,4-dioxane, emission maxima, band widths and Stokes shifts increase with increasing solvent polarity as expected for CT transitions. While the lifetimes of the CT state increase with decreasing fluorescence energy, the quantum yields do not reveal a clear trend. As expected from the Strickler-Berg equation¹⁹¹ k_f should be proportional to the cubic fluorescence energy. While this is not exactly fulfilled with the present data set, at least an increase of k_f with the fluorescence energy is clearly visible. According to the gap rule of Siebrand¹⁹² the nonradiative rate constant k_{nr} should increase with decreasing fluorescence energy. However, the opposite trend is observed. This unusual trend together with the same solvatochromic shifts and somewhat smaller Stokes shifts have also been observed for the monomer analogue,¹⁷⁹ but an explanation for the violation of Siebrand's gap rule is still missing. In comparison to the monomer, lifetimes of **P2** are about twice as high and k_f values are about one third of the values of the monomer, whereas k_{nr} values are the same for monomer and polymer. Therefore, the quantum yields of the polymer are lower than those of the monomer. Thus, counterintuitively, it is not any additional nonradiative pathway which leads to the decreased fluorescence quantum

yield of the polymer compared to the monomer but the smaller fluorescence rate constant.

Compared to the emission spectra of 3,6-linked *N*-alkyl-carbazole polymers, which emit at $\lambda_{em} = 426$ nm in dichloromethane,¹⁹³ the emission band of **P2** is much broader and is shifted to lower energy ($\lambda_{em} = 484$ nm in dichloromethane) because of its low lying CT state. The Stokes shift of 6700 cm^{-1} in dichloromethane is somewhat smaller than that of *N*-alkyl-3,6-carbazole polymers.^{185,187,193} Interestingly, fluorescence quantum yields are surprisingly high compared for example to poly-[*N*-decyl-3,6-carbazole] with $\Phi_f = 0.15$ in THF¹⁸⁵ and other 3,6-linked *N*-alkylcarbazole polymers with $\Phi_f = 0.04 - 0.06$ in dichloromethane.¹⁹³ The reason for the enhanced quantum yield obviously is the CT character of the fluorescing state. The improved quantum yield makes **P2** a promising candidate as light emitting polymer for the application in OLEDs.

The most interesting aspect about **P1** and **P2** is their absorption and emission properties being completely different (Figure 9a). The fact, that **P1** has a higher fluorescence quantum yield than **P2** was to be expected on the basis of the properties of other poly-*N*-alkyl-carbazoles. The higher k_f value compared to the k_{nr} value of **P1** is in accordance with its higher quantum yield. However, polymer **P2** shows negative solvatochromic absorption and positive solvatochromic fluorescence resulting from a low lying CT state. Because the same characteristics are found for the monomer analogue¹⁷⁹ we conclude that the fluorescent CT state in **P2** is localized within the monomer site. Much in contrast, no solvatochromic behaviour is observed for **P1** which fluoresces from a delocalized state of the polymer backbone ($S_{backbone}$). This is because **P1** forms a true conjugated (poly-*para*-phenylene type) polymer with low-lying delocalized states while **P2** is a polybenzidine with conjugation being interrupted by the nitrogen atoms. Thus, the state located at the polymer backbone ($S_{backbone}$) will be high-lying in **P2** compared to the localized CT state (Figure 11).

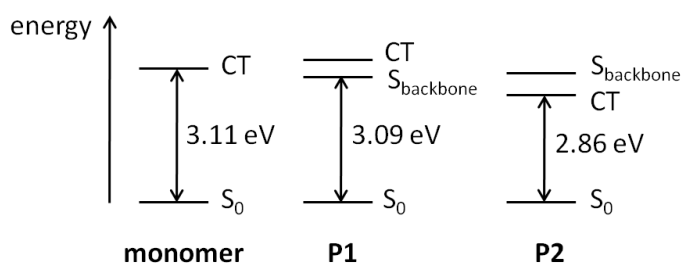


Figure 11. Qualitative energy diagram of ground and excited electronic states of P1, P2 and their monomer analogue. Gap energies are taken from the onsets of the absorption spectra of cyclohexane solutions.

While no pronounced solvent effect was visible in **P1**, a solvent effect was observed for a 2,7-linked polycarbazole substituted by 4-dioctylamino-benzene at the nitrogen atom which shows dual fluorescence in polar solvents.¹⁶⁴ The dual fluorescence possibly arises from a fluorescent delocalized state of the polymer backbone and from a fluorescent intramolecular CT state between the dioctylaminophenyl substituent and the carbazole moiety. Interestingly, the emission maximum of the supposed CT emission band and the Stokes shifts between the absorption maximum and the CT emission band in THF and dichloromethane are quite close to those observed for **P2** in these solvents. In case of **P1** such a CT state might be higher in energy than the delocalized state of the polymer backbone. Thus no solvent effect is observed for the fluorescence of **P1**.

Thin Films

Absorption and emission bands recorded of thin films of the polymers cast on quartz plates are slightly red shifted except for the solid state emission of **P2** which reveals an emission maximum of $\lambda_{em} = 461$ nm which is similar to the one in *tert*-butyl-methylether (459 nm) (Figure 9b, Tables 3 and 5). This indicates that the polymer itself provides a relatively apolar environment. In general, the fluorescence signals are not much broader in the solid state than in solution which is also favourable for OLED applications. Optical band gaps E_g^{opt} determined from the onsets of the absorption bands are 3.02, 2.92 and 2.97 eV for **P1**, **P2** and **P3**. These values fit well into the range of 2.89-3.2 eV observed for other 2,7-linked polycarbazoles depending on the conjugation length.^{161,164,166,183-184} In contrast, the

band gap of **P2** is considerably smaller compared to other 3,6-linked polycarbazoles which have E_g^{opt} values of about 3.2 eV^{165-166,194}. This is again due to the low lying CT state.

Table 5. Absorption and emission maxima λ_{abs} and λ_{em} , optical band gaps E_g^{opt} and fluorescence quantum yields Φ_f of powders and films.

	$\lambda_{\text{abs}}(\text{film})$ /nm	$\lambda_{\text{em}}(\text{film})$ /nm	$E_g^{\text{opt}}(\text{film})$ /eV	$\Phi_f(\text{powder})$	$\Phi_f(\text{film})$
P1	260, 363	418	3.02	0.21	0.09
P2	316, 379	461	2.92	0.28	0.15
P3	266, 373	422	2.97	0.23	0.25

Emission quantum yield measurements of powders of **P1**, **P2** and **P3** gave values of 0.21, 0.28 and 0.23, respectively, whereas quantum yields of the films (drop cast) are 0.09, 0.15 and 0.25 (Table 5). The latter values depend on the film quality and might be different for spin coated films. Nevertheless, solid state quantum efficiencies between 0.20 and 0.30 are reasonably high compared to other solid state quantum efficiencies of conjugated carbazole polymers.¹⁶⁴

2.4 Cyclic Voltammetry

Cyclic voltammetric measurements were carried out in acetonitrile (MeCN)/tetrabutylammonium perchlorate (TBAP) with the polymer being drop cast onto a Pt-working electrode from a dichloromethane solution. Redox potentials were referenced vs. ferrocene (Fc/Fc⁺) and results are listed in Tables 6 and 7.

Table 6. Oxidation and reduction potentials vs. Fc/Fc⁺ of P1, P2 and P3 drop cast onto a Pt electrode (MeCN) and in solution (THF).

	solvent	E_{ox}^1/V	E_{ox}^2/V	E_{ox}^3/V	E_{red}^1/V
P1	MeCN	+0.58 ^a	+0.83 ^a	+1.02 ^b	-2.51 ^a
P2	MeCN	+0.53 ^a	+0.83 ^a		-2.49 ^a
	THF				-2.49 ^a
P3	MeCN	+0.60 ^a	+0.84 ^a	+0.96 ^c	-2.40 ^b

^a half wave potential, $\nu = 100 \text{ mV s}^{-1}$; ^b peak potential, chemically irreversible, $\nu = 2 \text{ V s}^{-1}$; ^c peak potential, chemically irreversible, $\nu = 100 \text{ mV s}^{-1}$

Table 7. HOMO, LUMO and electrochemical band gap energies E_g of P1, P2 and P3 in MeCN.^a

	HOMO /eV	LUMO /eV	E_g /eV ^e	HOMO /eV ^d	LUMO /eV ^d	E_g /eV ^e
P1	-5.43 ^b	-2.42 ^b	3.01	-5.15	-2.52	2.63
P2				-5.17	-2.46	2.71
P3	-5.45 ^c	--	--	-5.23	--	--

^a values are calculated on the basis that Fc/Fc⁺ is 4.8 eV below the vacuum level¹⁹⁵; ^b from onset of oxidation /reduction of noncrosslinked **P1** ($\nu = 2 \text{ V s}^{-1}$); ^c from onset of the oxidation of noncrosslinked **P3** ($\nu = 100 \text{ mV s}^{-1}$); ^d from onset of the first reversible oxidation /reduction of **P2** and of crosslinked **P1** and **P3** ($\nu = 100 \text{ mV s}^{-1}$); ^e $E_g = \text{LUMO} - \text{HOMO}$

Polymers **P1** and **P3** are oxidized at $E_{pa} = +1.02 \text{ V}$ and at $E_{pa} = +0.96 \text{ V}$, respectively. This process is chemically irreversible for both polymers. Upon back reduction two new signals appear ($E_{1/2} = +0.58 \text{ V}$ and $E_{1/2} = +0.83 \text{ V}$ for **P1** and $E_{1/2} = +0.60 \text{ V}$ and $E_{1/2} = +0.84 \text{ V}$ for **P3**), which are reversible upon multi-sweep oxidation at high scan rates of 2 V s^{-1} . At lower scan rates (100 mV s^{-1}) the signals of **P1** drop due to detachment of the polymer from the electrode surface during the measurement. The irreversible oxidation signal disappears after the first redox cycle for both polymers. The new signals arise from CC bond formation between polymer chains at 3,6-position which leads to benzidine units which can typically be oxidized twice.^{163,167} A multi-sweep cyclic voltammogram (CV) of the oxidation processes of **P1** is displayed in Figure 12a. The CV of **P3** is qualitatively similar.

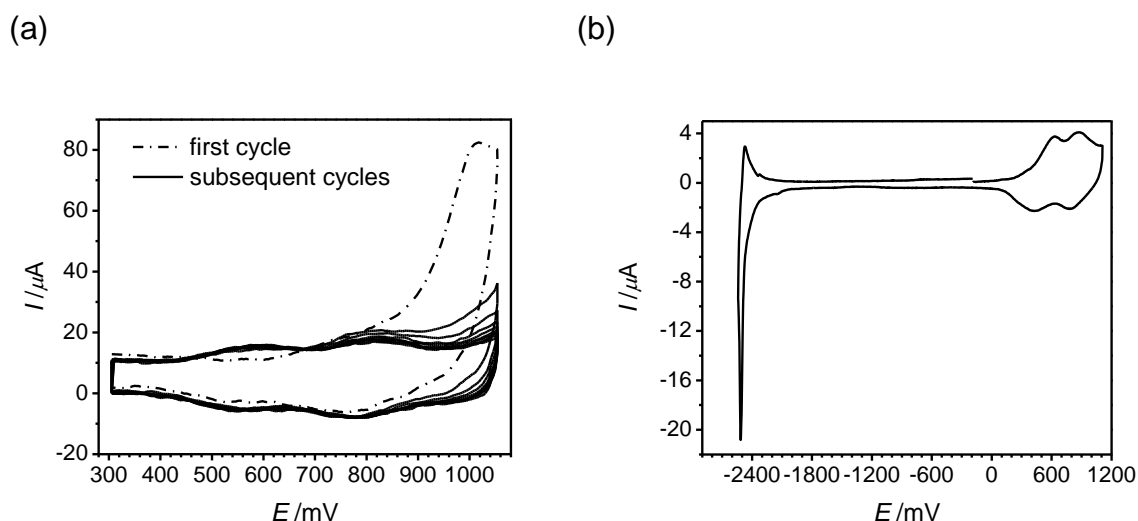


Figure 12. (a) Multi-sweep CV of **P1** drop cast onto a Pt-working electrode in MeCN/TBAP, $\nu = 2 \text{ V s}^{-1}$; (b) CV of **P2** drop cast onto a Pt-working electrode in MeCN/TBAP, $\nu = 100 \text{ mV s}^{-1}$.

Two reversible oxidation signals similar to the reversible oxidation signals of **P1** and **P3** are also observed for **P2** ($E_{1/2} = +0.53 \text{ V}$ and $E_{1/2} = +0.83 \text{ V}$) where the benzidine units are already present in the polymer backbone (Figure 12b). The reduction of **P2** is at $E_{1/2} = -2.49 \text{ V}$. However, the backoxidation peak is much smaller than the reduction peak and both peaks drop from one cycle to the next due to dissolution of the negatively charged polymer (Figure 13a). Therefore, a CV of **P2** dissolved in THF/TBAP was recorded additionally. This CV shows a fully reversible signal at $E_{1/2} = -2.49 \text{ V}$ (Figure 13b, Table 6).

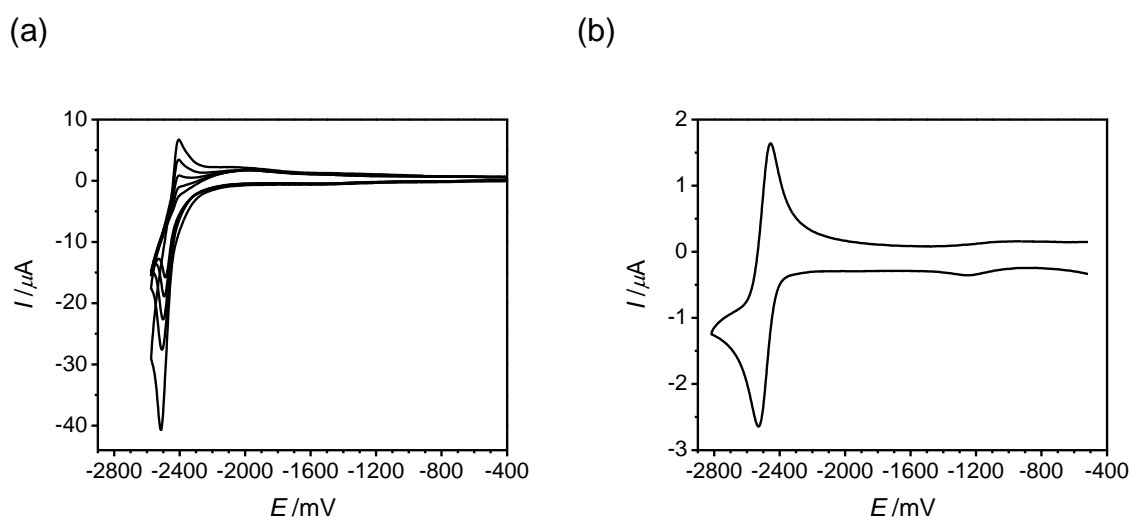


Figure 13. (a) Multi-sweep CV of **P2** drop cast onto a Pt-working electrode in MeCN/TBAP, $\nu = 100 \text{ mV s}^{-1}$; (b) CV of **P2** dissolved in THF/TBAP, $\nu = 100 \text{ mV s}^{-1}$.

The reduction of **P1** is chemically reversible only if the polymer film is crosslinked previously, which renders the polymer film insoluble avoiding its detachment from the electrode surface. Before crosslinking the reduction takes place at $E_{1/2} = -2.53$ V determined at a scan rate of $\nu = 2$ V s⁻¹. At a lower scan rate this peak is difficult to observe. At this high scan rate the peak separation between the reduction and the back oxidation peak is about 200 mV, which indicates a slow electron transfer between electrode surface and polymer film. After crosslinking $E_{1/2} = -2.51$ V and the signal becomes broader and more intense (Figure 14a).

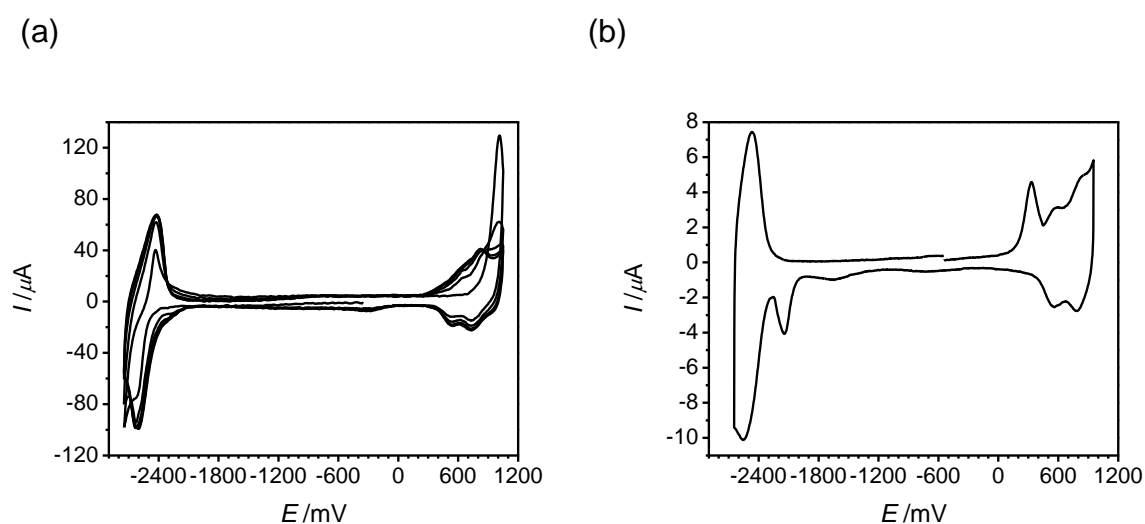


Figure 14. (a) Multi-sweep CV of **P1** drop cast onto a Pt-working electrode in MeCN/TBAP, $\nu = 2$ V s⁻¹; first cycle: reduction and oxidation before crosslinking; (b) CV of **P1** drop cast onto a Pt-working electrode in MeCN/TBAP, $\nu = 100$ mV s⁻¹, recorded after interchain coupling, second cycle of an oxidation-reduction-multi-sweep CV.

A CV of **P1** recorded at $\nu = 100$ mV s⁻¹ after crosslinking shows a peak separation of about 80 mV and irreversible signals at $E_{pc} = -2.14$ V and at $E_{pa} = +0.33$ V (Figure 14b) which are not observed if multi-sweep scans are exclusively run in one potential range (either between 0 and -2.80 V or between 0 and +1.10 V). These signals are more intense at scan rates of $\nu = 100$ mV s⁻¹ than at $\nu = 2$ V s⁻¹ (Figure 14a and b). Their origin is presently unclear.

No reduction process is observed for **P3**, if the polymer film is not crosslinked before. After crosslinking only an irreversible signal is observed at $E_{pc} = -2.38$ V which is not recovered in the following cycles, whereas the oxidation signals appear unchanged (Figure 15). It might result from an adduct being formed upon crosslinking

of the 2,7-linked carbazole backbone. Similar to **P1** there are irreversible signals at $E_{pc} = -2.14$ V and at $E_{pa} = +0.34$ V which are very small if multi-sweep scans are exclusively run in one potential range (inset of Figure 15).

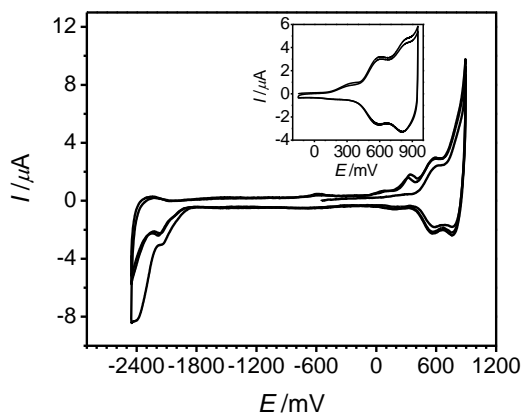


Figure 15. Multi-sweep CV of **P3** drop cast onto a Pt-working electrode in MeCN/TBAP, $\nu = 100$ mV s^{-1} , recorded after interchain-coupling; inset: two oxidation cycles after interchain-coupling, $\nu = 100$ mV s^{-1} .

Since no reversible reduction process is observed for **P3**, whereas reversible reductions at $E_{1/2} = -2.59$ V vs. Fc/Fc^+ (0.7 mM in THF/TBAP 0.3 M, $\nu = 250$ mV s^{-1} , Pt-working electrode) and at $E_{1/2} = -2.48$ V vs. Fc/Fc^+ (0.6 mM in THF/TBAP 0.3 M, $\nu = 100$ mV s^{-1} , Pt-working electrode) are observed for dimesityl(2,6-dimethylphenyl)borane and for the monomer analogue, the reduction processes of **P1** and **P2** can be ascribed to the reduction of the borane moiety. The reduction of the carbazole moiety is not seen for any of the three polymers as it seems to be the case for most polycarbazoles in the literature.¹⁸³ Only Zotti and coworker¹⁶⁷ reported the reduction of poly(*N*-octyl-2,7-carbazolediyl) at $E_{\text{red}} = -2.68$ V vs. $\text{Ag}/0.1$ M AgClO_4 in MeCN and Iraqi and coworker¹⁹⁶ found a reduction potential of $E_{\text{red}} = -2.1$ V vs. Ag/AgNO_3 for a drop cast polymer film of poly[3,6-dicyano-*N*-(2-hexyldecyl)-carbazole-2,7-diyl].

HOMO and LUMO energies determined from the onset of the first reversible oxidation and reduction processes of **P2** and of the noncrosslinked and crosslinked polymers **P1** and **P3** and the corresponding energy band gaps E_g are listed in Table 7. The HOMO energies of noncrosslinked **P1** and **P3** are -5.43 eV and -5.45 eV, respectively. HOMO energies of other 2,7-linked polycarbazoles are also around -5.4

eV^{163,182,197}. Crosslinking raises the HOMO levels of **P1** and **P3** resulting in quite similar HOMO energies for all three polymers (-5.15 eV (**P1**), -5.17 eV (**P2**), -5.23 eV (**P3**)) which, thus, lie in the range of those of 3,6-linked polycarbazoles (-5.0 eV¹⁶⁵, -5.1 eV¹⁹³). The lowering of the HOMO energies can be explained by the donating abilities of the nitrogen atoms arranged *para* to each other after crosslinking. The LUMO energy of **P1** is only slightly lowered from -2.42 eV before crosslinking to -2.52 eV after crosslinking which has to do with the broadening of the peak after crosslinking. Note that the half wave potentials of the reduction of **P2** and of noncrosslinked and crosslinked **P1** are all more or less the same, which means, that the reduction is not much affected by the type of carbazole connection and is located at the borane moiety. The LUMO energy of **P3** could not be determined since the origin of the irreversible reduction signal after crosslinking is unclear and might result from an adduct. Accordingly, the electrochemical band gap energy E_g of **P3** calculated as the difference between HOMO and LUMO energy could not be determined.⁵⁰ The band gap energies for **P1**, noncrosslinked and crosslinked, and for **P2** are $E_g = 3.01$, 2.63 and 2.71 eV, respectively.

Absorption spectra of polymer films of **P1** and **P3** on a Pt-working electrode in MeCN/TBAP before and after crosslinking were recorded additionally, which clearly reflect the narrowing of E_g upon crosslinking. Unfortunately, the spectra were of a rather poor quality so that optical band gap energies and shifts of absorption maxima could not be derived.

Comparison of the electrochemical band gap energies of **P2** and noncrosslinked **P1** with the optical band gap energies extracted from the solid state absorption spectra of thin films on quartz plates (Table 5) reveal nice agreement for **P1** ($E_g = 3.01$ eV and $E_g^{\text{opt}} = 3.02$ eV) and a major deviation for **P2** ($E_g = 2.71$ eV and $E_g^{\text{opt}} = 2.92$ eV). However, it has to be pointed out, that quite some of the HOMO and LUMO values are rather rough estimates, since the shape of the signals is distorted by adsorption (sharp signal in Figure 12b), solvent decomposition (steep signal raise, Figure 14a) and polymer interchain interactions (signal broadening, Figure 14a), which considerably affects the determination of the onset potentials. However, in order to make HOMO and LUMO values comparable to literature values which were also determined from onset potentials inaccuracies due to obscure onset potentials were accepted.

2.5 Single Layer OLED

A single layer OLED was constructed with **P2** as active layer in order to prove its electroluminescent properties: A solution of **P2** (6 mg/mL) in chloroform/toluene (25:1) was spin coated onto ITO coated glass plates and Al contacts (90 nm) were deposited on top as illustrated in Figure 16b. The electroluminescence spectrum was recorded at an applied voltage of 8.5 V (Figure 16a). The emission maximum is at $\lambda = 463$ nm, which is only a 2 nm red-shift compared to that of the photoluminescence spectrum of the polymer film (Table 5). The CIE coordinates are (0.17, 0.21). R. Liu and coworkers got CIE coordinates of (0.17, 0.14)¹⁹⁸ for a single layer OLED of 2,7-fluorene-co-3,9-carbazole copolymer which indicates a more saturated colour. Electroluminescence spectra of **P1** and **P3** could not be recorded reproducibly. This is possibly caused by their low solubility which results in very thin polymer layers.

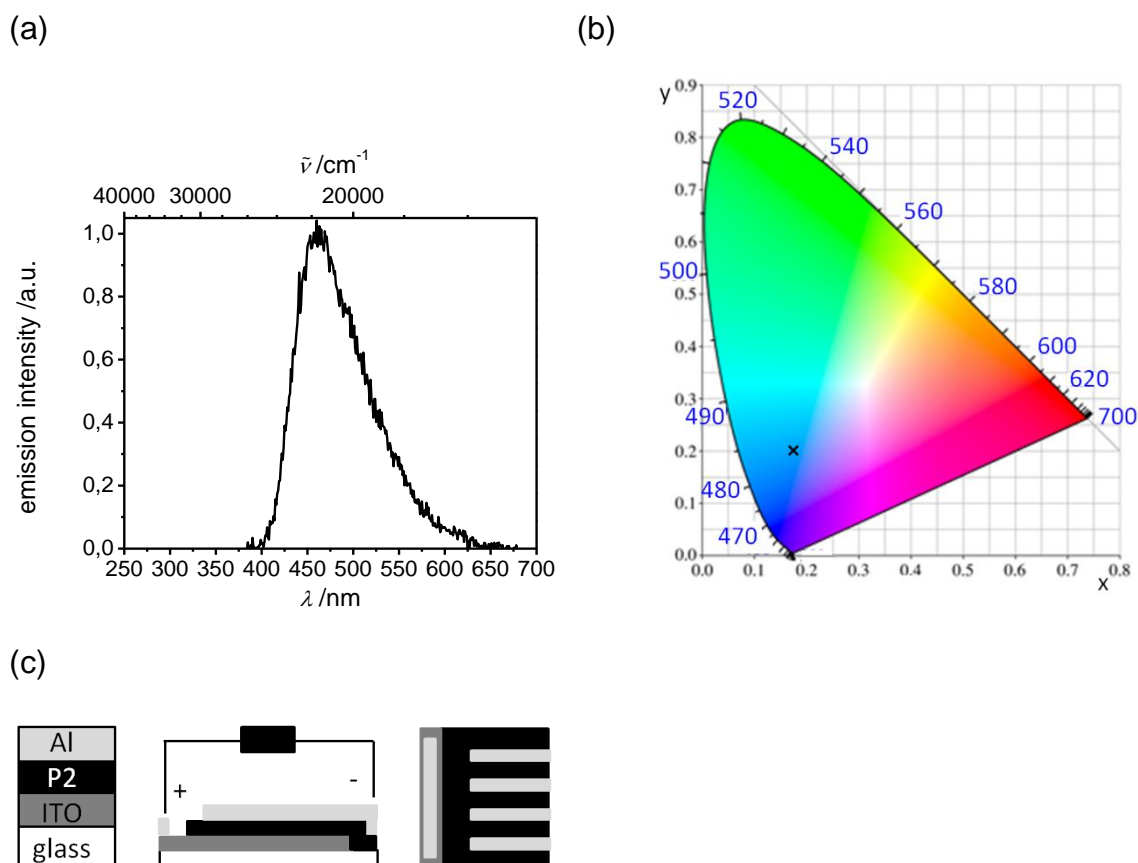


Figure 16. (a) Electroluminescence spectrum of the device ITO/**P2**/Al; (b) CIE 1931 (x,y) chromaticity diagram¹⁹⁹; wavelengths in nm are marked in blue; (c) lateral and top view of a single layer OLED of **P2**.

2.6 Conclusions

2,7- and 3,6-linked polycarbazoles with pendant triarylborane (**P1**, **P2**) and triphenylmethane (**P3**) substituents have been synthesized by Yamamoto coupling reaction. It was found that the triarylborane substituent in 2,7-linked polymer **P1** does not have any influence on absorption and emission properties evident by comparison with the reference polymer **P3** and with other known 2,7-linked polyalkylcarbazoles. This is possibly due to effective conjugation along the polymer backbone, which results in a polymer state being lower in energy than an intramolecular CT state involving the boron and nitrogen centers. However, the triarylborane substituent in 3,6-linked polymer **P2** has a pronounced influence on the optical properties of **P2**: a low energy CT-absorption band and an emission maximum also lower in energy than those of known 3,6-linked polyalkylcarbazoles are observed. This is, because conjugation along the polymer backbone is interrupted by the nitrogen atoms making the intramolecular CT state the lowest electronically excited state. Measurements in different solvents revealed negative solvatochromic absorption and positive solvatochromic emission. Fluorescence quantum efficiencies of **P2** are fairly high even in solid state which we attribute to the existence of the low lying CT state. Violation of Siebrand's rule leads in effect to a high fluorescence quantum yield for **P2** irrespective of the solvent polarity. Altogether, absorption and emission properties of **P2** are similar to the corresponding monomer, whereas absorption and emission properties of **P1** and **P3** are similar to 2,7-linked polyalkylcarbazoles.

CV measurements showed that end groups of 2,7-linked polymers **P1** and **P3** couple in 3,6 position upon oxidation resulting in two new reversible oxidations of the crosslinked polymer similar to the two reversible oxidation peaks of 3,6-linked polymer **P2**. Before (and after) crosslinking of **P1** and for **P2** one reversible reduction process at $E_{1/2} = -2.53$, (-2.51 V) (**P1**) and $E_{1/2} = -2.49$ V (**P2**) located at the borane moiety is observed, whereas for crosslinked **P3** one irreversible reduction at $E_{pc} = -2.38$ V is observed, which might arise from an adduct being formed during oxidation. Crosslinking raises the HOMO levels of **P1** and **P3** up to the range where the HOMO energies of 3,6-linked polycarbazoles lie, whereas the LUMO energy of **P1** is not much affected by crosslinking.

P2 seems to be a promising candidate for the application in OLEDs: It has an average degree of polymerization of twelve monomer units, it is soluble in common organic solvents, it consists of hole and electron transporting moieties and it is a blue emitter with CIE coordinates of (0.17, 0.21) and with a reasonable high quantum yield in solution and in solid state. Applications of **P1** and **P3** in organic electronic devices were not possible due to their low solubilities in common organic solvents.

3 Low Band Gap Donor-Acceptor Conjugated Polymer

3.1 Introduction and Aim of the Project

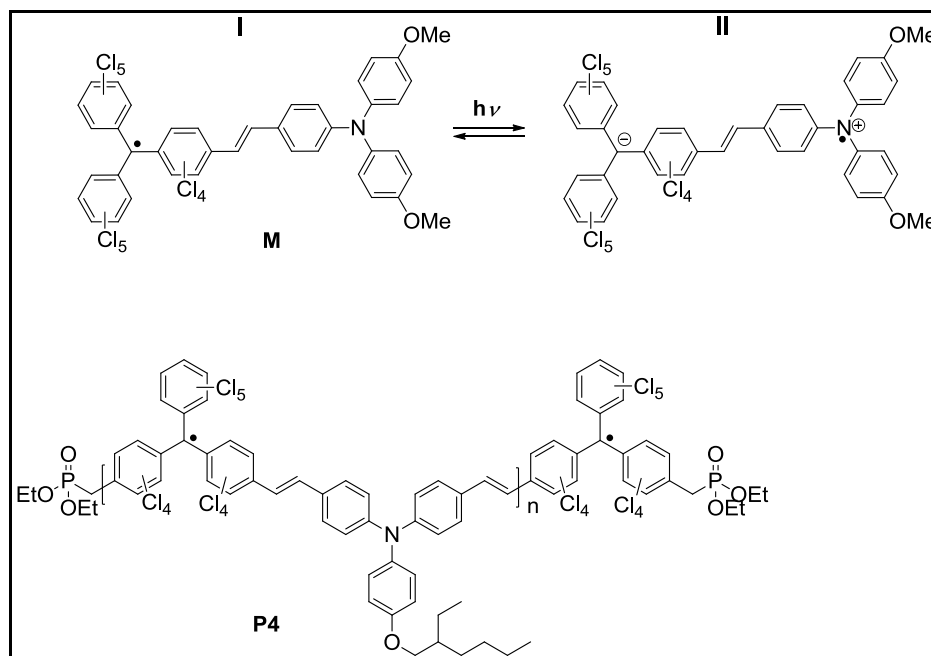
The ultimate goal in preparing low band gap polymers is to achieve intrinsic metal-like conductivity.²⁰⁰ Infinite delocalization along a polymer backbone would result in a zero band gap. This is however hampered by the Peierls instability, i.e. the relaxation of the delocalized electronic structure into a structure of alternating bond lengths.¹³³ One approach to reduce the band gap is to construct D-A conjugated polymers, in which the resonance structure $D^+=A^-$ contributes to the electronic delocalization by planarization of the polymer backbone (see also chapter 1.3).²⁰⁰ D-A conjugated polysquaraines and polycroconaines prepared by Havinga et al.¹³⁴ with optical band gaps of 0.8 and 0.5 eV showed conductivities of 10^{-7} and 10^{-5} S cm^{-1} (four-point measurement), respectively, which are however far from metallic conductivity. An even smaller optical band gap of 0.36 eV was obtained for an electropolymerized thiophene polymer,²⁰¹ which however is unsuitable for solution processing. Low band gap polymers are not only expected to be intrinsic conductors but they are also supposed to show balanced ambipolar charge transport due to low injection barriers into HOMO and LUMO levels. For example, a soluble spray-processable D-A polymer with a band gap as small as 0.54 eV exhibited hole and electron mobilities of 1×10^{-3} and 6×10^{-4} in OFET devices.⁶ However, as explained in chapter 1.1 there are several more important parameters apart from injection barriers that influence charge transport in OFETs. Another feature of low band gap polymers is that they usually absorb over a broad range of the solar spectrum up to the NIR. This has also been exploited in BHJ solar cells: A PCE of up to 2.7 %²⁰² was achieved for a polymer with a band gap of 1.13 eV. Since most of the efficient electronic devices incorporate polymers with band gaps above 1 eV and since no extraordinary electrical properties were found for very small band gap polymers the search for “zero” band gap polymers has ceased.

A low band gap *monomer* with attractive optical and redox properties, prepared and investigated by Heckmann²⁰³⁻²⁰⁵, is the D-A molecule **M** (Chart 8): Upon absorption of light an electron is transferred from the triarylamine donor to the perchlorotriphenylmethyl (PCTM) radical acceptor, apparent from the intervalence

charge transfer (IV-CT) absorption band found in the NIR. In case of **M** the energy maximum of the IV-CT band $\tilde{\nu}_{\max}$ is determined by the sum of ΔG^{00} and the Marcus reorganization energy λ : ΔG^{00} is the difference of the free energy between the two diabatic (= formally noninteracting) redox states I and II (Chart 8) and λ comprises the energy needed for the reorientation of the solvent molecules after the electron transfer (ET) event and the energy needed for the structural relaxation of the molecule during ET. In addition to the absorption over a broad range, which extends up to 1.1 μm , **M** also shows favourable redox potentials (+0.24 and -0.67 V vs. Fc/Fc^+) which makes it promising for the application in OFET devices and as acceptor material in solar cell devices.

Low molecular weight triarylamines are well-known hole injection and hole transport materials which have been widely used in OLEDs.⁹⁹⁻¹⁰³ PCTM radicals on the other hand are thermally and chemically very stable organic radicals that have been incorporated in polymers,²⁰⁶ used as the spin bearing unit in organic magnets,²⁰⁷⁻²⁰⁹ and attached to surfaces etc..²¹⁰⁻²¹³

Chart 8



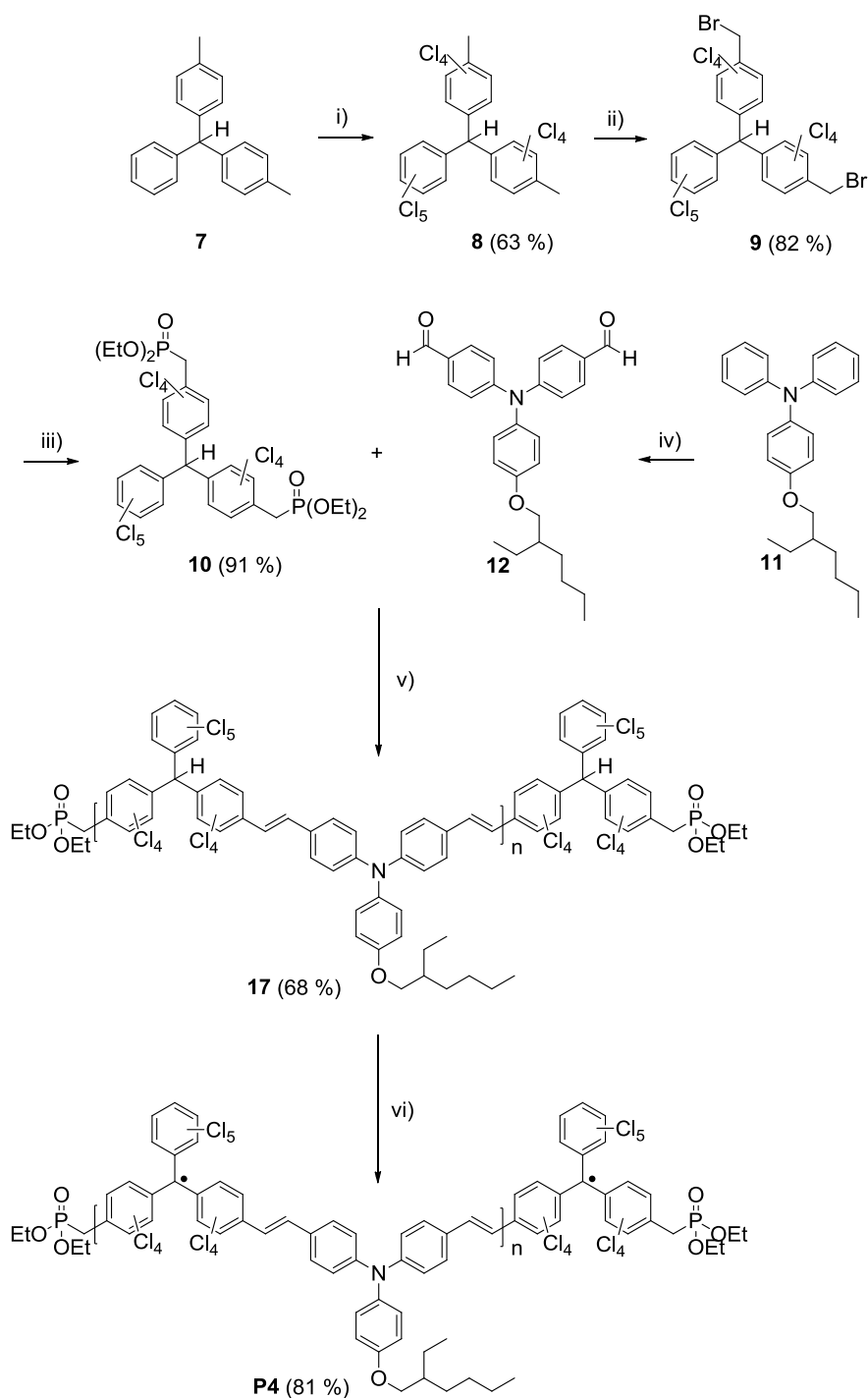
Molecules like **M** comprising two or more redox centers with different oxidation states, which are connected by a conjugated or nonconjugated bridge, are so-called mixed-valence (MV) compounds. This class of compounds has been intensively

studied during the past.²¹⁴⁻²²⁷ However, MV compounds have rarely been used as optoelectronic materials.²²⁸ Since the unsatisfactory film-forming properties of **M** hampered the application in electronic devices, the aim of this project was to synthesize the low band gap polyradical **P4** and investigate its optical and electrochemical properties as well as its applicability in OFET and BHJ solar cell devices. Furthermore, ET issues should be investigated by transient absorption spectroscopy in comparison to the monomeric MV compound.

3.2 Synthesis

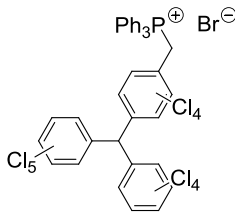
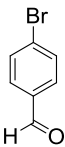
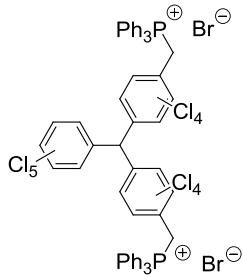
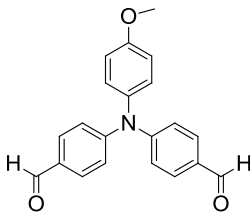
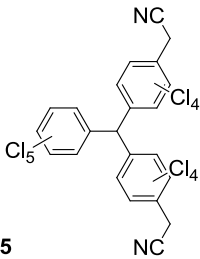
The monomer **M** was synthesized according to the literature procedure²⁰⁵ except for the radicalization step: Instead of KO^tBu in DMSO an aqueous *n*-Bu₄NOH solution in THF was used for the deprotonation of the α -H atom of the PCTM moiety, which gives the radical **M** free of α -H precursor impurities. The synthetic approach to **P4** is outlined in Scheme 2. Compound **10** is prepared in analogy to a procedure established by Veciana et al.²²⁶. A Horner-Emmons reaction of **10** and dialdehyde **12**^{92,229} in THF with KO^tBu as base yields polymer **17**. After the reaction has completed the reaction mixture was acidified in order to protonate PCTM anions, that may have formed, since the α -H compounds are rather strong acids.²³⁰ In the ¹H and ¹³C NMR spectra of polymer **17** no signals corresponding to the aldehyde group were visible whereas signals corresponding to the $-\text{CH}_2\text{P}(\text{O})(\text{OEt})_2$ group could be identified. The all-*E* configuration of the ethylene bridges was confirmed by IR, ¹H and ¹³C NMR spectroscopy: In the IR spectrum the band at 967 cm⁻¹ indicates *E*-configuration²³¹ and in the ¹H NMR spectrum no signals at around 6.6 ppm corresponding to the *Z*-configuration of the vinylene bridges were visible.²²⁶ Furthermore, in the ¹³C NMR spectra no additional carbon signals, but exactly six carbon signals corresponding to the 16 tertiary carbon atoms in the repeating unit (2 \times 4C and 2 \times 2C for the triarylamine moiety, and 2 \times 2C for the ethylene bridges) were found. This contrasts the findings of Veciana et al.²²⁶ who obtained a mixture of *Z*- and *E*-isomers by applying the Horner-Emmons reaction to the monophosphonate analogue of compound **10**. In case of polymer **17** the formation of the *Z*-isomer might well be suppressed due to steric hindrance.

Scheme 2. Synthesis of P4.



i) S_2Cl_2 , $AlCl_3$, SO_2Cl_2 , reflux, 8 h; ii) *N*-bromosuccinimide, AIBN, CCl_4 , reflux, 60 h; iii) $P(OEt)_3$, reflux, 2 h; iv) $POCl_3$, DMF, 100 °C, 15 h; v) 1. *n*-Bu₄NOH, THF, r. t., 1 h; 2. *p*-chloranil, r. t., 21 h

Table 8. Ethylene bridge formation.

triarylmethane	aldehyde	conditions	yield
 <p>13</p>		<p>CHCl₃, NaOH (50 %)</p>	<p><i>E</i>-stilbene (60 %)</p>
 <p>14</p>	 <p>16</p>	<p>CHCl₃, NaOH (50 %)</p>	<p>—</p>
 <p>15</p>	<p>16</p>	<p>THF, ^tBuOH, KO^tBu</p>	<p>—</p>
<p>10</p>	<p>16</p>	<p>THF, KO^tBu</p>	<p>insoluble product</p>
<p>10</p>	<p>12</p>	<p>THF, KO^tBu</p>	<p>17 (68%)</p>

Previously to the successful preparation of polymer **17**, it was attempted to form the ethylene bridge by reaction of bis(phosphonium) salt **14** and triarylamine-bis(aldehyde) **16**^{229,232} in refluxing chloroform/aqueous sodium hydroxide (50 %). The reaction failed in contrast to the successful ethylene bridge formation of **M** by the reaction of monophosphonium salt **13** and *p*-bromobenzaldehyde under the same experimental conditions (Table 8).²⁰³ This is possibly caused by the low solubility of the expected polymer in this solvent mixture and the lower reactivity of the donor-substituted aldehyde functionality in **16** as compared to the electron-deficient *p*-

bromobenzaldehyde. A Knoevenagel reaction of bis(cyanomethyl) derivative **15** and triarylamine **16** as performed in the synthesis of carbazolylenevinylene-based copolymers by Leclerc et. al.²³³, neither gave product, whereas a Horner-Emmons reaction of compounds **10** and **16** resulted in an insoluble product (Table 8). Replacement of the methoxy group of triarylamine **16** by the solubilizing 2-ethylhexyloxy substituent and using a Horner-Emmons reaction finally resulted in the soluble polymer **17** as outlined above.

Radicalization of **17** to give **P4** was achieved by deprotonation of the α -H atoms of the PCTM moieties with an aqueous *n*-Bu₄NOH solution in THF and subsequent oxidation with *p*-chloranil (Scheme 2) according to the procedure by Veciana et al.²²⁶. Polymer **P4** was isolated and purified by repeated dropwise addition of a concentrated THF solution of **P4** to an acetone/HCl mixture to give a dark brown precipitate that was further washed with acetone in a Soxhlet apparatus in order to remove excess *p*-chloranil and low molecular weight fractions. The completeness of the radicalization was confirmed by differential pulse voltammetry (DPV): Integration of the oxidation and reduction signal of **P4** measured in dichloromethane/tetrabutylammonium hexafluorophosphate (TBAPF₆) resulted in equal values as expected for equal amounts of donor and radical moieties thus proving **P4** to be fully radicalized. Again a band at 964 cm⁻¹ was visible in the IR-spectrum indicating *E*-configuration of the vinylene bridges.

Polymer **P4** is soluble in common organic solvents such as THF, chloroform, dichloromethane, toluene and chlorobenzene. Solid **P4** is stable for several months and even in solution (toluene 0.3 mg/mL) it can be stored for at least two months under ambient conditions. No phase transition was observed with differential scanning calorimetry (DSC) measurements. Instead **P4** starts to decompose at about 250 °C. GPC measurements performed in THF vs. polystyrene standards gave an average molecular weight $\bar{M}_w = 19300$ Da ($\bar{M}_n = 11200$ Da, PDI = 1.72) corresponding to $\bar{X}_w = 17$ and $\bar{X}_n = 10$ for **P4**, whereas for the nonradicalized precursor polymer **17** an average molecular weight $\bar{M}_w = 17100$ Da ($\bar{M}_n = 9600$ Da, PDI = 1.77) corresponding to $\bar{X}_w = 15$ and $\bar{X}_n = 9$ was found under the same experimental conditions. Endgroup analysis of the ¹H NMR spectrum of **17** revealed

polymer chains with $\bar{X}_n = 12$ terminated by diethylphosphonate groups on both ends as depicted in Scheme 2. The latter value seems to be more reliable because with GPC only rough estimates can be obtained. The small differences between the molecular weight data of **P4** and of **17** show that the radicalization and work-up did not influence the chain length distribution to a significant extent.

3.3 Absorption Spectroscopy

Absorption spectra of **P1** measured in dichloromethane and toluene are displayed in Figure 17a together with the absorption spectra of the reference molecule **M**. Energies of absorption bands $\tilde{\nu}$ and corresponding molar extinction coefficients ε are listed in Table 9.

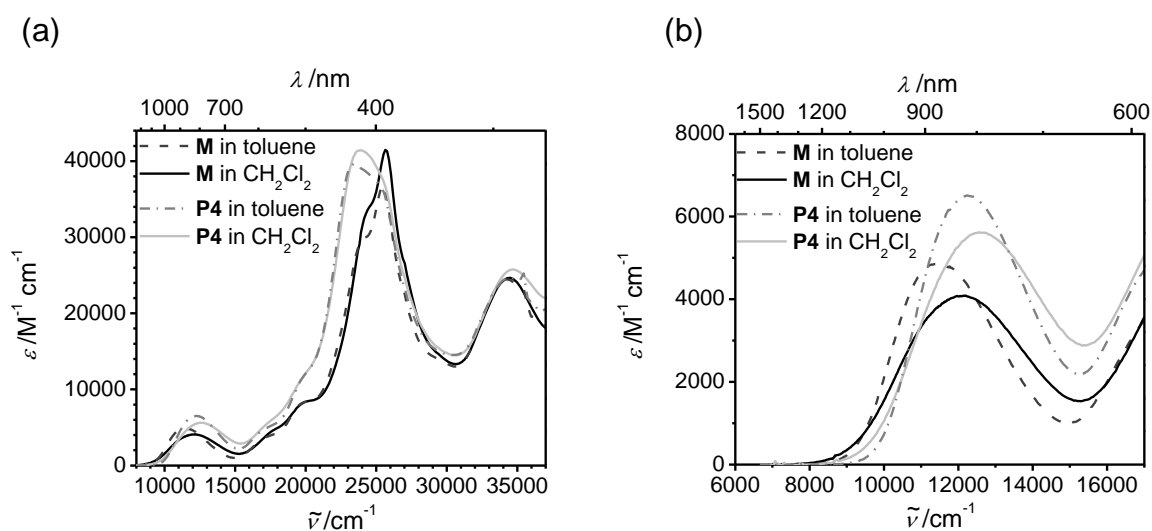


Figure 17. (a) Absorption spectra of **M** and **P4** in CH_2Cl_2 and toluene; (b) enhanced IV-CT bands of Figure 17a.

Absorption bands of **P4** resemble those of **M** and can be assigned as follows: Bands around 34500 cm^{-1} correspond to localized triarylamine transitions²³⁴ and bands between 25600 and 17200 cm^{-1} belong to the PCTM radical moiety²³⁵. The band of particular interest is the IV-CT band located around 12000 cm^{-1} .²⁰⁵ This transition is somewhat higher in energy for **P4** (12600 cm^{-1} , dichloromethane) than for **M** (12100 cm^{-1} , dichloromethane) which can be explained by the weaker donor

strength of the triarylamine moiety in **P4** compared to **M**. This interpretation is also supported by the differing oxidation potentials of **P4** and **M** (see chapter 3.4). A hypsochromic shift of the IV-CT band with decreasing donor strength of the triarylamine moiety was also found for a series of analogous compounds with biphenyl spacer.²³⁶ The shift and broadening of the IV-CT bands in going from the nonpolar solvent (toluene) to the polar solvent (dichloromethane) is similar for **M** and **P4** (Figure 17b) and has been explained previously.²⁰⁴⁻²⁰⁵ The full-width at half-maximum values are $\tilde{\nu}_{1/2} = 3900 \text{ cm}^{-1}$ and 3300 cm^{-1} for **M** and 3800 cm^{-1} and 3400 cm^{-1} for **P4** in dichloromethane and toluene, respectively. Similar to the smaller shift between $\tilde{\nu}_{\text{max,IV-CT}}(\text{dichloromethane})$ and $\tilde{\nu}_{\text{max,IV-CT}}(\text{toluene})$ for **P4** (400 cm^{-1}) compared to **M** (700 cm^{-1}) the difference in $\tilde{\nu}_{1/2}$ in these two solvents is also smaller for **P4** than for **M**. However, the fact that $\tilde{\nu}_{1/2}$ values of **M** and **P4** are still very similar to each other in the respective solvents indicates that the IV-CT transition in **P4** is confined to one repeating unit.

Table 9. Absorption band energies of M and P4 in CH₂Cl₂ and toluene solution and of a thin film of P4.

$\tilde{\nu} / \text{cm}^{-1} (\epsilon / \text{M}^{-1} \text{cm}^{-1})$				
M	P4	M	P4	P4
CH ₂ Cl ₂ ^a	CH ₂ Cl ₂	toluene	toluene	thin film
34500 (24700)	34700 (25800)	34200 (24500)	34500 (24700)	34200
25600 (41500)	--	25500 (36800)	25300 (36900)	25100
24500 (34000)	23900 (41400)	24200 (29900)	23400 (39600)	23300
20200 (8500)	19600 (1100)	20000 (8400)	20200 (12400)	20200
17900 (4900)	17200 (5500)	17400 (3900)	17400 (5100)	17200
12100 (4100)	12600 (5600)	11400 (4900)	12200 (6500)	11800

^a values differ from previously published data²⁰⁴⁻²⁰⁵ since those were measured on a batch of **M** which still contained a small fraction of nonradicalized PCTM moieties and thus a lower intensity for all bands was observed

In contrast to the close resemblance of the IV-CT bands of **M** and **P4**, the absorption maximum of **P4** at ca. $23000\text{-}25000 \text{ cm}^{-1}$ differs significantly from that of

M in that it is broadened and shifted to the red by 1700 cm^{-1} in dichloromethane. The seeming contradiction can be explained by exciton splitting, which stems from the dipole-dipole interaction of transition moments localized on adjacent molecular units (Figure 18). With increasing band intensity the exciton coupling energy \mathcal{E} rises, because it is proportional to the square of the transition moment μ_{ab} of the individual monomer: $\mathcal{E} \sim \mu_{ab}^2$.²³⁷ Since the transitions at $23000\text{--}25000\text{ cm}^{-1}$ have much higher intensities than the IV-CT band one can qualitatively expect a much higher exciton coupling of the former transitions and thus a significant broadening of the high energy bands.

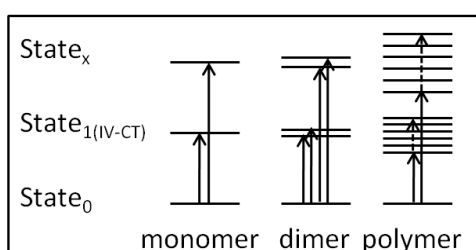


Figure 18. Band broadening due to exciton coupling interactions between adjacent molecular units in polymers.

The solid state absorption spectrum of **P4** spin coated from toluene onto a quartz plate reveals the same spectral shape as the toluene solution spectrum (Figure 19) except for a small red shift commonly observed for solid state spectra due to interchain interactions^{13,127,144,147} which are, however, weak in films of **P4**.

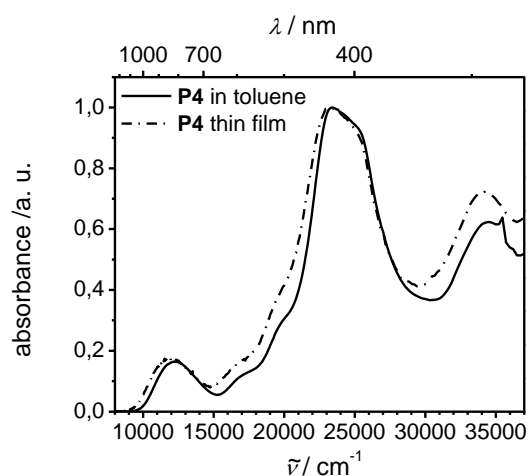


Figure 19. Normalized absorption spectra of **P4** in toluene and of a thin film spin coated from a toluene solution onto a quartz plate.

The same solid state spectrum is also obtained, when **P4** is spin coated from chlorobenzene under the same conditions. Annealing of as prepared films in air at 110 °C for 30 minutes did not alter the spectrum significantly. This points to a pronounced air stability and the amorphous character of the film, since a higher ordering which can be induced by annealing would shift the absorption edge farther to the red due to more effective interchain interactions.^{79,238-239}

The optical band gaps E_g^{opt} as determined from the onset absorptions (Table 10) are slightly smaller for **M** (1.13 eV in dichloromethane, 1.15 eV in toluene) than for **P4** (1.19 eV in dichloromethane, 1.23 eV in toluene, 1.17 eV in solid state) consistent with the higher energy of the IV-CT transition of **P4**.

Summarizing the optical properties **P4** is a low band gap polymer, that forms air and temperature stable, amorphous films and shows IV-CT characteristics similar to **M**.

3.4 Cyclic Voltammetry

Half wave potentials $E_{1/2}$ of oxidation and reduction processes were determined by cyclic voltammetry in dichloromethane/TBAPF₆ with potentials being referenced against Fc/Fc⁺. The oxidation of the amine moiety and the reduction of the PCTM radical of **P4** occur at $E_{1/2}^{\text{ox}} = +340$ mV and at $E_{1/2}^{\text{red}} = -690$ mV, respectively (Figure 20, Table 10). Both signals are chemically fully reversible as confirmed by multi-sweep experiments in a thin layer whereupon the signals did not alter significantly. Under semi-infinite conditions the peak separation ΔE_p decreases during subsequent scans from 82 mV (oxidation) and 72 mV (reduction) at the beginning to 33 and 32 mV, respectively, after 32 scans. This observation indicates adsorption of **P4** on the surface of the working electrode with increasing number of voltammetric cycles, which implies a transition from semi-infinite conditions (theoretical value for reversible one-electron processes at 25 °C: $\Delta E_p = 58$ mV²⁴⁰) to thin-layer conditions (theoretical value for reversible processes: $\Delta E_p = 0$ mV²⁴¹). Note that in practice ΔE_p values may be substantially larger than the theoretical values due to voltage drops of uncompensated solution resistance. The full-width at half-maximum of the signals

determined from DPV measurements are about 100 mV for both **P4** and **M**, which shows that the redox centers behave as independent units with negligible inhomogeneous distribution of redox potentials in the polymer **P4**. In comparison to the oxidation potential of **M** ($E_{1/2}^{\text{ox}} = +240 \text{ mV}$)²⁰⁵ the oxidation of **P4** occurs at considerably higher potential, whereas the reduction potentials are almost identical ($E_{1/2}^{\text{red}}(\mathbf{M}) = -670 \text{ mV}$)²⁰⁵. These findings agree well with previous results: The oxidation potentials of triarylamine molecules strongly depend on the donor/acceptor strength of the substituents,²³⁴ whereas the reduction potential of the PCTM radical moiety is nearly independent of the donor strength of the amine moiety if the two centers (C[•] and N) are connected by the same spacer.²⁰⁴ Thus the presence of two PCTM radical acceptors next to the amine moiety shifts the oxidation of **P4** to higher potentials as compared to **M**.

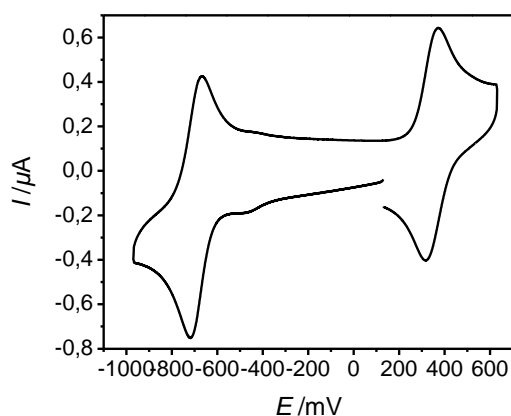


Figure 20. CV of **P4** in $\text{CH}_2\text{Cl}_2/\text{TBAPF}_6$, $\nu = 100 \text{ mV s}^{-1}$.

The important values for the application of **P4** in electronic devices are the HOMO and LUMO values which were determined from the half-wave potentials of the oxidation and the reduction process, respectively (see experimental section). Even though usually onset potentials are taken for the estimation of the electrochemical band gaps of polymers based on the work of Brédas in 1983,²⁴² here the half-wave potentials are used for the following reason: The half-wave potential is the thermodynamic quantity that is measured (relative to potentials of reference electrodes or an internal redox couple such as Fc/Fc^+) as the potential needed to bring the Fermi level of the electrode to the free energy of a 1:1 mixture of reduced

and oxidized species (= formal potential). This free energy can be set as the HOMO (or LUMO) energy provided differences of solvation and reorganizational effects of reduced and oxidized species are negligible or cancel out. These constrictions are important to mention since the HOMO/LUMO energies refer to vertical ionization and electron affinity values while redox potentials refer to adiabatic ionization and electron affinities.²⁴³ In cases where the determination of a half-wave potential is impossible because of strongly overlapping signals as e.g. in polymers, the onset potential may be used instead.²⁴² The HOMO and LUMO energies of **P4** determined from the half-wave potentials are -5.50 and -4.47 eV, respectively, resulting in an electrochemical band gap of $E_g = 1.03$ eV (Table 10). These values are perfectly suitable for the application of **P4** in an ambipolar OFET device with Au contacts, since the Au work function (4.7-5.2 eV)^{8,244} is close to these values and thus charge carrier injection barriers for both holes and electrons should be small. Moreover the low lying HOMO and LUMO make **P4** stable against redox reactions with wet air.⁶⁴

Table 10. Oxidation and reduction potentials, HOMO and LUMO values and electrochemical (E_g) and optical (E_g^{opt} , E_g^{BJ}) band gaps of **M and **P4**.**

	$E_{1/2}^{\text{ox}}$	$E_{1/2}^{\text{red}}$	HOMO	LUMO	E_g	E_g^{opt}	E_g^{BJ}
	/mV	/mV	/eV	/eV	/eV ^b	/eV ^c	/eV ^d
M							
CH ₂ Cl ₂	+240 ^{a, 205}	-670 ^{a, 205}	-5.40	-4.49	0.91	1.13	1.00
toluene						1.15	1.16
P4							
CH ₂ Cl ₂	+340 ^a	-690 ^a	-5.50	-4.47	1.03	1.19	1.24
toluene						1.23	1.24

^a half-wave potentials vs. Fc/Fc⁺; **P4**: CH₂Cl₂/TBAPF₆, $v = 100$ mV s⁻¹; **M**: CH₂Cl₂/TBAPF₆ (0.1 M), $v = 250$ mV s⁻¹; ^b $E_g = \text{LUMO} - \text{HOMO}$; ^c E_g^{opt} is determined from the onset absorptions; ^d $E_g^{\text{BJ}} = \Delta G^{00}$ (see chapter 3.1) is determined by a Bixon-Jortner band shape analysis of the IV-CT band, see ref. [204]

For comparison HOMO and LUMO values of **M** were determined from the CV of ref. [205] in the same way as it was done for **P4** giving -5.40 eV (HOMO) and -4.49 eV (LUMO) (Table 10). For both **M** and **P4** the optical band gap energies E_g^{opt} as

determined from the absorption onsets²⁴⁵ of the solution spectra (**P4**: 1.19 eV in CH₂Cl₂, **M**: 1.13 eV in CH₂Cl₂) are larger than the electrochemical E_g values (Table 10). The deviation is only slightly smaller if the absorption onsets are determined from the spectra of neutral species recorded during spectroelectrochemical measurements (see chapter 3.5) under experimental conditions (supporting electrolyte solution) similar to those of the CV measurements, which gave $E_g^{\text{opt}} = 1.17$ eV for **P4** and $E_g^{\text{opt}} = 1.13$ eV for **M**. In solid state (thin film on quartz plate) $E_g^{\text{opt}} = 1.17$ eV for **P4**. In general, the spectra in pure CH₂Cl₂ only marginally deviate from those with electrolyte. These findings suggest that the deviation between E_g^{opt} and E_g is not caused by medium effects. In theory, one would expect that E_g^{opt} is smaller than E_g because of the exciton binding energy. In **M** and **P4** this energy might be small because of the explicit CT character of the lowest-energy transition which already requires a spatial separation of hole and electron. In a previous work the band gap of **M** in CH₂Cl₂ was evaluated by a Bixon-Jortner analysis, in which a Golden Rule type equation is fitted to the IV-CT band in order to obtain $\Delta G^{00} = E_g^{\text{BJ}}$.²⁰⁴ For **M** in toluene and for **P4** an analogous analysis was performed in this work which rests on the assumption that the broadening of the IV-CT band of the polymer due to exciton coupling is negligible (see chapter 3.3). In fact, excellent agreement between E_g^{opt} and E_g^{BJ} is found for **M** in toluene and for **P4** in both solvents (see Table 10). This analysis excludes reorganizational effects to be the source of the deviations between optically and electrochemically determined band gaps. The major source for the discrepancies might still be ion pairing effects in the apolar CH₂Cl₂ solution which lowers the ionization energy and electron affinity in the electrochemical experiments. The overall good agreement of E_g^{opt} and E_g^{BJ} shows that the exciton binding energy is small in **P4**. However, given the systematical inaccuracy of the methods for determining the band gap we cannot rule out exciton binding energies in the order of 100-200 mV.

3.5 Spectroelectrochemistry

By spectroelectrochemistry the absorption spectra of oxidized triarylamine donor D^{+} and reduced PCTM acceptor A^- can be obtained independently. Since the IV-CT

band is caused by an ET from the triarylamine to the PCTM radical moiety (see chapter 3.1), the sum of the spectra of $D^{+\bullet}$ and $A^{\bullet-}$ should approximately give the transient absorption profile of the IV-CT state (lowest excited state), with exception of those contributions that are due to interactions between $D^{+\bullet}$ and $A^{\bullet-}$, i.e. the IV-CT band itself. Thus, the spectra obtained by spectroelectrochemistry may help for the interpretation of transient absorption spectra (see chapter 3.6). In Figure 21 the absorption spectra of reduced and oxidized **M** and **P4** are displayed together with the absorption spectra of the neutral species.

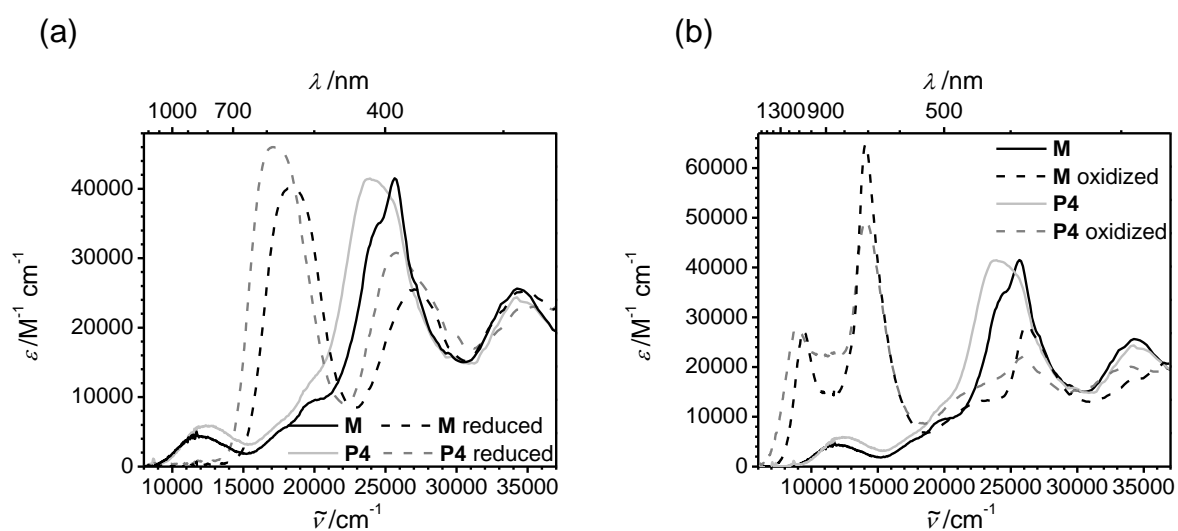


Figure 21. Absorption spectra of **M** (0.2 mM) and **P4** (0.2 mM) in $\text{CH}_2\text{Cl}_2/\text{TBAPF}_6$ in their fully reduced (a) and fully oxidized (b) states together with the spectra of the neutral species.

For both, reduced **M** and reduced **P4**, an intense broad band (**M**: 18400 cm^{-1} , $\epsilon = 40100\text{ M}^{-1}\text{ cm}^{-1}$ and **P4**: 17100 cm^{-1} , $\epsilon = 46000\text{ M}^{-1}\text{ cm}^{-1}$), typical of PCTM anions^{204,226,246} is observed (Figure 21a). The radical band of the neutral species at around 25000 cm^{-1} decreased and is blue shifted (**M**: 27000 cm^{-1} , $\epsilon = 25500\text{ M}^{-1}\text{ cm}^{-1}$; **P4**: 25800 cm^{-1} , $\epsilon = 30800\text{ M}^{-1}\text{ cm}^{-1}$) in the spectra of the reduced species. In addition, the IV-CT band is absent, since there is no ET possible upon excitation of the PCTM anion. The higher intensity of the bands of reduced **P4** as compared to those of **M** results from the additional PCTM radical moiety attached to each polymer chain end (Chart 8).

In the spectra of oxidized **M** and **P4** (Figure 21b) a sharp and intense band at 14100 cm^{-1} (**M**: $\epsilon = 64700\text{ M}^{-1}\text{ cm}^{-1}$; **P4**: $\epsilon = 49400\text{ M}^{-1}\text{ cm}^{-1}$) belonging to the

triarylamine radical cation^{204,234} and a new IV-CT band at 9500 cm⁻¹ ($\epsilon = 27200 \text{ M}^{-1} \text{ cm}^{-1}$) for **M** and at 8900 cm⁻¹ ($\epsilon = 27500 \text{ M}^{-1} \text{ cm}^{-1}$) for **P4** is visible. The latter arises from an ET from the PCTM radical to the triarylamine radical cation center.²⁰⁴ Thus, donor and acceptor functionalities of the moieties exchange in the oxidized species and the formerly weaker donor of neutral **P4** is now a stronger acceptor compared to the corresponding moiety of **M**, which causes the red shift of the IV-CT band of oxidized **P4** relative to the IV-CT band of oxidized **M**. Similar to the spectra of reduced **M** and **P4** the radical band of the neutral spectrum at around 25000 cm⁻¹ decreased and is blue shifted (**M**: 26300 cm⁻¹, $\epsilon = 28300 \text{ M}^{-1} \text{ cm}^{-1}$, shoulder at 22900 cm⁻¹; **P4**: 25900 cm⁻¹, $\epsilon = 22100 \text{ M}^{-1} \text{ cm}^{-1}$, shoulder at 22100 cm⁻¹) in the spectra of the oxidized species.

3.6 Transient Absorption Spectroscopy

In order to investigate the dynamics of photoinduced ET phenomena fs-pump-probe transient absorption spectroscopy was performed by Martin Kullmann and Stefan Rützel in the group of Prof. T. Brixner. Polymer **P4** and monomer **M** dissolved in toluene and dichloromethane were excited at 525 nm and their transient spectra were recorded with femtosecond time resolution. In toluene the transient spectra of **P4** show two bands at 18300 and 15200 cm⁻¹ (Figure 22a), which correspond to characteristic transitions of the anion (**P4**⁻) and radical cation (**P4**^{•+}), respectively, as was proved by comparison with spectroelectrochemistry (Figure 22c) although the bands in those experiments appear at lower energy (17100 and 14100 cm⁻¹). The transient band at 15200 cm⁻¹ shifts to 15600 cm⁻¹ at longer delay times. A ground state bleaching is observed at 23100 cm⁻¹. In dichloromethane initially two bands at 18100 and 15400 cm⁻¹ are observed similar to those in toluene. At longer delay times the bands in dichloromethane shift to 18500 cm⁻¹ and 15900 cm⁻¹ (Figure 22b). The reason for the band shifts in both solvents is presently unclear. In dichloromethane the spectral shape at longer times resembles that of the sum of oxidized (**P4**^{•+}) and reduced (**P4**⁻) polymer minus three times the ground state absorption of neutral **P4** obtained from spectroelectrochemistry (Figure 22c). The enlarged intensity of the ground state bleaching cannot be explained yet.

Almost no spectral shift with time is found for the monomer **M** in toluene (Figure 22d). Transient bands are observed at 20000 and 14000 cm^{-1} . In dichloromethane these bands are located at 19600 and 14100 cm^{-1} (Figure 22e). Comparison of the absorption profile of the sum of the spectra of \mathbf{M}^- and \mathbf{M}^{*+} minus **M** obtained by spectroelectrochemistry (Figure 22f), which exhibits two bands at 17700 and 14100 cm^{-1} , with the initial transient spectra of **M** in both solvents shows again qualitative similarity. The differences between the transient spectra and the sum of the spectroelectrochemistry spectra are due to interactions between the oxidized radical donor (\mathbf{D}^{*+}) and the reduced acceptor (\mathbf{A}^-) in the excited IV-CT state of monomer **M** and polymer **P4**. In the polymer interactions with neutral D and \mathbf{A}^- moieties add which are responsible for the generally more diffuse transient spectra of **P4**. Nevertheless, the optically induced ET process is unambiguously identified for both **P4** and **M**.

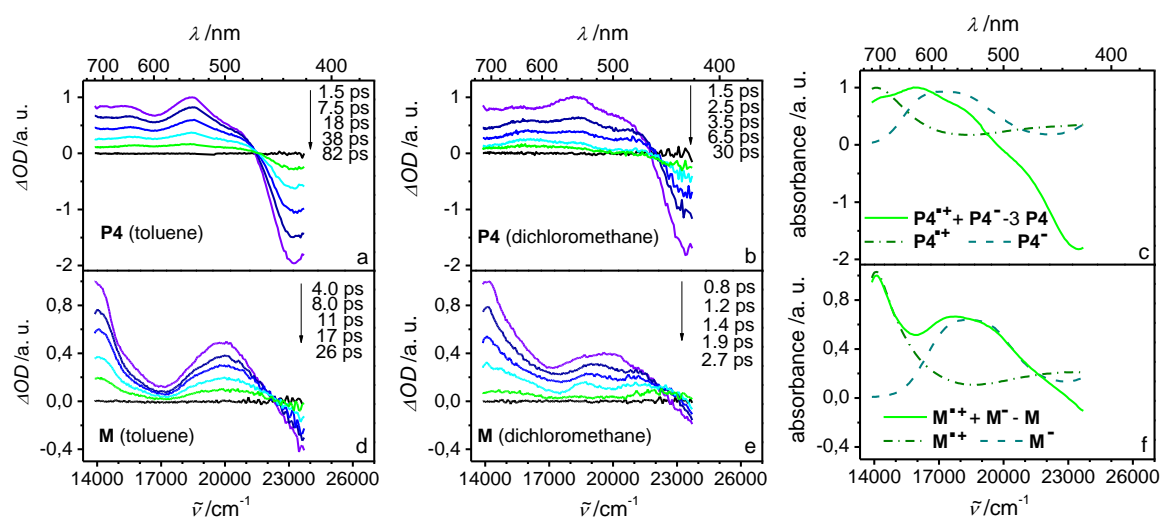


Figure 22. Normalized transient absorption spectra of **P4** in toluene (a) and CH_2Cl_2 (b) and of **M** in toluene (d) and CH_2Cl_2 (e) together with the sum of the spectra of reduced ($\mathbf{P4}^-$, \mathbf{M}^-) and oxidized ($\mathbf{P4}^{*+}$, \mathbf{M}^{*+}) polymer (c) and monomer (f) minus their respective ground state absorption (three times for **P4**) obtained by spectroelectrochemistry in $\text{CH}_2\text{Cl}_2/\text{TBAPF}_6$. All spectra are normalized to the absorption maximum. In the transient spectra the data points of the black curves were recorded before time zero.

By multiexponential fits, which were carried out by Sabine Keiber and Tatjana Quast in the group of Prof. T. Brixner, time constants τ were extracted from the decay curves at different wavelengths in the spectral region of the anion and radical cation band, respectively, which are compatible with the time constants extracted from the ground state bleaching. The time constants somewhat vary with wavelength (Table

11) which reflects the error of the measurements and the model used for their analysis. The decay curves of **P4** and **M** in dichloromethane and toluene are depicted in Figure 23. For **P4** in toluene a biexponential decay with two time constants $\tau_2 \approx 20$ ps and $\tau_3 \approx 70$ ps was found. However, in dichloromethane τ_2 is much smaller (≈ 2.5 ps), whereas the larger time constant τ_3 is hardly affected by the solvent (≈ 70 ps). This indicates that the smaller time constant is associated with the decay of the IV-CT state to the ground state. This decay is faster in more polar solvents because of a Marcus inverted region effect, as was found for a compound very similar to **M**.²⁴⁷ The larger time constant probably corresponds to a structural or electronic transformation within the polymer excited state. Much in contrast, for **M** only one short time constant, $\tau_2 \approx 13$ ps in toluene and $\tau_2 \approx 0.6$ ps in dichloromethane is found as well as a time constant for the rise of the IV-CT state, $\tau_1 \approx 1$ ps in toluene and $\tau_1 \approx 0.5$ ps in dichloromethane. The observed rise time likely refers to the solvent dynamic modulated ET process in good agreement with values obtained recently.²⁴⁷

Table 11. Time constants τ and amplitudes a for P4 and M at selected wavelengths.

	P4 (toluene)				P4 (dichloromethane)			
	540 nm	560 nm	625 nm	665 nm	540 nm	560 nm	625 nm	665 nm
τ_2 /ps	20	21	19	15	2.5	2.6	2.6	2.3
$a_2 / \Delta OD / 10^{-3}$	19	15	13	13	13	11	9.7	10
τ_3 /ps	69	80	78	60	78	79	51	63
$a_3 / \Delta OD / 10^{-3}$	9.9	7.3	8.1	9.6	0.75	0.88	0.93	0.46
	M (toluene)				M (dichloromethane)			
	500 nm	520 nm	700 nm	720 nm	500 nm	520 nm	700 nm	720 nm
τ_1 /ps	1	0.6	1	1	0.4	0.6	0.5	0.4
τ_2 /ps	13	13	13	12	0.7	0.6	0.6	0.6

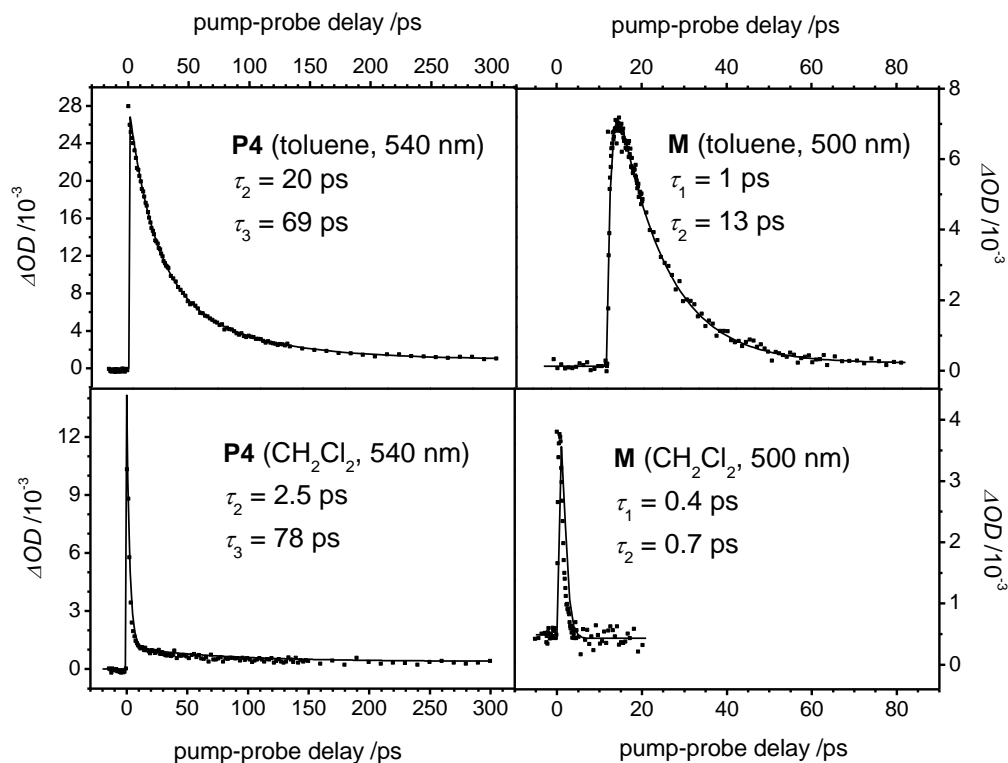


Figure 23. Experimental and fitted decay curves of **P4** and **M** in toluene and dichloromethane at selected wavelengths at a pump wavelength of 525 nm.

A schematic interpretation of the above results is given in Figure 24: It is assumed that no bimolecular or multiphotonic processes play a significant role as no influence of the pump power on the transient spectra dynamics was found. Because of the polyradical character **P4** may adopt different spin multiplicities in the ground and excited state. For simplicity, the discussion is restricted to the interaction of two spin bearing units that is to triplets and singlets. However, it is stressed that states of higher multiplicity might be involved. The spin-spin interaction in the ground state is expected to be quite weak, because PCTM-bridge-PCTM with shorter bridges than the triarylamine in **P4** already shows weak interactions.²⁰⁶ In State₀ (see Figure 24) the unpaired electrons of the PCTM radical moieties (A^{\bullet}) either have α or β spin. Thus in an $[A^{\bullet}\text{-D-A}^{\bullet}]$ moiety, where D denotes the triarylamine moiety, the two spins can either form a triplet state or a singlet state. These states are anticipated to be almost degenerate. Upon excitation of **P4** the IV-CT states - singlet and triplet - are populated from higher lying excited singlet and triplet states. The transient spectra of both triplet and singlet IV-CT states are expected to be very similar. The decay of the

IV-CT states to the respective ground states (triplet and singlet) occurs approximately with τ_2 and no differences in the decay kinetics depending on the different spin states are expected. Thus, the long time constant τ_3 cannot result from this kinetic scheme. For comparison population and decay of the IV-CT state of **M** is also depicted in Figure 24 (left side), which exclusively includes doublet states. However, for **P4** several transformations of the IV-CT state are conceivable as depicted in the upper part of Figure 24: The exciton may migrate by electron or hole transfer via an electron-deficient or electron-rich bridge. In that case ET is identical to an excitation energy transfer (EET) (processes i). Because these newly formed states are practically identical to the primarily formed IV-CT state with identical decay dynamics they cannot account for the third time constant τ_3 . Furthermore, the structure of **P4** could undergo structural relaxation into a quinoid form by combination of two adjacent radicals (process ii), which would result in the planarization of the polymer backbone. This seems to be less likely due to sterically demanding *ortho*-chlorine atoms. Another possible transformation of the IV-CT state could be the hole transfer from D^{+*} to D (or electron transfer from D to D^{+*}) via neutral A^* to give the charge separated species CS (process iii). While the transient spectra of CS should be quite similar to those of the IV-CT state $State_1$ (except for the absence of the D^{+*}/A^* interaction) the decay to the $State_0$ should only be possible via back electron transfer, i.e. via the IV-CT state, thus, making the back electron transfer to the IV-CT state the rate limiting step. This process is assumed to account for the slow decay component τ_3 which represents an averaged time constant for back electron transfer from next nearest neighbors and those even farther apart. While charge separation per se is an endergonic process, a reduced exciton binding energy in $State_{1(IV-CT)}$ of **P4** (see chapter 3.4) may result in an equilibrium of IV-CT state and CS state. In fact, a kinetic analysis²⁴⁸ involving the $^1[State_0]$, $^1[State_{1(IV-CT)}]$ and $^1[CS]$ species of **P4** ($^1[State_{1(IV-CT)}] \rightarrow ^1[State_0]$, $^1[State_{1(IV-CT)}] \leftrightarrow ^1[CS]$), with the relative amplitudes and lifetimes a_2/τ_2 and a_3/τ_3 yields the rate constants k_2 , k_3 and k_{-3} (Figure 24). In toluene k_2 is ca. $4 \times 10^{10} \text{ s}^{-1}$, k_3 is ca. $1 \times 10^{10} \text{ s}^{-1}$ and k_{-3} is ca. $2 \times 10^{10} \text{ s}^{-1}$. This gives an excited state equilibrium constant $K = k_3/k_{-3} \approx 0.5$. In dichloromethane k_2 is ca. $4 \times 10^{11} \text{ s}^{-1}$, k_3 is ca. $2.5 \times 10^{10} \text{ s}^{-1}$ and k_{-3} is ca. $2 \times 10^{10} \text{ s}^{-1}$ giving $K \approx 1.4$. The K values in the order of 1 suggest that both the IV-CT state and the CS state have almost the same free energy which is in agreement with a negligible exciton binding energy. A reason for this

might be that in the CS state spin-spin interactions of three adjacent spin bearing centers ($2 \times A^\bullet$ and $1 \times D^{\bullet+}$) lower the free energy of this state which would normally be expected to be higher in energy than the IV-CT state. Further analysis of model compounds will be necessary to support the above made hypothesis.

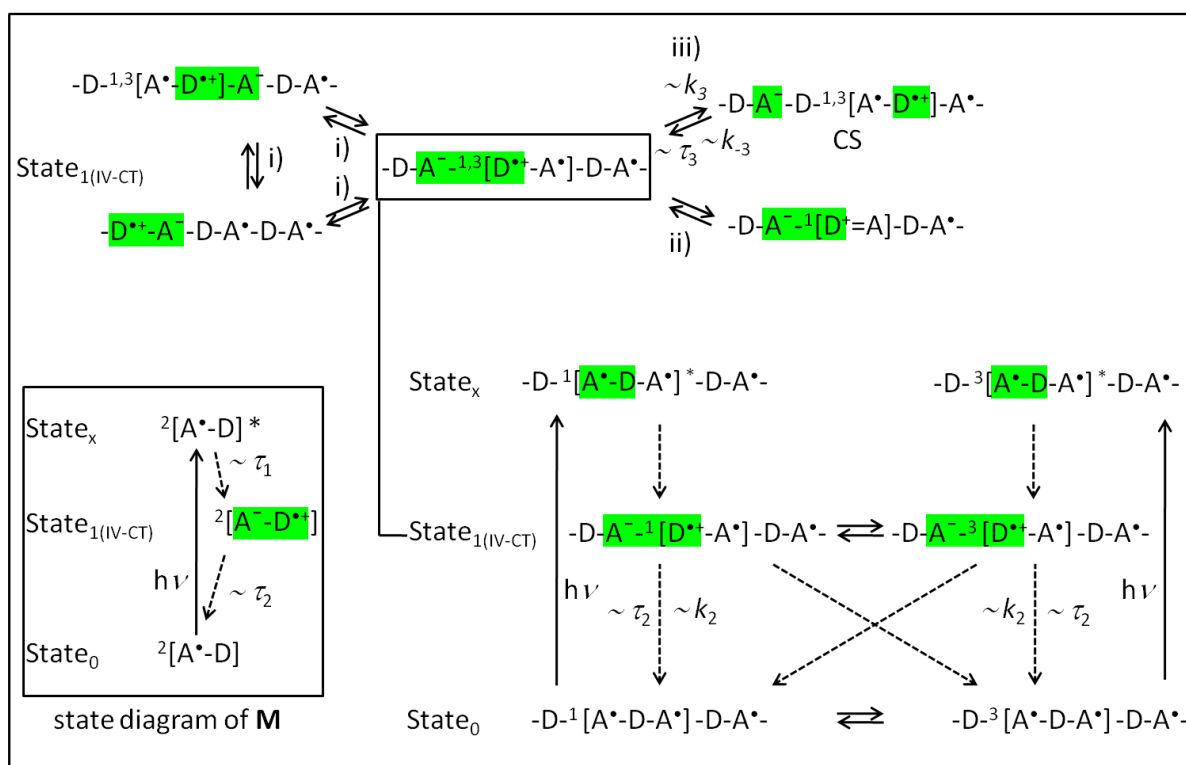


Figure 24. State diagram of **M** (box on the left side) and of **P4**. D: triarylamine moiety; A[•]: PCTM radical moiety, excitons are marked in green.

3.7 Field-Effect Transistors

OFET devices allow to measure electron and hole mobilities of bulk materials in a film separately. In order to assess the charge transport properties of polyradical **P4** OFETs were fabricated in two different device configurations: For device A, a BC/BG structure with SiO₂ as gate dielectric and Au source/drain contacts was chosen. For device B a TC/BG structure with an additional organic insulating layer of PPcB placed upon the SiO₂ surface and Au source/drain contacts evaporated on top of the **P4** layer was used. The staggered configuration (device B) offers the advantage of

enhanced charge injection.³¹ The use of the PPcB layer aims at the suppression of electron trapping often encountered at SiO₂ surfaces⁴³ and the lowering of energetic disorder at the semiconductor/insulator interface, which is achieved with low permittivity materials ($2.1 \leq \epsilon \leq 2.3$) like PPcB⁶². Device fabrication, measurements and calculations of mobilities were carried out by Maria Hammer in the group of Prof. V. Dyakonov (Physics Department).

Table 12. Device configurations and mobilities of holes μ_h and electrons μ_e of devices of P4.

type	gate	insulator	contacts	$T_a / ^\circ\text{C}$	$\mu_h / \text{cm}^2 \text{V}^{-1} \text{s}^{-1}$	$\mu_e / \text{cm}^2 \text{V}^{-1} \text{s}^{-1}$
A	Si BG	SiO ₂	Au BC	120	1×10^{-6}	4×10^{-6}
B	Si BG	SiO ₂ /PPcB	Au TC	120	3×10^{-5}	3×10^{-5}

T_a = annealing temperature

In Table 12 device configurations and mobilities calculated in the saturation regime are listed. Interestingly, in device A the hole mobility is lower than the electron mobility in contrast to what is anticipated for semiconductor mobilities measured on untreated SiO₂ surfaces. This is possibly caused by the high electron affinity (EA) of **P4**, since materials of high EA (> 4 eV) were found to be less affected by the presence of electron traps.⁶⁵ The suppression of the hole transport might originate from additional energetic disorder induced at the **P4**/SiO₂ interface by the polarity of the SiO₂ surface,⁶² which according to the charge transport model for disordered semiconductors proposed by Bäessler²⁴⁹, leads to a broadening of the Gaussian density of states and thus to an enhanced localization of charge carriers⁴⁴.

The output characteristics of device B in the hole and electron accumulation mode are displayed in Figures 25a and 25b, respectively, and the corresponding transfer characteristics are shown in Figure 26.

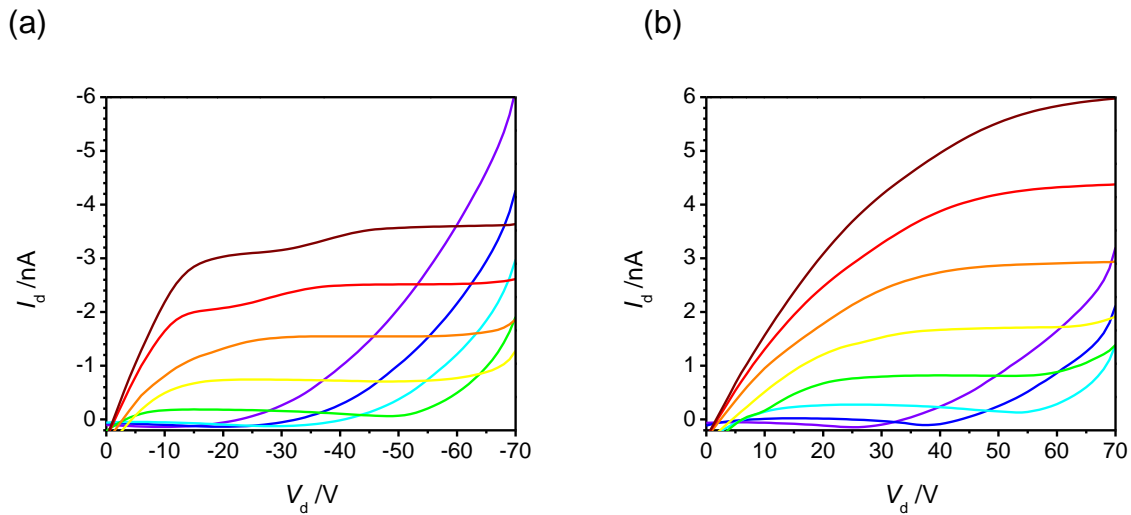


Figure 25. Output characteristics of device B in the hole (a) and electron (b) accumulation mode. V_g is varied from 0 to 70 V (violet, blue, ..., brown) in steps of 10 V. Transistor details: $W = 2$ mm, $L = 125$ μm .

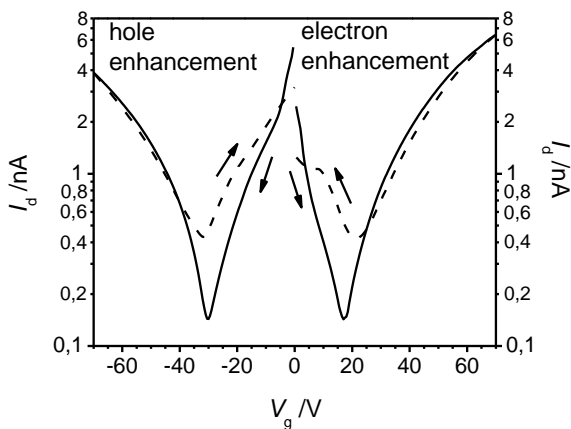


Figure 26. Transfer plot of device B, $|V_d| = 50$ V.

Nicely balanced ambipolar transport is clearly observed with hole and electron mobilities of $3 \times 10^{-5} \text{ cm}^2 \text{ V}^{-1} \text{ s}^{-1}$. The contact resistance does not dominate the charge transport as can be seen from the linear onset of the drain current of the output characteristics. This is expected from the HOMO and LUMO levels of **P4** estimated to be -5.5 eV and -4.5 eV, respectively. The threshold voltages for hole and electron accumulation are -19 V and 9 V, respectively, and a considerable hysteresis is observed in the ambipolar regime of the transfer characteristics. This hysteresis might arise from trap filling by the accumulated charge carrier species, which enhances the drain current in backward direction. These traps can have their

origin in the tail of the intrinsic density of states distribution, or in Coulomb interaction with trapped charges of the opposite sign. Also metallic or organic impurities could limit the charge transport. Another reason for the low mobilities could be a nonoptimized morphology. However, annealing did neither alter the field-effect transistor characteristics nor the absorption spectra of thin films of **P4** (see chapter 3.3) which points to an amorphous material. Since the film morphology of amorphous semiconductors is rather independent of processing procedures and the type of underlying dielectric, as is found for polytriarylamine OFET devices,⁴⁴ ordering by a morphology optimization is not expected to be achieved for **P4**. Note however, that even amorphous semiconductors (polytriarylaminines) may exhibit considerably high hole mobilities up to $0.01 \text{ cm}^2 \text{ V}^{-1} \text{ s}^{-1}$.⁶² Therefore, comparing the polymer structures of high mobility semiconductors to that of **P4**, the low mobility is presumably caused by the lack of close packing of the polymer chains: In contrast to the flat, planar backbone structures of diketopyrrolopyrrole based polymers⁷⁸⁻⁷⁹ **P4** has a flexible and twisted backbone structure. The weak intermolecular interactions are also visible by the close similarity of absorption spectra in solution and in the film which implies the absence of excitonic interactions in the solid state

3.8 Solar Cells

Due to the high electron affinity (LUMO at -4.5 eV) being higher than that of [60]PCBM (LUMO at -4.3 eV) and the broad absorption of **P4** extending to $1 \mu\text{m}$ BHJ all-polymer solar cells with P3HT as donor were fabricated. Device fabrication, measurements and calculations were carried out by Daniel Rauh in the group of Prof. V. Dyakonov (Physics Department). P3HT is a well studied donor polymer that yields PCEs around 5 %¹⁴⁹⁻¹⁵¹ in BHJ solar cells when combined with [60]PCBM and 1.8 %²⁴⁴ in all-polymer solar cells with F8TBT as acceptor, which is among the highest PCEs reported so far for all-polymer solar cells^{238,250-255}. The HOMO levels of P3HT (-5.2 eV)²⁵⁶ and **P4** (-5.4 eV) are offset by about 0.2 eV thus allowing for the maximum open-circuit voltage V_{OC} possible with this low band gap polymer to be achieved (eq. 6). Devices were fabricated with the structure glass/ITO/PEDOT:PSS/(P3HT/**P4**)/Ca/Al with five different weight ratios of P3HT/**P4**,

namely 4:1, 2:1, 1:1, 1:2 and 1:4. The best device efficiency was $3.1 \times 10^{-3} \%$ ($V_{OC} = 0.38$ V, $J_{SC} = 2.8 \times 10^{-2}$ mA cm⁻², FF = 0.29) obtained for the 1:4 (P3HT/**P4**) ratio (Figure 27a), which is unexpectedly low. Comparing the device characteristics of the different blends it is found that V_{OC} is enlarged, whereas the short-circuit current J_{SC} drops when the amount of **P4** in the blend is raised. The fill-factor FF does not vary much with blend ratio. Thus the higher V_{OC} causes the better PCE for the 1:4 blend. Note, that $V_{OC} = 0.38$ V is in agreement with the predicted value according to eq. 6. Even though V_{OC} values of BHJ solar cells comprising low band gap polymers are inherently low, a PCE of 2.7 % ($V_{OC} = 0.38$ V, $J_{SC} = 14.87$ mA cm⁻², FF = 0.48) has recently been reported for a polymer with E_g^{opt} (film) = 1.13 eV using [70]PCBM as acceptor.²⁰² In case of the P3HT/**P4** device the very low PCE is clearly caused by the extraordinarily low value of J_{SC} also being reflected in the EQE spectrum (incident photon to converted electron, Figure 27b). Note, that the main contribution to the maximum EQE at 29000 cm⁻¹ stems from P3HT (compare Figure 19). One of the reasons for the low photoresponse may be attributed to the low charge carrier mobilities found for **P4**. However, P3HT/F8TBT devices are among the most efficient all-polymer solar cells, despite of low and unbalanced mobilities of $\mu_h = 9.9 \times 10^{-5}$ cm² V⁻¹ s⁻¹ and $\mu_e = 8.9 \times 10^{-6}$ cm² V⁻¹ s⁻¹ found in ITO/TiO₂/(P3HT/F8TBT)/MoO₃/Au devices under continuous background illumination by time-of-flight (TOF) measurements²⁵⁷. Even the mobilities measured on OFET devices of pure F8TBT, which are an order of magnitude higher ($\mu_h = 8 \times 10^{-4}$ cm² V⁻¹ s⁻¹ and $\mu_e = 8 \times 10^{-5}$ cm² V⁻¹ s⁻¹)²⁴⁴, are still fairly low.

A more obvious reason for the low photoresponse of the P3HT/**P4** devices is clearly seen on the AFM height images (Figure 28) measured by V. Stepanenko in the group of Prof. F. Würthner: The P3HT/**P4** 1:2 and 1:4 blends do not form a bicontinuous network nor do they exhibit a high density of interfaces between the two phases necessary for efficient exciton dissociation. For the P3HT/**P4** 4:1, 2:1 and 1:1 blends the phase separation is on a smaller scale than for the blends with the higher **P4** content, but **P4** “drops” of about 1 μm size are also visible in the 2:1 and 1:1 blends. Moreover the high surface roughness discloses the inhomogeneity of the blend layers. The phase separation seems to be smallest for the P3HT/**P4** 4:1 blend for which the J_{SC} value is the largest among the different blend ratios. Thus the improper blend morphology is responsible for the bad device performance.

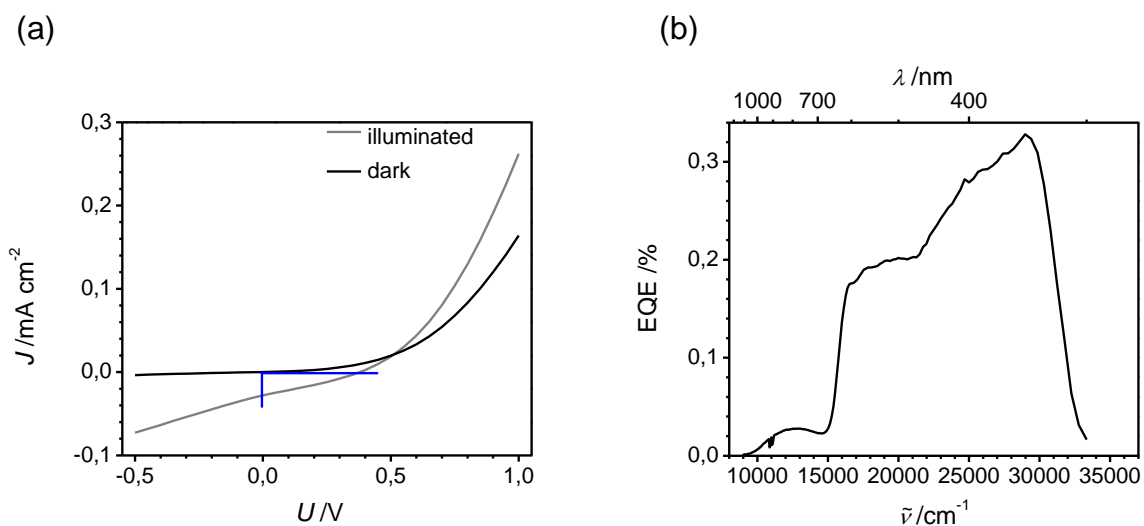


Figure 27. I-V curves of device glass/ITO/PEDOT:PSS/(P3HT/P4 1:4)/Ca/Al under AM1.5 simulated solar irradiation (a) and corresponding EQE spectrum (b).

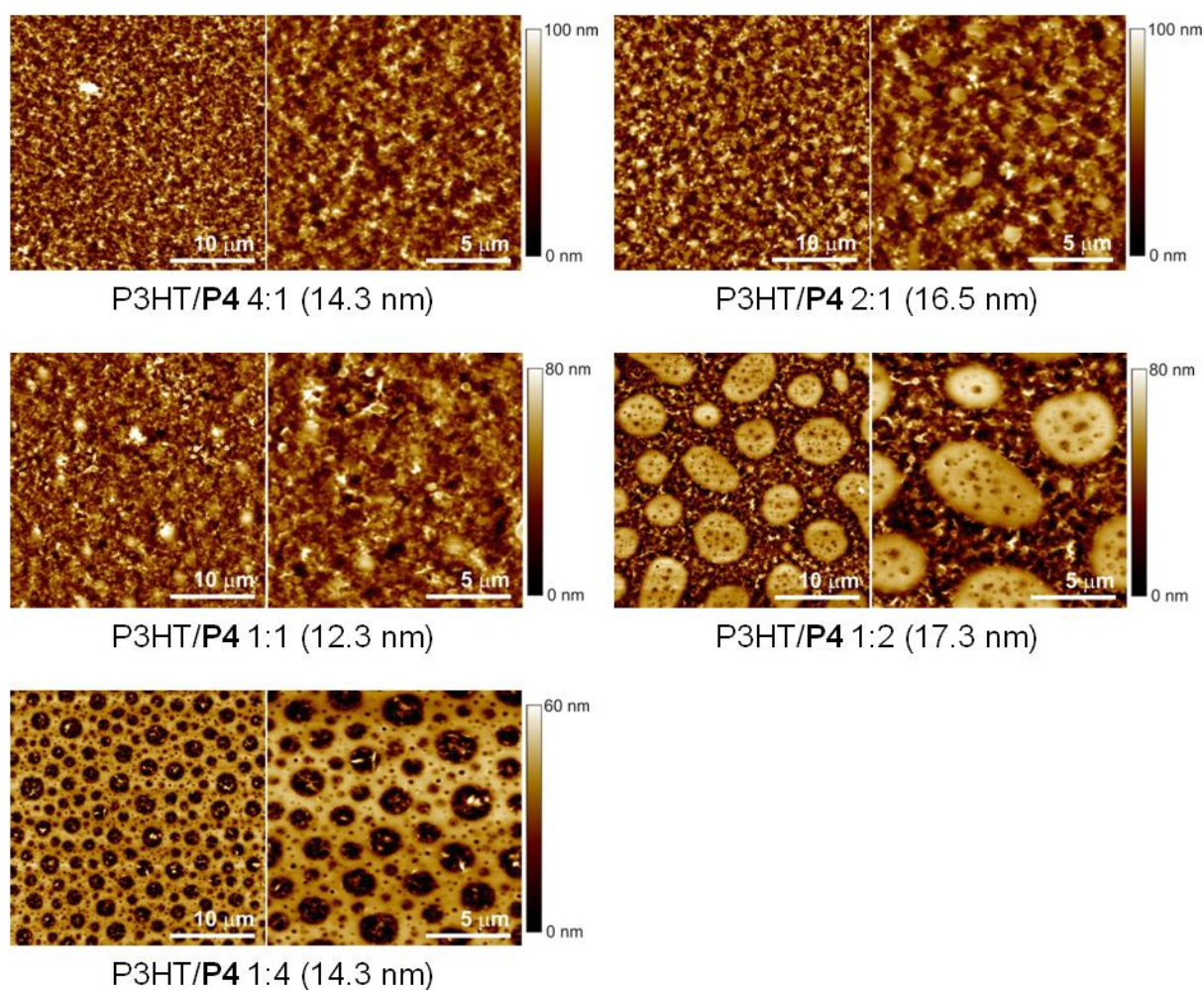


Figure 28: AFM height images of glass/ITO/PEDOT:PSS/(P3HT/P4)/Ca/Al devices. Root mean square (RMS) values are denoted in brackets.

3.9 Conclusions

The low band gap polyradical **P4**, containing alternating triarylamine and PCTM radical moieties, was synthesized by Horner-Emmons reaction to give a polymer with $\bar{M}_w = 19300$ Da ($\bar{M}_n = 11200$ Da, PDI = 1.72) corresponding to $\bar{X}_w = 17$ and $\bar{X}_n = 10$. Comparison with the monomer analogue **M** shows that the lowest-energy band of **P4** can be interpreted as an IV-CT transition that is associated with an optically induced transfer of an electron from the donor (triarylamine) to the radical acceptor (PCTM) unit. Despite the connection of repeating units by conjugated bridges the IV-CT transition of **P4** is confined to one donor-acceptor pair which is proved by the close similarity of polymer and monomer electronic spectra. However, for the more intense, higher energy transitions a distinct excitonic broadening of bands is observed. The band gap of the polymer was determined by both optical (1.2 eV) and electrochemical methods (1.0 eV). The somewhat lower electrochemical band gap compared to the optical band gap may be explained by ion pairing effects and indicates a very low exciton binding energy. The major difference between monomer and polymer is the good film-forming property of **P4** which forms amorphous films that are stable upon annealing at 110 °C in air.

The ET properties of **P4** were investigated in solution by fs-pump-probe transient absorption spectroscopy, which revealed distinct differences between monomer and polymer. The transient spectra of both systems unequivocally prove a charge separation in the IV-CT state as evidenced by the results of spectroelectrochemical measurements. While the monomer shows a single decay time which strongly depends on the solvent polarity the polymer has a biexponential decay with an additional - solvent independent - slow decay component. The short-living component is interpreted as the direct decay from the IV-CT state to the ground state and the long-living component as an equilibrium formation of the IV-CT state and a completely charge separated state. This hypothesis is supported by the observation of a small exciton binding energy as well as by the excited state equilibrium constants of ca. 0.5 and 1.4 in toluene and dichloromethane, respectively.

Charge carrier mobilities were measured in two different OFET configurations both for electron and for hole migration. Using an insulating organic PPcB layer increases the mobilities by one order of magnitude to ca. $3 \times 10^{-5} \text{ cm}^2 \text{ V}^{-1} \text{ s}^{-1}$ for both charge

carriers. While the **P4** films show a well balanced ambipolar transport promoted by the small injection barriers into HOMO (-5.5 eV) and LUMO (-4.5 eV) level, respectively, the overall mobilities are relatively low probably because of less densely packed polymer chains caused by the propeller-like PCTM and triarylamine moieties.

An improper morphology also caused a very low device performance of P3HT/**P4** BHJ solar cells (glass/ITO/PEDOT:PSS/(P3HT/**P4**)/Ca/Al), which yielded a PCE of 3.1×10^{-3} %, $V_{OC} = 0.38$ V, $J_{SC} = 2.8 \times 10^{-2}$ mA cm⁻² and FF = 0.29 for the 1:4 (P3HT/**P4**) blend ratio.

In conclusion, while **P4** is less suitable for OFET and solar cell applications the phenomenon of charge migration along the polymer backbone in the excited state as deduced from the slow solvent independent decay component is worth to be investigated in more detail.

4 Summary

In the first part of the work three polycarbazoles poly[*N*-((4-dimesitylboryl)-3,5-dimethylphenyl)-carbazole]-2,7-diyl **P1**, poly[*N*-((4-dimesitylboryl)-3,5-dimethylphenyl)-carbazole]-3,6-diyl **P2** and poly[*N*-(4-(diphenylmethylene)-phenyl)-carbazole]-2,7-diyl **P3** were synthesized by Yamamoto coupling reaction and their spectroscopic and electrochemical properties were investigated. Absorption and fluorescence characteristics of **P1** and **P3** were found to be similar to other 2,7-linked polycarbazoles, whereas **P2** shows a CT absorption band arising from a shift of electron density from the nitrogen of the carbazole donor to the triarylborane acceptor. This causes a negative solvatochromic absorption and a positive solvatochromic fluorescence behaviour and is responsible for the significantly enlarged fluorescence quantum efficiency in solution and solid state compared to other 3,6-linked polycarbazoles. Thus the spectroscopic properties are governed by the connection pattern: the 2,7-linked polycarbazoles are not affected by the acceptor substituent due to the rigid poly-*para*-phenylene-like backbone structure, whereas the 3,6-linked polycarbazole **P2** is dominated by the properties of the monomer unit due to its more flexible (less conjugated) structure.

The oxidative processes of **P1-P3** have been investigated in detail by cyclic voltammetry, which are similar to known 2,7- and 3,6-polycarbazoles. The reversible reduction found for **P1** and **P2**, respectively, is attributed to the reduction of the triarylborane moiety. No reduction process referring to the carbazole moiety was observed.

Due to its better solubility compared to **P1** and **P3** only **P2** was used as active layer in an OLED device (ITO/**P2**/Al). The electroluminescence spectrum revealed CIE coordinates of (0.17, 0.21).

In the second part of the work the low band gap polyradical poly{(((2,3,4,5,6-pentachlorophenyl)-bis(2,3,5,6-tetrachlorophenyl)methyl radical)-4,4'-diyl)-*alt*-4,4'-bis(vinylphenyl)-4-(2-ethylhexyloxy)phenylamin} **P4** was synthesized by Horner-Emmons reaction. It shows an IV-CT band in the NIR, which arises from an ET from the triarylamine donor to the PCTM radical acceptor. This transition is confined to one monomer unit as deduced from comparison with the monomer spectra.

HOMO and LUMO of **P4** determined by cyclic voltammetry are at -5.5 and -4.5 eV, respectively. The smaller electrochemical band gap (1.0 eV) compared to the optical band gap (1.2 eV) is probably caused by ion pairing effects in the electrochemical experiments and indicates a low exciton binding energy.

Femtosecond-pump-probe transient absorption spectroscopy revealed the spectral features of the oxidized triarylamine donor and the reduced PCTM acceptor similar to the spectra obtained separately for positive and negative potentials by spectroelectrochemistry. Thus the ET event causing the IV-CT absorption band could unambiguously be identified. The decay of the IV-CT state was found to be biexponential. The fast solvent dependent decay component is ascribed to the direct decay from the IV-CT state to the ground state, whereas the slow solvent independent decay component is tentatively attributed to an equilibrium formation of the IV-CT state and a completely charge separated state formed by charge migration along the polymer backbone.

Well balanced ambipolar charge transport with hole and electron mobilities of ca. $3 \times 10^{-5} \text{ cm}^2 \text{ V}^{-1} \text{ s}^{-1}$ was found in OFET devices (BG/TC structure) comprising an additional insulating organic PPcB layer.

Polymer/polymer BHJ solar cell devices with the structure glass/ITO/PEDOT:PSS/(P3HT/**P4**)/Ca/Al yielded a power conversion efficiency of $3.1 \times 10^{-3} \%$, $V_{OC} = 0.38 \text{ V}$, $J_{SC} = 2.8 \times 10^{-2} \text{ mA cm}^{-2}$ and $FF = 0.29$ for the 1:4 (P3HT/**P4**) blend ratio.

The improper solid state morphology of **P4** that causes the unsatisfying performance of OFET and solar cell devices renders **P4** less suitable for these applications, whereas the hypothesis of charge migration in the excited state is worth to be investigated in more detail.

5 Experimental Section

5.1 Apparatus and Methods

NMR spectra (^1H , ^{13}C , ^{31}P) were recorded with either a Bruker AVANCE 400 FT-NMR spectrometer or a Bruker AVANCE DMX 600 FT-NMR spectrometer at r. t.. Chemical shifts δ are given in ppm vs. tetramethylsilane. Carbon atoms connected to chlorine (CCI) were distinguished from those surrounded by only carbon (quart.) by the observation of a shoulder peak with one-third of the main peak's intensity according to the isotopic distribution of ^{35}Cl and ^{37}Cl .

Mass spectra were recorded with a Finnigan MAT 90 or with a Bruker Daltonics micrOTOF focus mass spectrometer equipped with an APCI ion source (Agilent G1947-60101). For calculation of the respective mass values of the isotopic distribution, the software modul "Bruker Daltonics IsotopePattern" of the software Compass 1.1 from Bruker Daltonik GmbH, Bremen was used. Due to the isotopic distribution over a broad m/z region caused by chlorine the signal of monoisotopic signals was too small for some compounds in intensity for an accurate mass measurement. In this case, typically the most intense signal (X+n) of this isotopic distribution was taken and compared with the respective calculated value. Mass spectra of **P1-P3** were recorded with a Bruker Daltonik autoflex II with samples being embedded in a DCTB matrix $[(\text{H}_3\text{C})_3\text{C}-p\text{-Ph}-\text{CH}=\text{C}(\text{CH}_3)\text{-trans-CH}=\text{C}(\text{CN})_2]$.

GPC measurements were performed with a setup consisting of a dual-plunger, tandem-flow pump (Shimadzu, LC-10AT), a He-degasser unit (Shimadzu, DGU-10B), two (**P4**) or three (**P1-P3**) SDV columns from PSS/Mainz (Germany) (pore size: 100, 10^3 and 10^5 Å; particle size: 5 μm ; column length: 300 mm each) and a Gynkotek model 160 UV detector. The eluent was THF (Acros, HPLC grade) at 35 °C with a flow rate of 1 mL min⁻¹. The calibration curve was made with a series of monodisperse polystyrene standards (PSS/Mainz, Germany; concentration: 1 mg/mL). The measurement of **P1** in 1,2,4-trichlorobenzene at 135 °C was performed at the MPI für Polymerforschung in Mainz by S. Seiwald (group of Prof. K. Müllen).

IR spectra were recorded on a JASCO FT/IR 4100 instrument using KBr pellets.

DSC measurements were performed on a Mettler-Toledo DSC 823 under nitrogen atmosphere.

UV/Vis/NIR absorption spectroscopy. Spectra were recorded on a JASCO V-570 UV/Vis/NIR spectrometer in 1 cm quartz cells (Hellma) at r. t.. All solvents were of spectroscopic grade and used as received. Solutions of **P1-P3** had to be filtered before the measurement which made the determination of the solution concentration impossible. The concentration of **P4** solutions was about 1×10^{-5} M. For solid state absorption spectra thin films were prepared by spin coating polymer solutions (**P1-P3**: saturated; **P4**: 5 mg/mL) onto quartz plates (4000 rpm, 60 s). For the determination of the full-width at half maximum $\tilde{\nu}_{1/2}$ the IV-CT band was fitted with three (dichloromethane) and four (toluene) Gaussian bands, respectively, and the sum of the two (dichloromethane) and three (toluene) Gaussian bands with the lowest energy was used for the determination of $\tilde{\nu}_{1/2}$.

Steady-state fluorescence spectroscopy. Spectra were recorded on a PTI (Photon Technology International) fluorescence spectrometer model QM-2000-4 with a cooled photomultiplier (R928 P) and a 75 W Xenon short arc lamp (UXL-75XE, Ushio). All spectra were recorded in 1 cm quartz cells (Hellma) in solvents of spectroscopic grade at r. t.. The fluorescence quantum yields were determined from the absorption and fluorescence spectra according to eq. 13, in which $I(\tilde{\nu})$, OD , and n_D^{20} denote the area below the emission band, the optical density of the solution at the excitation wavelength, and the refractive index of the solvent, respectively.

$$\phi_f = \phi_{ref} \left(\frac{I(\tilde{\nu}) \times OD_{ref} \times (n_D^{20})^2}{I(\tilde{\nu}) \times OD \times (n_{D,ref}^{20})^2} \right) \quad (13)$$

Quinine sulfate dihydrate (Fluka) in 1 N H₂SO₄ (Acros) was employed as fluorescence standard ($\phi_{f,ref} = 0.546$, $n_D^{20} = 1.3445$)²⁵⁸. For absorption measurements OD s were in the range of 0.01 to 0.045 in order to get sufficiently high signal to noise ratios.

Special care was taken for the determination of fluorescence quantum yields of **P1-P3**: For emission measurements samples were diluted by a factor of 1:10 since at

higher concentrations fluorescence quantum yields were quenched. In order to avoid mistakes arising from dilution, three samples per solvent were prepared. For each sample its absorption spectrum was recorded, it was diluted and its emission spectrum was recorded. The *OD* of the quinine sulfate dihydrate solution was about 0.01 and not altered before the emission measurement. Samples were not degassed thus avoiding concentration variations of solutions prepared from volatile solvents. Moreover, fluorescence quantum yields of polymers diluted in DMSO are only slightly higher when degassed by bubbling argon through the cuvette than that of samples not treated with an argon gas flow. Samples were excited at $\lambda = 340, 345$ and 350 nm which gave similar values for all three wavelengths for **P1** and **P3** and slightly differing values for the three wavelengths for **P2**. Results are only tabulated for $\lambda = 345$ nm excitation. Solid state emission spectra were recorded on thin films prepared by dropping saturated CH_2Cl_2 solutions of the polymers onto quartz plates. Solid state fluorescence quantum yields were determined on a Hamamatsu Absolute PL Quantum Yield Measurement System CC9920-02. The system is made up of an excitation source that uses a 150 W CW Xenon light source, a monochromator (250-700 nm, FWHM 10 nm), an integrating sphere, and a multi-channel spectrometer capable of simultaneously measuring multiple wavelengths between 300 and 950 nm and counting the number of absorbed and emitted photons. With this system the absolute fluorescence quantum yield of powders and thin films (drop cast, see above) were determined at r. t. on air upon excitation at $\lambda = 345$ nm.

Time-dependent fluorescence-decay.

Fluorescence lifetimes of **P1-P3** were measured with a PTI TM-2/2003 fluorescence-lifetime spectrometer with a nanosecond flash lamp charged with H_2/N_2 (1:1). The instrument response of the nanosecond flash lamp was determined by using colloidal silica (Ludox) in de-ionized water as a scatterer. The fluorescence-decay curves were fitted with a single-exponential decay function in order to obtain the corresponding fluorescence lifetimes. Measurements were performed in 1 cm quartz cells (Hellma) in solvents of spectroscopic grade at r. t..

Cyclic voltammetry. Experiments were carried out with a BAS CV-50 W instrument (Software Version 2.0). A conventional three-electrode setup consisting of a Pt-disc working electrode ($\phi = 2$ mm), an Ag/AgCl pseudoreference electrode, and a Pt-wire counter electrode was used. The redox potentials were referenced against the Fc/Fc⁺ redox couple as an internal standard. Measurements were performed under an argon atmosphere with TBAP or TBAPF₆ as the supporting electrolyte: 0.1 M in MeCN, 0.2 M in CH₂Cl₂ and 0.3 M in THF. CH₂Cl₂ (Baker, HPLC grade) and MeCN (Baker, HPLC grade) were predried over molecular sieves 4 Å (Acros, 8-12 mesh) and 3 Å (Merck), respectively and distilled over CaH₂. THF was predried over KOH and distilled over sodium/benzophenone. Polymer concentrations of solution measurements are unknown since the solution had to be filtered due to the low solubility of the polymers. For thin film measurements a solution of the polymer in CH₂Cl₂ was drop cast onto the working electrode and dried in a nitrogen gas flow. For thin layer measurements (20 ± 5 μm) the working electrode was placed on top of a flexible hemisphere ($\phi = 8$ mm). For **P1-P3** HOMO and LUMO values were determined from the onset potentials and calculated under the assumption that Fc/Fc⁺ = -4.8 eV vs. vacuum¹⁹⁵ in order to make values comparable to literature data. For **P4** HOMO and LUMO values were determined from the half-wave potentials in CH₂Cl₂/TBAPF₆ solution and calculated according to $E(\text{HOMO/LUMO}) = -5.16 \text{ eV} - E_{1/2}^{\text{ox/red}}$. It was assumed that Fc/Fc⁺ = +0.46 eV vs. SCE (0.1 M TBAPF₆ in CH₂Cl₂)²⁵⁹ and SCE = 0.24 eV vs. the Standard Hydrogen Electrode (SHE).²⁶⁰ The absolute potential of SHE was found to be 4.46 eV.²⁶¹ Differential Pulse Voltammetry (DPV) was carried out with the same instrument and under identical experimental conditions.

Spectroelectrochemistry. Experiments were performed in a specially designed sample compartment consisting of a cylindrical quartz cell, a Pt-disc electrode ($\phi = 6$ mm), a gold-covered metal (V2A) plate as the counter electrode and an Ag/AgCl pseudo-reference electrode. Solvents and electrolytes were the same as those used for CV experiments and measurements were performed under argon atmosphere. Spectra were recorded with a JASCO V-570 UV/Vis/NIR spectrometer in reflection mode. The vertical position of the working electrode was adjusted with a micrometer screw 100 μm above the bottom of the cell. The potential was applied by an EG & G

Princeton Applied Research Model 283 potentiostat and was varied in steps of 20–100 mV.

Transient absorption spectroscopy. The laser system used for the femtosecond transient absorption measurements consists of an ultrafast Ti:sapphire amplifier (Spectra Physics Solstice) with a repetition rate of 1 kHz, a central wavelength of 800 nm, and a pulse duration of 100 fs. One part of the output power was used to seed a noncollinear optical parametric amplifier (Light Conversion TOPAS White) which produced the pump pulses centered at 525 nm with a duration of about 55 fs as verified by frequency-resolved optical gating measurements.²⁶² A small fraction of the Ti:sapphire output was focused into a linearly moving CaF₂-plate to produce a supercontinuum between 390 nm and 750 nm which acted as the probe beam. After passing the sample the probe pulses were detected via a spectrograph (Acton SP2558) with a CCD camera (Princeton Instruments Pixis 2k). A mechanical chopper, working at 500 Hz, blocks every second pump pulse, thus enabling low noise shot-to-shot-measurements, eliminating the need for a reference beam. By comparing the transmitted spectral intensity of consecutive pulses [$I(\lambda, \tau)$, $I_0(\lambda)$] the photoinduced change in the optical density can be directly recorded as: $\Delta OD = -\log \left[\frac{I(\lambda, \tau)}{I_0(\lambda)} \right]$. For the measurements pump and probe pulses were focused noncollinearly and spatially overlapped in a 500 μm flow cell with beam diameters of 40 μm and less than 30 μm , respectively, while the polarizations were set to the magic angle of 54.7°. The pump power was attenuated resulting in pulse energies of 100 nJ (**M** in toluene and CH₂Cl₂ and **P4** in CH₂Cl₂) and 260 nJ (**P4** in toluene). The relative temporal delay between pump and probe pulses was varied over a maximum range of 3.6 ns with a motorized, computer controlled linear stage. The delay interval between two consecutive data points was 100 fs for small delay times and was increased up to 30 ps for very large delay times. The data were analyzed by a least squares fitting algorithm. The nonlinear fit model was a multiexponential function in combination with a Heaviside step function. In case of the polymer a biexponential decay was assumed. For the monomer a sum of monoexponential rise and decay functions was used. Where the coherent artifact²⁶³ was observable, selected data points around time zero were omitted from the fit.

OLED Fabrication. An ITO coated glass plate (2.5 × 2.5 cm², 125 nm, sheet resistance ~25 Ω, Merck KGaA) was covered with tape except for a bar of about 0.5 cm width. This bar was treated with a Zn/H₂O suspension and HCl in order to remove ITO from the glass plate. The plate was cleaned mechanically with dish liquid and then with acetone and isopropanol in an ultrasonic bath and subsequently heated to 140 °C for 24 h in order to remove residual solvent. **P2** dissolved in CHCl₃/toluene (25:1, 6 mg/mL) was spin coated onto the plate (800 rpm, 60 s). Opposite to the bar of pure glass, a bar of the polymer layer was scratched off (about 0.5 cm). On top Al contacts (90 nm, Mateck GmbH) were deposited through a shadow mask (aluminium) by thermal evaporation at high vacuum (1 × 10⁻⁶ mbar, deposition rate 0.2 nm s⁻¹) in a BOC Edwards Auto 306/500 deposition system. Voltage was applied by the electrochemical workstation BAS CV-50 W. Spectra were recorded on a PTI (Photon Technology International) fluorescence spectrometer model QM-2000-4 with a cooled photomultiplier (R928 P). CIE 1931 (x,y) chromaticity coordinates were calculated according to eqs. 14 and 15:²⁶⁴

$$y = \frac{X}{X+Y+Z} \quad (14)$$

$$y = \frac{Y}{X+Y+Z} \quad (15)$$

The XYZ values are derived from eqs. 16-18:

$$X = k \int \varphi_{\lambda}(\lambda) \times \bar{x}(\lambda) d\lambda \quad (16)$$

$$Y = k \int \varphi_{\lambda}(\lambda) \times \bar{y}(\lambda) d\lambda \quad (17)$$

$$Z = k \int \varphi_{\lambda}(\lambda) \times \bar{z}(\lambda) d\lambda \quad (18)$$

in which $\bar{x}(\lambda)$, $\bar{y}(\lambda)$ and $\bar{z}(\lambda)$ are the CIE 1931 XYZ colour matching functions. $\varphi_{\lambda}(\lambda)$ is the spectral colour stimulus function (\equiv electroluminescence EL(λ)) and k is a normalization constant.

OFET fabrication. Heavily doped n-type Si substrates as the gate and thermally grown 200 nm silicon dioxide as the dielectric layer (Si-Mat) were cleaned in an ultrasonic bath with acetone and isopropanol. For device A (BG/BC structure) first source and drain electrodes (1 nm Ti adhesion layer/19 nm Au) were patterned using standard photolithography. Then the semiconductor layer was spin coated (1500 rpm, 60 s) on top from a 1 wt% solution of **P4** in chlorobenzene inside a nitrogen-filled glove box. For device B (BG/TC structure) PPcB (12 wt% 1-butene, Aldrich) was dissolved in anhydrous decaline (cis/trans mixture, Aldrich) at 190 °C (20 mg/mL) and spin coated in air on top of the SiO₂ surface using a preheated copper chuck (2500 rpm, 60 s). The device was heated for one minute at 200 °C in air and then transferred to the glove box where **P4** was spin coated (1 wt% in chlorobenzene, 1500 rpm, 60 s) on top. As final layer Au source and drain contacts (50 nm) were evaporated through a shadow mask. The as prepared devices (A and B) were heated at 120 °C for 20 h in vacuum prior to the measurements using an Agilent Parameter Analyzer 4155C. Mobilities μ were calculated from the transfer curves in the saturation regime at a drain voltage $|V_D| = 50$ V according to eq. 4.

Solar Cell Fabrication. Structured ITO covered glass plates were cleaned with dish liquid, acetone and isopropanol in an ultrasonic bath prior to spin coating of a PEDOT:PSS layer (40-50 nm) followed by heating of the substrates at 130 °C for 10 min in a nitrogen-filled glove box. Subsequent processing steps and measurements were then exclusively performed under inert atmosphere. The blend layer was spin coated from different ratios of regioregular P3HT (Rieke Metals, 20 mg/mL in chlorobenzene) and **P4** (20 mg/mL in chlorobenzene) with the two solutions being mixed directly before spin coating. Samples were annealed at 130 °C for 15 min prior to thermal evaporation of Ca(3 nm)/Al(100 nm) metal contacts. The active area was 3 mm². Measurements were performed under AM1.5 simulated solar light irradiation with the light intensity being adjusted by using a Si reference solar cell with an optical filter.

5.2 Syntheses

5.2.1 Materials

Solvents were dried by standard procedures and stored under nitrogen atmosphere. 9*H*-Carbazole was recrystallized from ethanol. Only fresh batches of dimesitylboron fluoride were used. CuBr₂ and K₂CO₃ were dried in vacuum above 200 °C and stored under nitrogen atmosphere. 18-crown-6 was distilled under reduced pressure and stored under nitrogen atmosphere.

Activation of Cu powder:

Cu powder (2 g) was stirred in acetone (20 mL) with I₂ (40.0 mg) for 10 min, filtered and stirred in conc. HCl/acetone (1:1, 20 mL) for 5 min. The activated Cu powder was filtered, washed thoroughly with acetone until neutral and dried in vacuum.

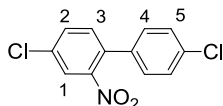
Preparation of anhydrous NiCl₂:

Under nitrogen atmosphere SOCl₂ (183 mmol) was carefully added to NiCl₂·6H₂O (24.0 mmol) and the suspension was stirred at 80 °C for 1 h. NiCl₂ was filtered off under nitrogen atmosphere and dried in vacuum to give a rose solid, which turned yellow upon exposure to air.

All other chemicals and reagents were used as received. For reactions carried out under nitrogen atmosphere standard Schlenk techniques were used.

5.2.2 Synthesis of Polycarbazoles

4,4'-Dichloro-2-nitrobiphenyl **2**



CA [192942-45-3]

Synthesis according to lit.¹⁷³

4,4'-Dichlorobiphenyl 1 ¹⁷²	16.3 g (73.1 mmol)
Glacial acetic acid	343 mL
HNO ₃ (100 %)	105 mL
H ₂ O	8.6 mL

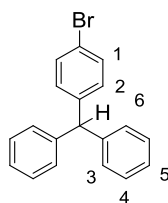
The reaction mixture was poured onto ice and neutralized by the addition of aqueous NaOH. The yellow precipitate was collected by filtration, dissolved in CHCl₃ and washed with aqueous NaHCO₃ (2 x) and water (2 x). The organic phase was dried over MgSO₄, filtered and the solvent was evaporated.

Formula: C₁₂H₇Cl₂NO₂

Yield: 19.3 g (72.0 mmol, 98 %) of a yellow solid.

¹H NMR (400 MHz, [D₆]acetone): δ = 8.06 (d, 1H, ⁴J_{HH} = 2.1 Hz, H1), 7.83 (dd, 1H, ³J_{HH} = 8.3 Hz, ⁴J_{HH} = 2.1 Hz, H2), 7.61 (d, 1H, ³J_{HH} = 8.3 Hz, H3), 7.52 (AA', 2H, H4), 7.41 (BB', 2H, H5).

4-Bromophenyl-diphenylmethane 4b



CA: [5410-05-9]

Synthesis according to lit.¹⁸⁰

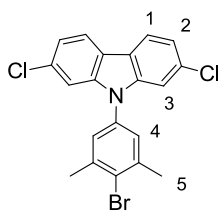
To a solution phenylmagnesium bromide (4.68 g, 29.8 mmol) in 63 mL Et₂O a solution of *p*-bromobenzophenone (4.94 g, 18.9 mmol) in 37 mL Et₂O was added dropwise over a period of 1 h. Subsequently the red reaction mixture was stirred over night at r. t. upon which it turned brown. Then it was poured onto crushed ice and acidified with 6 N HCl (pH 3-4). The phases were separated and the aqueous phase was extracted with Et₂O (3 x). The combined organic extracts were washed with NaHCO₃ (1 x) and water (3 x) and dried over MgSO₄. After removal of the solvent formic acid (23.5 mL, 98-100 %) was added and the red-orange mixture was refluxed for 3 h whereupon it turned red-brown and a yellow solid appeared. Then the mixture was poured onto crushed ice and after addition of Et₂O the aqueous phase was separated and extracted with Et₂O (3 x). The combined organic phases were washed with aqueous NaOH (5 %, 6 x) and dried over MgSO₄. The solvent was evaporated and the oily product was purified by flash chromatography (100 % PE → PE/DCM 3:1) and recrystallized from PE.

Formula: C₁₉H₁₅Br

Yield: 4.49 g (13.9 mmol, 73 %) of a slightly yellow solid.

¹H NMR (400 MHz, [D₆]acetone): δ = 7.40 (AA', 2H, H1), 7.32-7.26 (m, 4H, H4), 7.25-7.20 (m, 2H, H5), 7.11-7.07 (m, 4H, H3), 6.99 (BB', 2H, H2), 5.50 (s, 1H, H6).

***N*-(4-Bromo-3,5-dimethylphenyl)-2,7-dichlorocarbazole 5a**



Synthesis according to lit.¹⁷⁹

3a¹⁷⁰ (8.31 g, 35.2 mmol), **4a**¹⁷⁸ (5.57 g, 21.1 mmol), CuI (224 mg, 1.18 mmol), *trans*-1,2-cyclohexanediamine (290 μ L, 2.41 mmol) and K₃PO₄ (15.7 g, 74.0 mmol) were suspended in dry 1,4-dioxane (22 mL) under nitrogen atmosphere and heated at 110 °C for 72 h. The reaction mixture was diluted in CH₂Cl₂ and washed with water. The combined aqueous phases were extracted with CH₂Cl₂ and the CH₂Cl₂ phases were dried over MgSO₄. The crude product was purified by flash chromatography (PE/CH₂Cl₂ 10:1).

Formula: C₂₀H₁₄BrCl₂N

Yield: 6.52 g (15.6 mmol, 74 %) of a colourless solid.

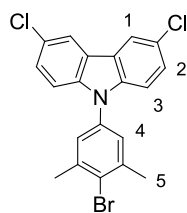
Melting point: 240-242 °C (PE/CH₂Cl₂).

¹H NMR (400 MHz, [D₆]acetone): δ = 8.22 (dd, 2H, ³J_{HH} = 8.3 Hz, ⁵J_{HH} = 0.5 Hz, H1), 7.47 (s, 2H, H4), 7.38 (dd, 2H, ⁴J_{HH} = 1.9 Hz, ⁵J_{HH} = 0.5 Hz, H3), 7.32 (dd, 2H, ³J_{HH} = 8.3 Hz, ⁴J_{HH} = 1.9 Hz, H2), 2.56 (s, 6H, H5).

¹³C NMR (101 MHz, CD₂Cl₂): δ = 142.3 (quart.), 141.1 (quart.), 135.3 (quart.), 132.3 (quart.), 127.6 (quart.), 127.0 (CH, C4), 121.7 (quart.), 121.6 (CH, C1), 121.2 (CH, C2), 110.5 (CH, C3), 24.2 (CH₃, C5).

APCI positive (high resolution): calcd. for [M]⁺⁺ = C₂₀H₁₄BrCl₂N⁺⁺ 416.96812, found 416.96700, Δ = 2.69 ppm.

***N*-(4-Bromo-3,5-dimethylphenyl)-3,6-dichlorocarbazole 5b**



Synthesis according to the preparation of **5a**.

3b ¹⁷⁵	1.00 g (4.24 mmol)
4a ¹⁷⁸	670 mg (2.54 mmol)
CuI	27.0 mg (142 μ mol)
<i>trans</i> -1,2-Cyclohexanediamine	34.9 μ L (290 μ mol)
K ₃ PO ₄	1.89 g (8.90 mmol)
1,4-Dioxane (dry)	2.65 mL

The reaction time was 19 h instead of 72 h. The crude product was purified by flash chromatography (100 % PE).

Formula: C₂₀H₁₄BrCl₂N

Yield: 550 mg (1.31 mmol, 52 %) of a colourless solid.

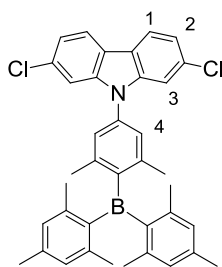
Melting point: 201-203 °C (PE).

¹H NMR (400 MHz, CD₂Cl₂): δ = 8.06 (dd, 2H, ⁴J_{HH} = 2.0 Hz, ⁵J_{HH} = 0.5 Hz, H1), 7.40 (dd, 2H, ³J_{HH} = 8.8 Hz, ⁴J_{HH} = 2.0 Hz, H2), 7.31 (dd, 2H, ³J_{HH} = 8.7 Hz, ⁵J_{HH} = 0.5 Hz, H3), 7.25 (s, 2H, H4), 2.52 (s, 6H, H5).

¹³C NMR (101 MHz, CD₂Cl₂): δ = 140.9 (quart.), 140.1 (quart.), 135.7 (quart.), 127.1 (CH, C2), 126.7 (CH, C4), 126.0 (quart.), 123.8 (quart.), 120.5 (CH, C1), 111.6 (CH, C3), 24.2 (CH₃, C5), CBr is missing.

APCI positive (high resolution): calcd. for [M]⁺ = C₂₀H₁₄BrCl₂N⁺ 416.96812, found 416.96829, Δ = 0.41 ppm.

2,7-Dichloro-*N*-((4-dimesitylboryl)-3,5-dimethylphenyl)-carbazole 6a



Synthesis according to lit.¹⁷⁹

To a suspension of **5a** (370 mg, 883 μmol) in dry Et_2O (10 mL) *tert*-butyllithium (1.17 mL, 1.76 mmol, 1.5 M in *n*-pentane) was added at $-68\text{ }^\circ\text{C}$ under nitrogen atmosphere. The reaction mixture was stirred for 3 h and then slowly added via cannula to a $-68\text{ }^\circ\text{C}$ cold solution of dimesitylboron fluoride (268 mg, 999 μmol) in dry Et_2O (5 mL). The reaction mixture was allowed to warm up to r. t. over night, diluted in CH_2Cl_2 , washed with water and dried over MgSO_4 . The crude product was purified by flash chromatography (PE/ CH_2Cl_2 20:1).

Formula: $\text{C}_{38}\text{H}_{36}\text{BCl}_2\text{N}$

Yield: 285 mg (484 μmol , 55 %) of a colourless solid.

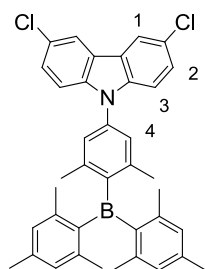
Melting point: 265-267 $^\circ\text{C}$ (PE/ CH_2Cl_2).

^1H NMR (400 MHz, CD_2Cl_2): δ = 8.02 (d, 2H, $^3J_{\text{HH}} = 8.3\text{ Hz}$, H1), 7.38 (d, 2H, $^4J_{\text{HH}} = 1.9\text{ Hz}$, H3), 7.26 (dd, 2H, $^3J_{\text{HH}} = 8.3\text{ Hz}$, $^4J_{\text{HH}} = 1.9\text{ Hz}$, H2), 7.07 (s, 2H, H4), 6.84 (s, 2H, CH), 6.81 (s, 2H, CH), 2.30 (s, 6H, CH_3), 2.12 (s, 6H, CH_3), 2.11 (s, 6H, CH_3), 2.04 (s, 6H, CH_3).

^{13}C NMR (101 MHz, CD_2Cl_2): δ = 143.2 (quart.), 142.2 (quart.), 141.2 (quart.), 141.0 (quart.), 140.2 (quart.), 137.2 (quart.), 132.2 (quart.), 129.2 (CH), 129.1 (CH), 125.9 (CH, C4), 121.7 (quart.), 121.5 (CH, C1), 121.1 (CH, C2), 111.1 (quart.), 110.7 (CH, C3), 108.9 (quart.), 23.1 (CH_3), 23.08 (CH_3), 23.0 (CH_3), 21.4 (CH_3).

APCI positive (high resolution): calcd. for $[\text{M}+\text{H}]^+ = \text{C}_{38}\text{H}_{37}^{10}\text{BCl}_2\text{N}^+$ 587.24269, found 587.24185, $\Delta = 1.43\text{ ppm}$.

3,6-Dichloro-*N*-((4-dimesitylboryl)-3,5-dimethylphenyl)-carbazole 6b



Synthesis according to the preparation of **6a**.

5b	500 mg (1.19 mmol)
in Et ₂ O (dry)	13.5 mL
<i>tert</i> -Butyllithium	1.40 mL (2.38 mmol, 1.7 M in <i>n</i> -pentane)
Dimesitylboron fluoride	362 mg (1.21 mmol)
in Et ₂ O (dry)	6.5 mL

The crude product was precipitated by dropwise addition of a concentrated CH₂Cl₂ solution into MeOH and recrystallized from ethyl acetate.

Formula: C₃₈H₃₆¹⁰BCl₂N

Yield: 220 mg (374 μmol, 31 %) of a colourless solid.

Melting point: 302-303 °C (ethyl acetate).

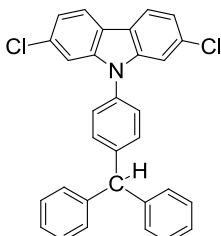
¹H NMR (600 MHz, CD₂Cl₂): δ = 8.05 (dd, 2H, ⁴J_{HH} = 1.8 Hz, ⁵J_{HH} = 0.7 Hz, H1), 7.40 (dd, 2H, ³J_{HH} = 8.7 Hz, ⁴J_{HH} = 1.8 Hz, H2), 7.38 (dd, 2H, ³J_{HH} = 8.7 Hz, ⁵J_{HH} = 0.7 Hz, H3), 7.08 (s, 2H, H4), 6.82 (s, 2H, CH), 6.80 (s, 2H, CH), 2.29 (s, 6H, CH₃), 2.10 (s, 6H, CH₃), 2.09 (s, 6H, CH₃), 2.03 (s, 6H, CH₃).

¹³C NMR (151 MHz, CD₂Cl₂): δ = 147.8 (quart.), 143.9 (quart.), 142.9 (quart.), 141.1 (quart.), 140.9 (quart.), 140.2 (quart.), 139.9 (quart.), 137.5 (quart.), 129.09 (CH), 129.06 (CH), 126.9 (CH, C2), 125.73 (CH, C4), 125.69 (quart.), 123.7 (quart.), 120.3 (CH, C1), 111.8 (CH, C3), 23.02 (CH₃), 23.00 (CH₃), 22.99 (CH₃), 21.3 (CH₃).

APCI positive (high resolution): calcd. for [M]⁺ = C₃₈H₃₆BCl₂N⁺ 586.23487, found

586.23460, $\Delta = 0.46$ ppm.

2,7-Dichloro-*N*-(4-(diphenylmethylene)-phenyl)-carbazole **6c**



Synthesis according to the preparation of **5a**.

3a ¹⁷⁰	600 mg (2.54 mmol)
4b	492 mg (1.52 mmol)
CuI	16.2 mg (85.1 μ mol)
<i>trans</i> -1,2-Cyclohexanediamine	20.9 μ L (174 μ mol)
K ₃ PO ₄	1.13 g (5.32 mmol)
1,4-Dioxane (dry)	1.56 mL

Formula: C₃₁H₂₁Cl₂N

Yield: 620 mg (1.30 mmol, 86 %) of a colourless solid.

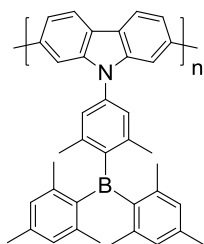
Melting point: 203-205 °C (PE/CH₂Cl₂).

¹H NMR (400 MHz, CDCl₃): $\delta = 7.98$ (dd, 2H, ³J_{HH} = 8.3 Hz, ⁵J_{HH} = 0.38 Hz, arom.), 7.44-7.34 (m, 10H, arom.), 7.31-7.21 (m, 8H, arom.), 5.68 (s, 1H, benzylic).

¹³C NMR (101 MHz, CD₂Cl₂): $\delta = 144.4$ (quart.), 143.5 (quart.), 142.0 (quart.), 134.8 (quart.), 132.2 (quart.), 131.3 (CH), 129.6 (CH), 128.7 (CH), 126.87 (CH), 126.83 (CH), 121.5 (quart.), 121.2 (CH), 121.0 (CH), 110.3 (CH).

EI-MS (high resolution, PI): m/z calcd. for C₃₁H₂₁Cl₂N 477.10456, found 477.10449, $\Delta = 0.14$ ppm.

Poly[*N*-((4-dimesitylboryl)-3,5-dimethylphenyl)-carbazole]-2,7-diyl P1



Synthesis according to lit.¹⁷⁰

Triphenylphosphine (58.1 mg, 221 μmol), Zn powder (81.7 mg, 1.25 mmol), 2,2'-bipyridyl (2.84 mg, 18.2 μmol), **6a** (225 mg, 383 μmol) and anhydrous NiCl_2 (2.34 mg, 18.1 μmol) were suspended in dry *N,N*-dimethylacetamide (0.61 mL) under nitrogen atmosphere and stirred at 70 °C for 3 days. Then 50 mL of HCl (10 %)/MeOH (1:5) were added to the grey-brown suspension and it was stirred until all Zn powder had been dissolved. The solid was filtered off, washed with water and transferred into a Soxhlet apparatus where it was washed with acetone for 48 h.

Formula: $[\text{C}_{38}\text{H}_{36}\text{BN}]_n + 2\text{H}$

Yield: 94.0 mg (182 μmol , 48 %) of a pale yellow solid.

Decomposition: 341 °C (acetone).

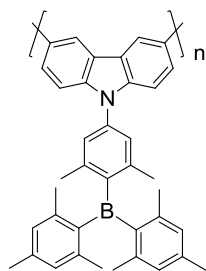
^1H NMR (400 MHz, CDCl_3): δ = 8.28-8.19, 8.18-8.14, 8.07-8.03, 7.70-7.50, 7.44-7.38, 7.20-7.13, 7.12-7.08, 6.83-6.68, 2.32-2.23, 2.14-2.05, 2.05-1.96;

^{13}C NMR: could not be recorded because of low solubility.

MALDI-MS: m/z calcd. for $\text{C}_{228}\text{H}_{218}\text{B}_6\text{N}_6$ 3107.08, found 3106.98, Δ = 35 ppm;
 m/z calcd. for $\text{C}_{266}\text{H}_{254}\text{B}_7\text{N}_7$ 3624.59, found 3624.68, Δ = 23 ppm;
 m/z calcd. for $\text{C}_{304}\text{H}_{290}\text{B}_8\text{N}_8$ 4142.10, found 4142.27, Δ = 39 ppm;
 m/z calcd. for $\text{C}_{342}\text{H}_{326}\text{B}_9\text{N}_9$ 4659.61, found 4659.81, Δ = 41 ppm;
 m/z calcd. for $\text{C}_{380}\text{H}_{362}\text{B}_{10}\text{N}_{10}$ 5177.12, found 5177.51, Δ = 74 ppm;
 m/z calcd. for $\text{C}_{418}\text{H}_{398}\text{B}_{11}\text{N}_{11}$ 5694.63, found 5694.61, Δ = 4 ppm.

GPC (THF): \bar{M}_w = 2300 Da, \bar{M}_n = 2100 Da, PDI = 1.1; in 1,2,4-trichlorobenzene: \bar{M}_w = 4000 Da, \bar{M}_n = 2300 Da, PDI = 1.8.

Poly[*N*-((4-dimesitylboryl)-3,5-dimethylphenyl)-carbazole]-3,6-diyl P2



Synthesis according to the preparation of **P1**.

Triphenylphosphine	38.5 mg (147 μmol)
Zn powder	54.1 mg (827 μmol)
2,2'-Bipyridyl	1.88 mg (12.0 μmol)
6b	149 mg (253 μmol)
Anhydrous NiCl ₂	1.55 mg (12.0 μmol)
<i>N,N</i> -Dimethylacetamide	0.40 mL

Formula: [C₃₈H₃₆BN]_n + 2H

Yield: 70.0 mg (135 μmol , 53 %) of a pale yellow solid.

Decomposition: 324 °C (acetone).

¹H NMR (600 MHz, [D₈]THF): δ = 8.9-8.1 (2H, arom.), 8.0-7.6 (2H, arom.), 7.6-7.3 (2H, arom.), 7.3-7.0 (2H, arom.), 6.8 (4H, arom.), 2.3-2.2 (6H, CH₃), 2.2-1.9 (18H, CH₃).

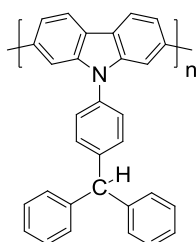
¹³C NMR (151 MHz, [D₈]THF): δ = 147.5 (quart.), 144.8 (quart.), 143.5 (quart.), 141.6 (quart.), 141.4 (quart.), 141.1 (quart.), 140.5 (quart.), 139.8 (quart.), 135.3 (quart.), 129.8 (CH), 129.7 (CH), 126.3 (CH), 125.5 (quart.), 119.6 (CH), 111.2 (CH), 22.3 (CH₃), 20.4 (CH₃).

MALDI-MS: m/z calcd. for C₂₂₈H₂₁₈B₆N₆ 3107.08, found 3106.99, Δ = 29 ppm;
m/z calcd. for C₂₆₆H₂₅₄B₇N₇ 3624.59, found 3624.64, Δ = 14 ppm;
m/z calcd. for C₃₀₄H₂₉₀B₈N₈ 4142.10, found 4142.09, Δ = 2.4 ppm;
m/z calcd. for C₃₄₂H₃₂₆B₉N₉ 4659.61, found 4659.86, Δ = 54 ppm;
m/z calcd. for C₃₈₀H₃₆₂B₁₀N₁₀ 5177.12, found 5177.29, Δ = 33 ppm;
m/z calcd. for C₄₁₈H₃₉₈B₁₁N₁₁ 5694.63, found 5694.72, Δ

= 16 ppm; m/z calcd. for $C_{456}H_{434}B_{12}N_{12}$ 6212.14, found 6212.50, Δ = 58 ppm; m/z calcd. for $C_{494}H_{470}B_{13}N_{13}$ 6729.65, found 6729.62, Δ = 4.5 ppm; m/z calcd. for $C_{532}H_{506}B_{14}N_{14}$ 7247.16, found 7247.47, Δ = 43 ppm.

GPC (THF): \bar{M}_w = 6000 Da, \bar{M}_n = 4900 Da, PDI = 1.2.

Poly[*N*-(4-(diphenylmethyl)-phenyl)-carbazole]-2,7-diyl **P3**



Synthesis according to the preparation of **P1**.

Triphenylphosphine	47.6 mg (182 μ mol)
Zn powder	67.1 mg (1.03 mmol)
2,2'-Bipyridyl	2.33 mg (14.9 μ mol)
6c	150 mg (314 μ mol)
Anhydrous NiCl ₂	1.92 mg (14.9 μ mol)
<i>N,N</i> -Dimethylacetamide	0.50 mL

Formula: $[C_{31}H_{21}N]_n + 2H$

Yield: 67.0 mg (164 μ mol, 52 %) of a yellow solid.

Decomposition: 335 °C (acetone).

¹H NMR (400 MHz, CDCl₃): δ = 8.21-8.00 (2H, arom.), 7.68-7.28 (12H, arom.), 7.23-7.17 (6H, arom.), 5.66-5.58 (1H, benzylic).

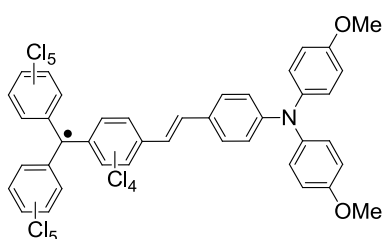
¹³C NMR: could not be recorded because of low solubility.

MALDI-MS: m/z calcd. for $C_{93}H_{65}N_3$ 1223.52, found 1223.49, Δ = 24 ppm; m/z calcd. for $C_{124}H_{86}N_4$ 1630.68, found 1630.69, Δ = 4 ppm; m/z calcd. for $C_{155}H_{107}N_5$ 2037.85, found 2037.92, Δ = 35 ppm.

GPC (THF): $\bar{M}_w = 1900$ Da, $\bar{M}_n = 1700$ Da, PDI = 1.1.

5.2.3 Synthesis of the Low Band Gap Polymer

Bis(2,3,4,5,6-pentachlorophenyl)-2,3,5,6-tetrachloro-4-((1E),2-[4-(bis(4-methoxyphenyl)amino)-phenyl]ethenyl)phenylmethyl radical **M**



CA: [828300-28-3]

Synthesis according to lit.²²⁶

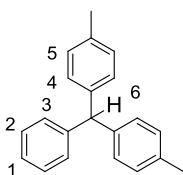
To a solution of the α -H compound²⁰⁵ of **M** (55.6 mg, 52.6 μ mol) in dry THF (5 mL) *n*-Bu₄NOH (70.1 μ L, 105 μ mol, ~1.5 M in H₂O) was added under the exclusion of air and light and the deep blue solution was stirred for 1 h during which it turned deep purple. After the addition of *p*-chloranil (33.2 mg, 135 μ mol) the resulting brown solution was stirred for 16 h. The solvent was removed and the mixture was diluted in dichloromethane and washed with slightly acidic water (HCl ~0.01 N, 2 x), with NaOH solution (5 %, 4 x) and with water (2 x). The organic phase was dried over MgSO₄, the solvent was removed and the raw product was purified by flash chromatography (PE/CH₂Cl₂ 1:1). Further purification by repeated dropwise addition of a concentrated acetone solution into methanol gave a brown solid.

Formula: C₄₁H₂₀Cl₁₄NO₂[•]

Yield: 31.8 mg (30.1 μ mol, 57 %) of a brown solid.

UV/vis/NIR(CH₂Cl₂): $\tilde{\nu}/\text{cm}^{-1}$ ($\epsilon/\text{M}^{-1} \text{cm}^{-1}$) = 34500 (24700), 25600 (41500), 24500 (34000), 20200 (8500), 17900 (4900), 12100 (4100).

4,4'-Dimethyltriphenylmethane 7



CA: [69511-00-8]

Synthesis according to lit.¹⁸⁰

To a solution of 4-methylphenylmagnesium bromide (40.6 g, 237 mmol) in 180 mL diethylether a solution of *p*-methylbenzophenone (28.1 g, 143 mmol) in 150 mL Et₂O was added dropwise over a period of 1 h. Subsequently the red reaction mixture was refluxed for 1 h, poured onto crushed ice and acidified with 6 N HCl (pH 3-4). The phases were separated and the aqueous phase was extracted with Et₂O (3 × 100 mL). The combined organic extracts were washed with water (3 × 100 mL) and dried over MgSO₄. After removal of the solvent formic acid (175 mL, 98-100 %) was added and the dark green mixture was refluxed for 3 h whereupon it turned brown. Then it was poured onto crushed ice and after addition of diethylether the aqueous phase was separated and extracted with Et₂O (3 × 75 mL). The combined organic phases were washed with saturated NaHCO₃ until neutral and dried over MgSO₄. Evaporation of the solvent and purification by flash chromatography (PE/CH₂Cl₂ 10:1) gave an oily product, which could be crystallized from *n*-hexane at -30 °C.

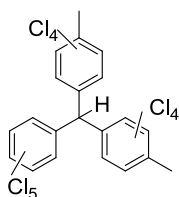
Formula: C₂₁H₂₀

Yield: 22.8 g (83.7 mmol, 59 %) of colourless needles.

¹H NMR (400 MHz, CDCl₃): δ = 7.30-7.24 (m, 2H, H2), 7.22-7.17 (m, 1H, H1), 7.13-7.10 (m, 2H, H3), 7.09 (AA', 4H, H4 or H5), 7.00 (BB', 4H, H4 or H5), 5.48 (s, 1H, H6), 2.32 (s, 6H, CH₃).

[Bis(4-methyl-2,3,5,6-tetrachlorophenyl)-(2,3,4,5,6-pentachlorophenyl)]methane

8



Synthesis according to lit.²⁰⁴

To a hot solution (70 °C) of S_2Cl_2 (3.42 g, 25.3 mmol) and anhydrous $AlCl_3$ (1.73 g, 13.0 mmol) in SO_2Cl_2 (400 mL) a solution of **7** (9.07 g, 33.3 mmol) in SO_2Cl_2 (200 mL) was added dropwise during 1 h. After 8 h of heating during which the reaction volume was kept constant by addition of further SO_2Cl_2 the latter was removed by distillation at atmospheric pressure and then in vacuum. 500 mL of water were then added and the mixture was made basic by the addition of $NaHCO_3$ whereupon it was heated to reflux during 1 h. The cooled mixture was acidified with conc. HCl (about 50 mL) and the solid was filtered off and washed with water. The crude product was repeatedly heated to reflux in *n*-hexane and filtered off until the *n*-hexane remained colourless.

Formula: $C_{21}H_7Cl_{13}$

Yield: 15.0 g (20.8 mmol, 63 %) of a grey solid.

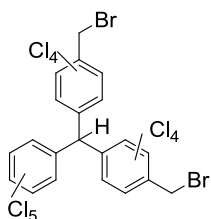
Decomposition: 313 °C (*n*-hexane).

1H NMR (600 MHz, $CDCl_3$): δ = 6.99 (s, 1H, CH), 2.62 (s, 6H, CH_3).

^{13}C NMR (151 MHz, $CDCl_3$): δ = 137.2 (quart.), 137.11 (quart.), 137.09 (quart.), 135.53 (quart.), 135.49 (quart.), 135.2 (CCI), 134.3 (CCI), 134.224 (CCI), 134.220 (CCI), 134.1 (CCI), 134.0 (CCI), 133.32 (CCI), 133.25 (CCI), 133.24 (CCI), 133.22 (CCI), 133.11 (CCI), 133.05 (CCI), 132.2 (CCI), 56.4 (CH), 20.633 (CH_3), 20.631 (CH_3).

APCI neg. (high resolution): calcd. for $[M-H]^+ = C_{21}H_6Cl_{13}^-$ 712.64258, found 712.64225, Δ = 0.47 ppm.

[Bis(4-bromomethyl-2,3,5,6-tetrachlorophenyl)-(2,3,4,5,6-pentachlorophenyl)]-methane **9**



Synthesis according to lit.²⁶⁵

A mixture of **8** (5.00 g, 6.94 mmol), *N*-bromosuccinimide (12.4 g, 69.4 mmol), azobis(isobutyronitrile) (273 mg, 1.67 mmol) and CCl₄ (150 mL) was refluxed (60 h). During the reaction *N*-bromosuccinimide (4 × 2.48 g, 4 × 13.9 mmol) and azobis(isobutyronitrile) (4 × 227 mg, 4 × 1.39 mmol) were added every 10-14 h. The reaction mixture was cooled to r. t., filtered, washed with CCl₄ and dried in vacuum. The crude product was refluxed in MeOH/CHCl₃ (5:1 and 1:1), cooled to r. t., filtered off and dried in vacuum.

Formula: C₂₁H₅Br₂Cl₁₃

Yield: 4.98 g (5.67 mmol, 82 %) of a yellowish solid.

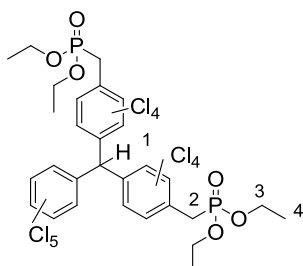
Decomposition: 218 °C (MeOH/CHCl₃).

¹H NMR (600 MHz, CDCl₃): δ = 7.02 (s, 1H, CH), 4.816 (s, 2H, CH₂), 4.814 (s, 2H, CH₂).

¹³C NMR (151 MHz, CDCl₃): δ = 138.0 (quart.), 136.25 (quart.), 136.21 (quart.), 136.20 (quart.), 135.09 (CCI), 135.07 (CCI), 135.0 (CCI), 134.59 (CCI), 134.58 (CCI), 134.03 (CCI), 134.01 (CCI), 133.96 (CCI), 133.7 (CCI), 133.53 (CCI), 133.47 (CCI), 133.46 (CCI), 132.5 (CCI), 56.7 (CH), 28.9 (CH₂).

ESI neg. (high resolution): calcd. for X+8 of [M]⁻ = C₂₁H₅Br₂Cl₁₃⁻ 876.45291, found 876.45248, Δ = 0.50 ppm.

[Bis(4-diethylphosphonomethyl-2,3,5,6-tetrachlorophenyl)-(2,3,4,5,6-penta-chlorophenyl)]methane 10



Synthesis according to lit.²²⁶

Under nitrogen atmosphere a mixture of **9** (3.42 g, 3.90 mmol) in degassed triethyl phosphite (15.6 mL) was heated to 180 °C (2 h). Triethyl phosphite was removed under reduced pressure (155 °C/0.03 mbar at the end of removal). The crude product was purified by flash chromatography (ethyl acetate/acetone 5:1).

Formula: C₂₉H₂₅Cl₁₃O₆P₂

Yield: 3.54 g (3.57 mmol, 91 %) of a colourless solid.

Meltig point: 89 °C (ethyl acetate/acetone).

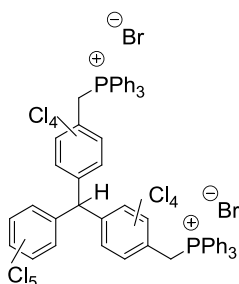
¹H NMR (400 MHz, CD₂Cl₂): δ = 7.01 (t, ⁷J_{PH} = 1.9 Hz, 1H, H1), 4.04 (m, 8H, H3), 3.73 (d, ²J_{PH} = 22.5 Hz, 4H, H2), 1.24 (td, ³J_{HH} = 7.1 Hz, ⁴J_{PH} = 1.3 Hz, 12H, H4).

¹³C NMR (101 MHz, CDCl₃, P decoupled): δ = 136.8 (quart.), 136.66 (quart.), 136.63 (quart.), 135.0 (CCI), 134.78 (CCI), 134.76 (CCI), 134.73 (CCI), 133.9 (CCI), 133.75 (CCI), 133.72 (CCI), 133.68 (CCI), 133.67 (CCI), 133.52 (CCI), 133.47 (CCI), 132.69 (quart.), 132.67 (quart.), 132.4 (CCI), 62.5 (C3), 56.7 (C1), 33.1 (C2), 16.33 (C4), 16.32 (C4).

³¹P NMR (162 MHz, CDCl₃): δ = 21.9.

ESI pos. (high resolution): calcd. for X+6 of [M + NH₄⁺]⁺ = C₂₉H₂₉Cl₁₃NO₆P₂⁺
1009.73325, found 1009.73317, Δ = 0.08 ppm.

[Bis(4-methylene-2,3,5,6-tetrachlorophenyl)-(2,3,4,5,6-pentachlorophenyl)]-methane bis(triphenyl)phosphonium dibromide 14



Synthesis according to lit.²²⁶

A mixture of **9** (3.00 g, 3.42 mmol) and triphenylphosphine (2.86 g, 10.9 mmol) in dry benzene (78 mL) was refluxed (18 h), cooled to r. t. and then filtered and washed with benzene. The crude product was refluxed in toluene and filtered off several times and then the solid was dried at 140 °C/0.1 mbar, whereupon it turned lilac. After cooling it turned nearly colourless again.

Formula: C₅₇H₃₅Br₂Cl₁₃P₂

Yield: 3.40 g (2.42 mmol, 71 %) of a slightly lilac solid.

Decomposition: 221 °C (toluene).

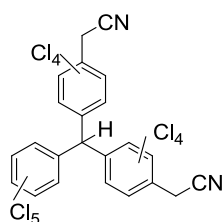
¹H NMR (400 MHz, [D₆]DMSO, P decoupled): δ = 7.96-7.90 (m, 6H, phenyl), 7.78-7.68 (m, 24H, phenyl), 6.81 (s, 1H, CH), 5.42 (d, ²J_{HH} = 16.0 Hz, 1H, CH₂), 5.41 (d, ²J_{HH} = 15.7 Hz, 1H, CH₂), 5.223 (d, ²J_{HH} = 15.7 Hz, 1H, CH₂), 5.215 (d, ²J_{HH} = 16.0 Hz, 1H, CH₂).

¹³C NMR (151 MHz, [D₆]DMSO): δ = 137.5 (quart.), 137.42 (quart.), 135.61 (quart.), 135.57 (CH_{para}), 135.5 (quart.), 135.3 (quart.), 134.5 (quart.), 134.3 (quart. and CH_{meta}), 134.1 (quart.), 133.6 (quart.), 133.5 (quart.), 133.4 (quart.), 133.1 (quart.), 132.9 (quart.), 131.8 (quart.), 130.3 (CH_{ortho}), 130.0 (quart.), 129.9 (quart.), 117.0 (quart., C_{ipso}), 56.3 (CH_{PCTM}), 31.02 (CH₂), 31.01 (CH₂).

³¹P NMR (162 MHz, [D₆]DMSO): δ = 20.31, 20.29.

ESI pos. (high resolution): calcd. for [M²⁺ - H⁺]⁺ = C₅₇H₃₄Cl₁₃P₂⁺ 1234.80811, found 1234.80810, Δ = 0.01 ppm.

[Bis(4-cyanomethyl-2,3,5,6-tetrachlorophenyl)-(2,3,4,5,6-pentachlorophenyl)]-methane 15



Synthesis according to lit.²⁶⁵

To a solution of **9** (1.28 g, 1.46 mmol) in 1,4-dioxane (200 mL) KCN (3.83 g, 58.8 mmol) dissolved in water was added and the resulting solution was stirred at r. t. (24 h). Water (100 mL) was added and the mixture was extracted with CHCl₃. The combined organic phases were washed with water and dried over MgSO₄. After evaporation of the solvent the crude product was purified by flash chromatography (PE/ethyl acetate 5:1), followed by reprecipitation by dropwise addition of a concentrated CH₂Cl₂ solution into PE and recrystallization from Et₂O/CH₂Cl₂ 2:1.

Formula: C₂₃H₅Cl₁₃N₂

Yield: 480 mg (623 μmol, 43 %) of a dark orange solid.

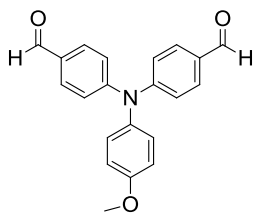
Decomposition: 304 °C (Et₂O/CH₂Cl₂).

¹H NMR (600 MHz, CDCl₃): δ = 7.03 (s, 1H, CH), 4.157 (s, 2H, CH₂), 4.155 (s, 2H, CH₂).

¹³C NMR (151 MHz, CDCl₃): δ = 138.47 (quart.), 138.43 (quart.), 135.8 (quart.), 135.30 (CCI), 135.25 (CCI), 134.9 (CCI), 134.62 (CCI), 134.57 (CCI), 134.23 (CCI), 134.22 (CCI), 134.0 (CCI), 133.9 (CCI), 133.6 (CCI), 133.53 (CCI), 133.49 (CCI), 132.7 (CCI), 129.64 (quart.), 129.62 (quart.), 114.5 (NC), 56.6 (CH), 22.7 (CH₂).

ESI neg. (high resolution): calcd. for [M - H⁺]⁻ = C₂₃H₄Cl₁₃N₂⁻ 762.63308, found 762.63265, Δ = 0.57 ppm.

4',4''-diformyl-4-methoxytriphenylamine 16



CA: [149676-16-4]

Synthesis according to lit.²²⁹

4-Methoxytriphenylamine ²³²	2.37 g (8.61 mmol)
Phosphoryl chloride	12.7 g (82.9 mmol)
DMF	32 mL

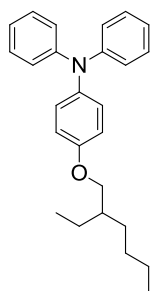
The crude product was dissolved in CH₂Cl₂ and washed with brine (4 x). The organic phase was dried over MgSO₄ and the solvent was evaporated to give an oil, which was purified by flash chromatography (*n*-hexane/ethyl acetate 4:1).

Formula: C₂₁H₁₇NO₃

Yield: 1.06 g (3.20 mmol, 37 %) of a yellow viscous liquid, which solidified on standing.

¹H NMR (400 MHz, CDCl₃): δ = 9.88 (s, 2H, COH), 7.76 (AA', 4H, arom.), 7.16 (BB', 4H, arom.), 7.11 (AA', 2H, arom.), 6.94 (BB', 4H, arom.), 3.85 (s, 3H, CH₃).

4-(2-Ethylhexyloxy)triphenylamine 11



CA: [450944-92-0]

Synthesis according to lit.⁹²

4-[2-(Ethylhexyl)oxy]-1-iodobenzene ⁹²	8.00 g (24.1 mmol)
Diphenylamine	2.72 g (16.1 mmol)
K ₂ CO ₃	11.2 g (81.0 mmol)
Cu powder	2.56 g (40.3 mmol)
18-Crown-6	533 mg (2.02 mmol)
1,2-Dichlorobenzene (dry)	36.0 mL

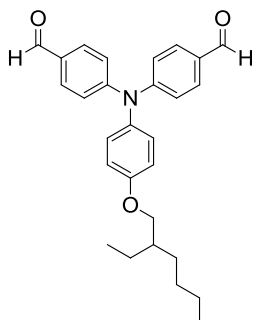
The reaction time was 4 d.

Formula: C₂₆H₃₁NO

Yield: 3.80 g (10.2 mmol, 63 %) of a colourless, viscous liquid which solidified on standing.

¹H NMR (400 MHz, [D₆]acetone): δ = 7.27-7.19 (m, 4H, arom.), 7.06-6.89 (m, 10H, arom.), 3.90 (d, 2H, OCH₂), 1.77-1.69 (m, 1H, CH), 1.58-1.29 (m, 8H, CH₂), 0.98-0.88 (m, 6H, CH₃).

4',4''-diformyl-4-(2-ethylhexyloxy)-triphenylamine 12



CA: [437769-71-6]

Synthesis according to lit.²²⁹

11	900 mg (2.41 mmol)
Phosphoryl chloride	3.87 g (25.3 mmol)
DMF	4.74 mL

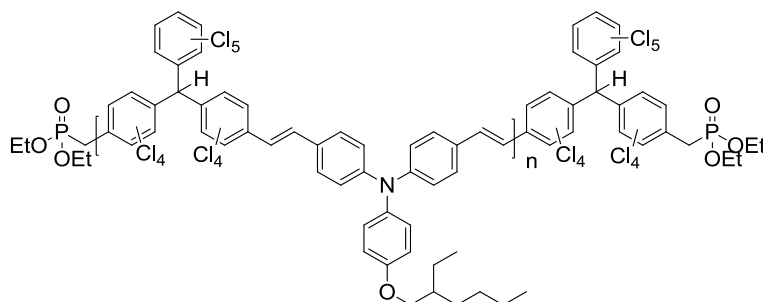
The crude product was dissolved in CH₂Cl₂ and washed with brine (4 x). The organic phase was dried over MgSO₄ and the solvent was evaporated to give an oil, which was purified by flash chromatography with *n*-hexane/ethyl acetate 5:1 → 4:1.

Formula: C₂₈H₃₁NO₃

Yield: 420 mg (978 μmol, 41 %) of a yellow oil.

¹H NMR (400 MHz, [D₆]acetone): δ = 9.91 (s, 2H, COH), 7.83 (AA', 4H, arom.), 7.23-7.16 (broad, 6H, arom.), 7.06 (BB', 2H, arom.), 3.96 (d, 2H, OCH₂), 1.80-1.71 (m, 1H, CH), 1.60-1.31 (m, 8H, CH₂), 1.01-0.84 (m, 6H, CH₃).

Poly{[[(2,3,4,5,6-pentachlorophenyl)-bis(2,3,5,6-tetrachlorophenyl)methane)-4,4'-diyl]-*alt*-4,4'-bis(vinylphenyl)-4-(2-ethylhexyloxy)phenylamine} 17



Under nitrogen atmosphere **10** (475 mg, 479 μmol) and **12** (200 mg, 466 μmol) were dissolved in dry THF (4.65 mL). To the yellow solution KO^tBu (113 mg, 1.01 mmol) was added in four portions and the mixture was stirred at r. t. (3 h). The resulting black, viscous liquid was poured onto HCl (0.01 M, 100 mL) to give a yellow precipitate that was stirred for a few minutes, filtered off and washed with water and acetone. The crude product was washed in a Soxhlet apparatus with acetone over night, dried, dissolved in THF and precipitated by dropwise addition of the concentrated THF solution into *n*-hexane.

Formula: $[\text{C}_{49}\text{H}_{34}\text{Cl}_{13}\text{NO}]_n + \text{C}_{29}\text{H}_{25}\text{Cl}_{13}\text{O}_6\text{P}_2$

Yield: 378 mg (339 μmol , 73 %) of a yellow solid.

Decomposition: 293 $^\circ\text{C}$ (THF/*n*-hexane).

^1H NMR (600 MHz, $[\text{D}_8]\text{THF}$): $\delta = 7.47$ (AA', 4H, arom.), 7.13 (s, 1H, CH_{PCTM}), 7.12-7.01 (m, 10H, AA', BB' and C-CH=CH-C), 6.92 (BB', 2H, arom.), 3.88 (d, $^3J_{\text{HH}} = 5.6$ Hz, 2H, OCH_2 , ethylhexyl), 1.72 (s, 1H, $\text{CH}_{\text{ethylhexyl}}$)²⁶⁶, 1.59-1.30 (m, 8H, CH_2 , ethylhexyl), 0.96 (t, $^3J_{\text{HH}} = 7.5$ Hz, 3H, CH_3 , ethylhexyl), 0.92 (t, $^3J_{\text{HH}} = 6.9$ Hz, 3H, CH_3 , ethylhexyl).

^{13}C NMR (151 MHz, $[\text{d}_8]\text{THF}$): $\delta = 157.9$ (quart.), 149.4 (quart.), 140.4 (quart.), 139.21 (quart.), 139.18 (quart.), 139.1 (CH), 138.3 (quart.), 136.98 (quart.), 136.95 (quart.), 136.1 (quart.), 135.7 (quart.), 135.6 (quart.), 134.9 (quart.), 134.71 (quart.), 134.68 (quart.), 134.32 (quart.), 134.28 (quart.), 134.22 (quart.), 134.17 (quart.),

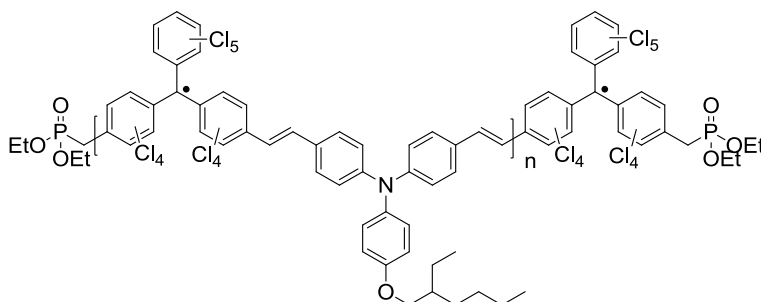
133.2 (quart.), 133.11 (quart.), 133.08 (quart.), 130.8 (quart.),
128.8 (CH), 128.6 (CH), 123.5 (CH), 121.7 (CH), 116.3 (CH),
71.1 (OCH₂, ethylhexyl), 57.8 (CH_{PCTM}), 40.6 (CH_{ethylhexyl}), 31.5 (CH₂,
ethylhexyl), 30.0 (CH₂, ethylhexyl), 24.8 (CH₂, ethylhexyl), 23.9 (CH₂,
ethylhexyl), 14.4 (CH₃, ethylhexyl), 11.5 (CH₃, ethylhexyl).

GPC (THF): $\bar{M}_w = 17100$ Da, $\bar{M}_n = 9600$ Da, PDI = 1.77.

IR: $\tilde{\nu}/\text{cm}^{-1} = 3037$ (w), 2956 (m), 2927 (m), 2869 (m), 2860 (m),
1628 (w), 1595 (s), 1540 (w), 1506 (s), 1466 (w), 1365 (m), 1316
(s), 1292 (s), 1269 (v), 1240 (s), 1191 (w), 1178 (m), 1164 (w),
1139 (w), 1105 (w), 1028 (w), 967 (w), 910 (w), 809 (m), 728 (w).

UV/vis(CH₂Cl₂): $\tilde{\nu}/\text{cm}^{-1}$ ($\epsilon/\text{M}^{-1} \text{cm}^{-1}$) = 34500 (34000), 24500 (42100).

Poly{[(((2,3,4,5,6-pentachlorophenyl)-bis(2,3,5,6-tetrachlorophenyl)methyl radical)-4,4'-diy)]-*alt*-4,4'-bis(vinylphenyl)-4-(2-ethylhexyloxy)phenylamin} P4



Synthesis according to lit.²²⁶

Under nitrogen atmosphere polymer **17** (100 mg, 89.8 μmol) was dissolved in dry THF (4.5 mL). $n\text{Bu}_4\text{NOH}$ (125 μL , 188 μmol , ~ 1.5 M in H_2O) was added whereupon the colour of the reaction mixture immediately changed from yellow to dark blue. After 1 h of stirring at r. t. *p*-chloranil (57.4 mg, 233 μmol) was added and the dark brown mixture was further stirred at r. t. (21 h) before it was dropped into a mixture of acetone (70 mL) and 2 N HCl (0.12 mL) to give a dark brown precipitate which was separated by centrifugation and washed with MeOH. The product was dissolved in THF, dropped into acetone (70 mL)/2 N HCl (0.12 mL), centrifuged and washed with MeOH two more times. Finally it was washed with acetone in a Soxhlet apparatus over night.

Formula: $[\text{C}_{49}\text{H}_{33}\text{Cl}_{13}\text{NO}]_n + \text{C}_{29}\text{H}_{25}\text{Cl}_{13}\text{O}_6\text{P}_2$

Yield: 88.6 mg (79.6 μmol , 89 %) of a dark brown powder.

Decomposition: 250 $^\circ\text{C}$ (DSC measurement, acetone).

GPC (THF): $\bar{M}_w = 19300$ Da, $\bar{M}_n = 11200$ Da, PDI = 1.72.

IR: $\tilde{\nu}/\text{cm}^{-1} = 3033$ (w), 2953 (m), 2924 (m), 2869 (m), 2860 (m), 1592 (s), 1506 (s), 1467 (w), 1426 (w), 1379 (w), 1335 (v), 1323 (s), 1287 (m), 1259 (s), 1239 (s), 1225 (v), 1192 (w), 1178 (s), 1164 (m), 1027 (w), 964 (w), 814 (w), 737 (w), 661 (w).

UV/vis/NIR(CH_2Cl_2): $\tilde{\nu}/\text{cm}^{-1}$ ($\epsilon/\text{M}^{-1} \text{cm}^{-1}$) = 34700 (28600), 23800 (43300), 20000 (shoulder), 17600 (shoulder), 12600 (6300).

6 References

- (1) Chiang, C. K.; Druy, M. A.; Gau, S. C.; Heeger, A. J.; Louis, E. J.; MacDiarmid, A. G.; Park, Y. W.; Shirakawa, H. *J. Am. Chem. Soc.* **1978**, *100*, 1013-1015.
- (2) Heeger, A. J. *Angew. Chem.* **2001**, *113*, 2660-2682.
- (3) MacDiarmid, A. G. *Angew. Chem.* **2001**, *113*, 2649-2659.
- (4) Shirakawa, H. *Angew. Chem.* **2001**, *113*, 2642-2648.
- (5) Moerner, W. E.; Silence, S. M. *Chem. Rev.* **1994**, *94*, 127-155.
- (6) Steckler, T. T.; Zhang, X.; Hwang, J.; Honeyager, R.; Ohira, S.; Zhang, X.-H.; Grant, A.; Ellinger, S.; Odom, S. A.; Sweat, D.; Tanner, D. B.; Rinzler, A. G.; Barlow, S.; Brédas, J.-L.; Kippelen, B.; Marder, S. R.; Reynolds, J. R. *J. Am. Chem. Soc.* **2009**, *131*, 2824-2826.
- (7) Usta, H.; Facchetti, A.; Marks, T. J. *J. Am. Chem. Soc.* **2008**, *130*, 8580-8581.
- (8) Zaumseil, J.; Sirringhaus, H. *Chem. Rev.* **2007**, *107*, 1296-1323.
- (9) Zhu, Z.; Waller, D.; Gaudiana, R.; Morana, M.; Mühlbacher, D.; Scharber, M.; Brabec, C. *Macromolecules* **2007**, *40*, 1981-1986.
- (10) Chen, M. X.; Perzon, E.; Robisson, N.; Jönsson, S. K. M.; Andersson, M. R.; Fahlman, M.; Berggren, M. *Synth. Met.* **2004**, *146*, 233-236.
- (11) Gong, X.; Wang, S. Polymer Light-Emitting Diodes: Devices and Materials. In *Introduction to Organic Electronic and Optoelectronic Materials and Devices*; Sun, S.-S. and Dalton, L. R., Eds.; CRC Press: Boca Raton, 2008.
- (12) Kulkarni, A. P.; Kong, X.; Janekhe, S. A. *Macromolecules* **2006**, *39*, 8699-8711.
- (13) Blouin, N.; Michaud, A.; Gendron, D.; Wakim, S.; Blair, E.; Neagu-Plesu, R.; Belletête, M.; Durocher, G.; Tao, Y.; Leclerc, M. *J. Am. Chem. Soc.* **2008**, *130*, 732-742.
- (14) Bundgaard, E.; Krebs, F. C. *Sol. Energy Mater. Sol. Cells* **2007**, *91*, 954-985.
- (15) Sun, S.-S.; Zhang, C. Organic and Polymeric Photovoltaic Materials and Devices. In *Introduction to Organic Electronic and Optoelectronic Materials and Devices*; Sun, S.-S. and Dalton, L. R., Eds.; CRC Press: Boca Raton, 2008.
- (16) Wienk, M. M.; Turbiez, M.; Gilot, J.; Janssen, R. A. J. *Adv. Mater.* **2008**, *20*, 2556-2560.
- (17) Arias, A. C.; Ready, S. E.; Lujan, R.; Wong, W. S.; Paul, K. E.; Salleo, A.; Chabinyc, M. L.; Apte, R.; Street, R. A.; Wu, Y.; Liu, P.; Ong, B. *Appl. Phys. Lett.* **2004**, *85*, 3304-3306.
- (18) de Gans, B.-J.; Duineveld, P. C.; Schubert, U. S. *Adv. Mater.* **2004**, *16*, 203-213.
- (19) Allard, S.; Forster, M.; Souharce, B.; Thiem, H.; Scherf, U. *Angew. Chem. Int. Ed.* **2008**, *47*, 4070-4098.
- (20) Sandberg, H. G. O. Polymer Field-Effect Transistors. In *Introduction to Organic Electronic and Optoelectronic Materials and Devices*; Sun, S.-S. and Dalton, L. R., Eds.; CRC Press: Boca Raton, 2008.
- (21) Gelinck, G. H.; Huitema, H. E. A.; van Veenendaal, E.; Cantatore, E.; Schrijnemakers, L.; van der Putten, J. B. P. H.; Geuns, T. C. T.; Beenhakkers, M.; Giesbers, J. B.; Huisman, B.-H.; Meijer, E. J.; Benito, E. M.; Touwslager, F. J.; Marsman, A. W.; van Rens, B. J. E.; de Leeuw, D. M. *Nat. Mater.* **2004**, *3*, 106-110.

- (22) Rogers, J. A.; Bao, Z. *J. Polym. Sci. A: Polym. Chem.* **2002**, *40*, 3327-3334.
- (23) Sheraw, C. D.; Zhou, L.; Huang, J. R.; Gundlach, D. J.; Jackson, T. N.; Kane, M. G.; Hill, I. G.; Hammond, M. S.; Campi, J.; Greening, B. K.; Francl, J.; West, J. *Appl. Phys. Lett.* **2002**, *80*, 1088-1090.
- (24) <https://projects.imec.be/oricla/>.
- (25) <http://www.polyic.com/en/projects.php#>.
- (26) <http://www.polyic.com/en/poly-logo.php>.
- (27) Sirringhaus, H. *Adv. Mater.* **2005**, *17*, 2411-2425.
- (28) Arias, A. C.; Endicott, F.; Street, R. A. *Adv. Mater.* **2006**, *18*, 2900-2904.
- (29) Hoshino, S.; Yoshida, M.; Uemura, S.; Kodzasa, T.; Takada, N.; Kamata, T.; Yase, K. *J. Appl. Phys.* **2004**, *95*, 5088-5093.
- (30) Russell, D. M.; Kugler, T.; Newsome, C. J.; Li, S. P.; Ishida, M.; Shimoda, T. *Synth. Met.* **2006**, *156*, 769-772.
- (31) Street, R. A.; Salleo, A. *Appl. Phys. Lett.* **2002**, *81*, 2887-2889.
- (32) Cho, J. H.; Kim, D. H.; Jang, Y.; Lee, W. H.; Ihm, K.; Han, J.-H.; Chung, S.; Cho, K. *Appl. Phys. Lett.* **2006**, *89*, 132101.
- (33) Gao, Y. Organic/Metal Interface Properties. In *Introduction to Organic Electronic and Optoelectronic Materials and Devices*; Sun, S.-S. and Dalton, L. R., Eds.; CRC Press: Boca Raton, 2008.
- (34) Cheng, X.; Noh, Y.-Y.; Wang, J.; Tello, M.; Frisch, J.; Blum, R.-P.; Vollmer, A.; Rabe, J. P.; Koch, N.; Sirringhaus, H. *Adv. Funct. Mater.* **2009**, *19*, 2407-2415.
- (35) Schmechel, R.; Ahles, M.; von Seggern, H. *J. Appl. Phys.* **2005**, *98*, 084511.
- (36) Bürgi, L.; Richards, T. J.; Friend, R. H.; Sirringhaus, H. *J. Appl. Phys.* **2003**, *94*, 6129-6137.
- (37) Kawase, T.; Shimoda, T.; Newsome, C.; Sirringhaus, H.; Friend, R. H. *Thin Solid Films* **2003**, *438*, 279-287.
- (38) Sele, C. W.; von Werne, T.; Friend, R. H.; Sirringhaus, H. *Adv. Mater.* **2005**, *17*, 997-1001.
- (39) Sirringhaus, H.; Kawase, T.; Friend, R. H.; Shimoda, T.; Inbasekaran, M.; Wu, W.; Woo, E. P. *Science* **2000**, *290*, 2123-2126.
- (40) Lefenfeld, M.; Blanchet, G.; Rogers, J. A. *Adv. Mater.* **2003**, *15*, 1188-1191.
- (41) Mäkelä, T.; Jussila, S.; Kosonen, H.; Bäcklund, T. G.; Sandberg, H. G. O.; Stubb, H. *Synth. Met.* **2005**, *153*, 285-288.
- (42) Lee, K. S.; Smith, T. J.; Dickey, K. C.; Yoo, J. E.; Stevenson, K. J.; Loo, Y.-L. *Adv. Funct. Mater.* **2006**, *16*, 2409-2414.
- (43) Chua, L.-L.; Zaumseil, J.; Chang, J.-F.; Ou, E. C.-W.; Ho, P. K.-H.; Sirringhaus, H.; Friend, R. H. *Nature* **2005**, *434*, 194-199.
- (44) Veres, J.; Ogier, S. D.; Leeming, S. W.; Cupertino, D. C.; Khaffaf, S. M. *Adv. Funct. Mater.* **2003**, *13*, 199-204.
- (45) Menard, E.; Podzorov, V.; Hur, S.-H.; Gaur, A.; Gershenson, M. E.; Rogers, J. A. *Adv. Mater.* **2004**, *16*, 2097-2101.
- (46) Podzorov, V.; Menard, E.; Borissov, A.; Kiryukhin, V.; Rogers, J. A.; Gershenson, M. E. *Phys. Rev. Lett.* **2004**, *93*, 086602.
- (47) Yan, H.; Chen, Z.; Zheng, Y.; Newman, C.; Quinn, J. R.; Dötz, F.; Kastler, M.; Facchetti, A. *Nature* **2009**, *457*, 679-686.
- (48) Facchetti, A. Molecular Semiconductors for Organic Field-Effect Transistors. In *Introduction to Organic Electronic and Optoelectronic Materials and Devices*; Sun, S.-S. and Dalton, L. R., Eds.; CRC Press: Boca Raton, 2008.

- (49) Sirringhaus, H.; Brown, P. J.; Friend, R. H.; Nielsen, M. M.; Bechgaard, K.; Langeveld-Voss, B. M. W.; Spiering, A. J. H.; Janssen, R. A. J.; Meijer, E. W.; Herwig, P.; de Leeuw, D. M. *Nature* **1999**, *401*, 685-688.
- (50) Tanase, C.; Wildeman, J.; Blom, P. W. M.; Benito, M. E. M.; de Leeuw, D. M.; van Breemen, A. J. J. M.; Herwig, P. T.; Chlon, C. H. T.; Sweelssen, J.; Schoo, H. F. M. *J. Appl. Phys.* **2005**, *97*, 123703.
- (51) van Breemen, A. J. J. M.; Herwig, P. T.; Chlon, C. H. T.; Sweelssen, J.; Schoo, H. F. M.; Benito, E. M.; de Leeuw, D. M.; Tanase, C.; Wildeman, J.; Blom, P. W. M. *Adv. Funct. Mater.* **2005**, *15*, 872-876.
- (52) Ullmann, A.; Ficker, J.; Fix, W.; Rost, H.; Clemens, W.; McCulloch, I.; Giles, M. *Mater. Res. Soc. Proc.* **2001**, *665*, C7.5.
- (53) Wang, G.; Swensen, J.; Moses, D.; Heeger, A. J. *J. Appl. Phys.* **2003**, *93*, 6137-6141.
- (54) Kline, R. J.; McGehee, M. D.; Kadnikova, E. N.; Liu, J.; Fréchet, J. M. J. *Adv. Mater.* **2003**, *15*, 1519-1522.
- (55) Kline, R. J.; McGehee, M. D.; Kadnikova, E. N.; Liu, J.; Fréchet, J. M. J.; Toney, M. F. *Macromolecules* **2005**, *38*, 3312-3319.
- (56) Zen, A.; Pflaum, J.; Hirschmann, S.; Zhuang, W.; Jaiser, F.; Asawapirom, U.; Rabe, J. P.; Scherf, U.; Neher, D. *Adv. Funct. Mater.* **2004**, *14*, 757-764.
- (57) Chen, T.-A.; Wu, X.; Rieke, R. D. *J. Am. Chem. Soc.* **1995**, *117*, 233-244.
- (58) Pan, H.; Li, Y.; Wu, Y.; Liu, P.; Ong, B. S.; Zhu, S.; Xu, G. *J. Am. Chem. Soc.* **2007**, *129*, 4112-4113.
- (59) McCulloch, I.; Heeney, M.; Bailey, C.; Genevicius, K.; MacDonald, I.; Shkunov, M.; Sparrowe, D.; Tierney, S.; Wagner, R.; Zhang, W.; Chabinyk, M. L.; Kline, R. J.; McGehee, M. D.; Toney, M. F. *Nat. Mater.* **2006**, *5*, 328-333.
- (60) Zhang, M.; Tsao, H. N.; Pisula, W.; Yang, C.; Mishra, A. K.; Müllen, K. *J. Am. Chem. Soc.* **2007**, *129*, 3472-3473.
- (61) Liu, J.; Zhang, R.; Sauv e, G.; Kowalewski, T.; McCullough, R. D. *J. Am. Chem. Soc.* **2008**, *130*, 13167-13176.
- (62) Veres, J.; Ogier, S.; Lloyd, G.; de Leeuw, D. *Chem. Mater.* **2004**, *16*, 4543-4555.
- (63) Zielke, D.; H ubler, A. C.; Hahn, U.; Brandt, N.; Bartzsch, M.; F ugmann, U.; Fischer, T.; Veres, J.; Ogier, S. *Appl. Phys. Lett.* **2005**, *87*, 123508.
- (64) de Leeuw, D. M.; Simenon, M. M. J.; Brown, A. R.; Einerhand, R. E. F. *Synth. Met.* **1997**, *87*, 53-59.
- (65) Yoon, M.-H.; Kim, C.; Facchetti, A.; Marks, T. J. *J. Am. Chem. Soc.* **2006**, *128*, 12851-12869.
- (66) Letizia, J. A.; Salata, M. R.; Tribout, C. M.; Facchetti, A.; Ratner, M. A.; Marks, T. J. *J. Am. Chem. Soc.* **2008**, *130*, 9679-9694.
- (67) Zhan, X.; Tan, Z.; Domercq, B.; An, Z.; Zhang, X.; Barlow, S.; Li, Y.; Zhu, D.; Kippelen, B.; Marder, S. R. *J. Am. Chem. Soc.* **2007**, *129*, 7246-7247.
- (68) Babel, A.; Jenekhe, S. A. *J. Am. Chem. Soc.* **2003**, *125*, 13656-13657.
- (69) Meijer, E. J.; de Leeuw, D. M.; Setayesh, S.; van Veenendaal, E.; Huisman, B.-H.; Blom, P. W. M.; Hummelen, J. C.; Scherf, U.; Klapwijk, T. M. *Nat. Mater.* **2003**, *2*, 678-682.
- (70) Singh, T. B.; Marjanovi c, N.; Matt, G. J.; G unes, S.; Sariciftci, N. S.; Moutaigne Ramil, A.; Andreev, A.; Sitter, H.; Schw odiauer, R.; Bauer, S. *Org. Electron.* **2005**, *6*, 105-110.
- (71) Wang, J.; Wang, H.; Yan, X.; Huang, H.; Yan, D. *Appl. Phys. Lett.* **2005**, *87*, 093507.

- (72) Wang, S. D.; Kanai, K.; Ouchi, Y.; Seki, K. *Org. Electron.* **2006**, *7*, 457-464.
- (73) Liu, C.; Sirringhaus, H. *Org. Electron.* **2010**, *11*, 558-563.
- (74) Szendrei, K.; Jarzab, D.; Chen, Z.; Facchetti, A.; Loi, M. A. *J. Mater. Chem.* **2010**, *20*, 1317-1321.
- (75) Swensen, J. S.; Yuen, J.; Gargas, D.; Buratto, S. K.; Heeger, A. J. *J. Appl. Phys.* **2007**, *102*, 013103.
- (76) Zaumseil, J.; Friend, R. H.; Sirringhaus, H. *Nat. Mater.* **2006**, *5*, 69-74.
- (77) Kajii, H.; Koiwai, K.; Hirose, Y.; Ohmori, Y. *Org. Electron.* **2010**, *11*, 509-513.
- (78) Bijleveld, J. C.; Zoombelt, A. P.; Mathijssen, S. G. J.; Wienk, M. M.; Turbiez, M.; de Leeuw, D. M.; Janssen, R. A. J. *J. Am. Chem. Soc.* **2009**, *131*, 16616-16617.
- (79) Bürgi, L.; Turbiez, M.; Pfeiffer, R.; Bienewald, F.; Kirner, H.-J.; Winnewisser, C. *Adv. Mater.* **2008**, *20*, 2217-2224.
- (80) Zaumseil, J.; Donley, C. L.; Kim, J.-S.; Friend, R. H.; Sirringhaus, H. *Adv. Mater.* **2006**, *18*, 2708-2712.
- (81) Naber, R. C. G.; Bird, M.; Sirringhaus, H. *Appl. Phys. Lett.* **2008**, *93*, 023301.
- (82) Zoombelt, A. P.; Mathijssen, S. G. J.; Turbiez, M. G. R.; Wienk, M. M.; Janssen, R. A. J. *J. Mater. Chem.* **2010**, *20*, 2240-2246.
- (83) <http://www.oled.at/produkte.htm>.
- (84) <http://www.novaled.com/aboutoleds/oledsindisplay.html>.
- (85) http://www.novaled.com/news/2010_05_20_pr.html.
- (86) Reineke, S.; Lindner, F.; Schwartz, G.; Seidler, N.; Walzer, K.; Lussem, B.; Leo, K. *Nature* **2009**, *459*, 234-U116.
- (87) http://www.newscenter.philips.com/de_de/standard/news/lighting/20100913_Philips_praesentiert_weltweit_erstes_Weisslicht_OLED_Modul.wpd.
- (88) <http://www.lighting.philips.com/main/lightcommunity/trends/led/lumiblade.wpd>.
- (89) Hertel, D.; Müller, C. D.; Meerholz, K. *Chem. Unserer Zeit* **2005**, *39*, 336-347.
- (90) Fu, Y.; Sun, M.; Wu, Y.; Bo, Z.; Ma, D. *J. Polym. Sci. A: Polym. Chem.* **2008**, *46*, 1349-1356.
- (91) Huang, J.; Niu, Y.; Xu, Y.; Hou, Q.; Yang, W.; Mo, Y.; Yuan, M.; Cao, Y. *Synth. Met.* **2003**, *135-136*, 181-182.
- (92) Karastatiris, P.; Mikroyannidis, J. A.; Spiliopoulos, I. K. *J. Polym. Sci. A: Polym. Chem.* **2008**, *46*, 2367-2378.
- (93) Mazzeo, M.; Vitale, V.; Della Sala, F.; Anni, M.; Barbarella, G.; Favaretto, L.; Sotgiu, G.; Cingolani, R.; Gigli, G. *Adv. Mater.* **2005**, *17*, 34-39.
- (94) Yuan, M.-C.; Shih, P.-I.; Chien, C.-H.; Shu, C.-F. *J. Polym. Sci. A: Polym. Chem.* **2007**, *45*, 2925-2937.
- (95) *Conjugated Polymers and Molecular Interfaces*. Salaneck, W. R., et al., Eds.; Marcel Dekker: New York, 2002.
- (96) Wang, L.; Matson, D. W.; Polikarpov, E.; Swensen, J. S.; Bonham, C. C.; Cosimbescu, L.; Berry, J. J.; Ginley, D. S.; Gaspar, D. J.; Padmaperuma, A. B. *J. Appl. Phys.* **2010**, *107*, 043103.
- (97) Matsumoto, N.; Miyazaki, T.; Nishiyama, M.; Adachi, C. *J. Phys. Chem. C* **2009**, *113*, 6261-6266.
- (98) Kulkarni, A. P.; Zhu, Y.; Babel, A.; Wu, P. T.; Jenekhe, S. A. *Chem. Mater.* **2008**, *20*, 4212-4223.
- (99) Kinoshita, M.; Kita, H.; Shirota, Y. *Adv. Funct. Mater.* **2002**, *12*, 780-786.
- (100) Murata, H.; Kafafi, Z. H.; Uchida, M. *Appl. Phys. Lett.* **2002**, *80*, 189-191.

- (101) Palilis, L. C.; Mäkinen, A. J.; Uchida, M.; Kafafi, Z. H. *Appl. Phys. Lett.* **2003**, *82*, 2209-2211.
- (102) Shirota, Y.; Kuwabara, Y.; Inada, H.; Wakimoto, T.; Nakada, H.; Yonemoto, Y.; Kawami, S.; Imai, K. *Appl. Phys. Lett.* **1994**, *65*, 807-809.
- (103) van Slyke, S. A.; Chen, C. H.; Tang, C. W. *Appl. Phys. Lett.* **1996**, *69*, 2160-2162.
- (104) Jia, W. L.; Feng, X. D.; Bai, D. R.; Lu, Z. H.; Wang, S.; Vamvounis, G. *Chem. Mater.* **2005**, *17*, 164-170.
- (105) Jin, S.-H.; Kim, W.-H.; Song, I.-S.; Kwon, S.-K.; Lee, K.-S.; Han, E.-M. *Thin Solid Films* **2000**, *363*, 255-258.
- (106) Zhang, H.; Huo, C.; Zhang, J.; Zhang, P.; Tian, W.; Wang, Y. *Chem. Commun.* **2006**, 281-283.
- (107) Morin, J.-F.; Beaupré, S.; Leclerc, M.; Lévesque, I.; D'lorio, M. *Appl. Phys. Lett.* **2002**, *80*, 341-343.
- (108) Romero, D. B.; Schaer, M.; Leclerc, M.; Adès, D.; Siove, A.; Zuppiroli, L. *Synth. Met.* **1996**, *80*, 271-277.
- (109) Doi, H.; Kinoshita, M.; Okumoto, K.; Shirota, Y. *Chem. Mater.* **2003**, *15*, 1080-1089.
- (110) Noda, T.; Shirota, Y. *J. Am. Chem. Soc.* **1998**, *120*, 9714-9715.
- (111) Jia, W. L.; Moran, M. J.; Yuan, Y.-Y.; Lu, Z. H.; Wang, S. *J. Mater. Chem.* **2005**, *15*, 3326-3333.
- (112) Jia, W.-L.; Bai, D.-R.; McCormick, T.; Liu, Q.-D.; Motala, M.; Wang, R.-Y.; Seward, C.; Tao, Y.; Wang, S. *Chem. Eur. J.* **2004**, *10*, 994-1006.
- (113) Noda, T.; Shirota, Y. *J. Lumin.* **2000**, *87-89*, 1168-1170.
- (114) <http://www.oled.at/oled-herstellung.htm>.
- (115) Huang, S.-T.; Liaw, D.-J.; Hsieh, L.-G.; Chang, C.-C.; Leung, M.-K.; Wang, K.-L.; Chen, W.-T.; Lee, K.-R.; Lai, J.-Y.; Chan, L.-H.; Chen, C.-T. *J. Polym. Sci. A: Polym. Chem.* **2009**, *47*, 6231-6245.
- (116) Li, H.; Hu, Y.; Zhang, Y.; Ma, D.; Wang, L.; Jing, X.; Wang, F. *J. Polym. Sci. A: Polym. Chem.* **2004**, *42*, 3947-3953.
- (117) Peng, Z.; Bao, Z.; Galvin, M. E. *Chem. Mater.* **1998**, *10*, 2086-2090.
- (118) Pu, Y.-J.; Kurata, T.; Soma, M.; Kido, J.; Nishide, H. *Synth. Met.* **2004**, *143*, 207-214.
- (119) Shu, C.-F.; Dodda, R.; Wu, F.-I.; Liu, M. S.; Jen, A. K.-Y. *Macromolecules* **2003**, *36*, 6698-6703.
- (120) <http://www.solarmer.com>.
- (121) Thompson, B. C.; Fréchet, J. M. J. *Angew. Chem. Int. Ed.* **2008**, *47*, 58-77.
- (122) Spanggaard, H.; Krebs, F. C. *Sol. Energy Mater. Sol. Cells* **2004**, *83*, 125-146.
- (123) Yu, G.; Gao, J.; Hummelen, J. C.; Wudl, F.; Heeger, A. J. *Science* **1995**, *270*, 1789-1791.
- (124) Dennler, G.; Scharber, M. C.; Brabec, C. J. *Adv. Mater.* **2009**, *21*, 1323-1338.
- (125) Brabec, C. J.; Zerza, G.; Cerullo, G.; De Silvestri, S.; Luzzati, S.; Hummelen, J. C.; Sariciftci, S. *Chem. Phys. Lett.* **2001**, *340*, 232-236.
- (126) Chen, C.-P.; Chan, S.-H.; Chao, T.-C.; Ting, C.; Ko, B.-T. *J. Am. Chem. Soc.* **2008**, *130*, 12828-12833.
- (127) Mühlbacher, D.; Scharber, M.; Morana, M.; Zhu, Z.; Waller, D.; Gaudiana, R.; Brabec, C. *Adv. Mater.* **2006**, *18*, 2884-2889.
- (128) Wienk, M. M.; Kroon, J. M.; Verhees, W. J. H.; Knol, J.; Hummelen, J. C.; van Hal, P. A.; Janssen, R. A. J. *Angew. Chem.* **2003**, *115*, 3493-3497.
- (129) Winder, C.; Sariciftci, N. S. *J. Mater. Chem.* **2004**, *14*, 1077-1086.

- (130) Scharber, M. C.; Mühlbacher, D.; Koppe, M.; Denk, P.; Waldauf, C.; Heeger, A. J.; Brabec, C. J. *Adv. Mater.* **2006**, *18*, 789-794.
- (131) Po, R.; Maggini, M.; Camaioni, N. *J. Phys. Chem. C* **2010**, *114*, 695-706.
- (132) Cai, W.; Gong, X.; Cao, Y. *Sol. Energy Mater. Sol. Cells* **2010**, *94*, 114-127.
- (133) Roncali, J. *Chem. Rev.* **1997**, *97*, 173-205.
- (134) Havinga, E. E.; ten Hoeve, W.; Wynberg, H. *Polym. Bull.* **1992**, *29*, 119-126.
- (135) Havinga, E. E.; ten Hoeve, W.; Wynberg, H. *Synth. Met.* **1993**, *55*, 299-306.
- (136) Brédas, J. L.; Heeger, A. J.; Wudl, F. *J. Chem. Phys.* **1986**, *85*, 4673-4678.
- (137) Meng, H.; Wudl, F. *Macromolecules* **2001**, *34*, 1810-1816.
- (138) Wudl, F.; Kobayashi, M.; Heeger, A. J. *J. Org. Chem.* **1984**, *49*, 3382-3384.
- (139) Blouin, N.; Michaud, A.; Leclerc, M. *Adv. Mater.* **2007**, *19*, 2295-2300.
- (140) Boudreault, P.-L. T.; Michaud, A.; Leclerc, M. *Macromol. Rapid Commun.* **2007**, *28*, 2176-2179.
- (141) Chen, H.-Y.; Hou, J.; Zhang, S.; Liang, Y.; Yang, G.; Yang, Y.; Yu, L.; Wu, Y.; Li, G. *Nat. Photon.* **2009**, *3*, 649-653.
- (142) Colladet, K.; Fourier, S.; Cleij, T. J.; Lutsen, L.; Gelan, J.; Vanderzande, D. *Macromolecules* **2007**, *40*, 65-72.
- (143) Liang, Y.; Feng, D.; Wu, Y.; Tsai, S.-T.; Li, G.; Ray, C.; Yu, L. *J. Am. Chem. Soc.* **2009**, *131*, 7792-7799.
- (144) Mikroyannidis, J. A.; Sharma, G. D.; Sharma, S. S.; Vijay, Y. K. *J. Phys. Chem. C* **2010**, *114*, 1520-1527.
- (145) Peet, J.; Kim, J. Y.; Coates, N. E.; Ma, W. L.; Moses, D.; Heeger, A. J.; Bazan, G. C. *Nat. Mater.* **2007**, *6*, 497-500.
- (146) Wong, W.-Y.; Wang, X.-Z.; He, Z.; Djurišić, A. B.; Yip, C.-T.; Cheung, K.-Y.; Wang, H.; Mak, C. S. K.; Chan, W.-K. *Nat. Mater.* **2007**, *6*, 521-527.
- (147) Yue, W.; Zhao, Y.; Tian, H.; Song, D.; Xie, Z.; Yan, D.; Geng, Y.; Wang, F. *Macromolecules* **2009**, *42*, 6510-6518.
- (148) Zhang, F.; Mammo, W.; Andersson, L. M.; Admassie, S.; Andersson, M. R.; Inganäs, O. *Adv. Mater.* **2006**, *18*, 2169-2173.
- (149) Ma, W.; Yang, C.; Gong, X.; Lee, K.; Heeger, A. J. *Adv. Funct. Mater.* **2005**, *15*, 1617-1622.
- (150) Reyes-Reyes, M.; Kim, K.; Carroll, D. L. *Appl. Phys. Lett.* **2005**, *87*, 083506.
- (151) Reyes-Reyes, M.; Kim, K.; Dewald, J.; López-Sandoval, R.; Avadhanula, A.; Curran, S.; Carroll, D. L. *Org. Lett.* **2005**, *7*, 5749-5752.
- (152) Al-Ibrahim, M.; Ambacher, O.; Sensfuss, S.; Gobsch, G. *Appl. Phys. Lett.* **2005**, *86*, 201120.
- (153) Chirvase, D.; Parisi, J.; Hummelen, J. C.; Dyakonov, V. *Nanotechnol.* **2004**, *15*, 1317-1323.
- (154) Li, G.; Yao, Y.; Yang, H.; Shrotriya, V.; Yang, G.; Yang, Y. *Adv. Funct. Mater.* **2007**, *17*, 1636-1644.
- (155) Padinger, F.; Rittberger, R. S.; Sariciftci, N. S. *Adv. Funct. Mater.* **2003**, *13*, 85-88.
- (156) Yang, X.; Loos, J.; Veenstra, S. C.; Verhees, W. J. H.; Wienk, M. M.; Kroon, J. M.; Michels, M. A. J.; Janssen, R. A. J. *Nano Lett.* **2005**, *5*, 579-583.
- (157) Morin, J.-F.; Leclerc, M.; Adès, D.; Siove, A. *Macromol. Rapid Commun.* **2005**, *26*, 761-778.
- (158) Paliulis, O.; Ostrauskaite, J.; Gaidelis, V.; Jankauskas, V.; Strohriegl, P. *Macromol. Chem. Phys.* **2003**, *204*, 1706-1712.
- (159) Lmimouni, K.; Legrand, C.; Chapoton, A. *Synth. Met.* **1998**, *97*, 151-155.
- (160) Stéphan, O.; Vial, J.-C. *Synth. Met.* **1999**, *106*, 115-119.

- (161) Morin, J.-F.; Leclerc, M. *Macromolecules* **2002**, *35*, 8413-8417.
- (162) Tirapattur, S.; Belletête, M.; Drolet, N.; Leclerc, M.; Durocher, G. *Chem. Phys. Lett.* **2003**, *370*, 799-804.
- (163) Iraqi, A.; Wataru, I. *Chem. Mater.* **2004**, *16*, 442-448.
- (164) Iraqi, A.; Simmance, T. G.; Yi, H.; Stevenson, M.; Lidzey, D. G. *Chem. Mater.* **2006**, *18*, 5789-5797.
- (165) Kulasi, A.; Yi, H.; Iraqi, A. *J. Polym. Sci. A: Polym. Chem.* **2007**, *45*, 5957-5967.
- (166) Sonntag, M.; Stroehriegl, P. *Chem. Mater.* **2004**, *16*, 4736-4742.
- (167) Zotti, G.; Schiavon, G.; Zecchin, S.; Morin, J.-F.; Leclerc, M. *Macromolecules* **2002**, *35*, 2122-2128.
- (168) Shirota, Y.; Kinoshita, M.; Noda, T.; Okumoto, K.; Ohara, T. *J. Am. Chem. Soc.* **2000**, *122*, 11021-11022.
- (169) Uchida, M.; Ono, Y.; Yokoi, H.; Nakano, T.; Furukawa, K. *J. Photopolym. Sci. Technol.* **2001**, *14*, 305-310.
- (170) Morin, J.-F.; Leclerc, M. *Macromolecules* **2001**, *34*, 4680-4682.
- (171) Ullmann, F.; Meyer, G. M.; Loewenthal, O.; Gilli, E. *Ann.* **1904**, *332*, 38-81.
- (172) Hammann, W. C.; Schisla, R. M. *J. Chem. Eng. Data* **1972**, *17*, 112-115.
- (173) Dierschke, F.; Grimsdale, A. C.; Müllen, K. *Synthesis* **2003**, *16*, 2470-2472.
- (174) Cadogan, J. I. G.; Cameron-Wood, M.; Mackie, R. K.; Searle, R. J. G. *J. Chem. Soc.* **1965**, 4831-4837.
- (175) Chmielewski, M. J.; Charon, M.; Jurczak, J. *Org. Lett.* **2004**, *6*, 3501-3504.
- (176) Doyle, M. P.; Siegfried, B.; Dellaria, J. F. *J. Org. Chem.* **1977**, *42*, 2426-2431.
- (177) de Groot, J. H.; Dillingham, K.; Deuring, H.; Haitjema, H. J.; van Beijma, F. J.; Hodd, K.; Norrby, S. *Biomacromolecules* **2001**, *2*, 1271-1278.
- (178) Stahl, R. *Dissertation* **2005**, University of Würzburg.
- (179) Stahl, R.; Lambert, C.; Kaiser, C.; Wortmann, R.; Jakober, R. *Chem. Eur. J.* **2006**, *12*, 2358-2370.
- (180) Brook, A. G.; Gilman, H.; Miller, L. S. *J. Am. Chem. Soc.* **1953**, *75*, 4759-4765.
- (181) Yamamoto, T.; Morita, A.; Miyazaki, Y.; Maruyama, T.; Wakayama, H.; Zhou, Z.-h.; Nakamura, Y.; Kanbara, T.; Sasaki, S.; Kubota, K. *Macromolecules* **1992**, *25*, 1214-1223.
- (182) Fu, Y.; Bo, Z. *Macromol. Rapid Commun.* **2005**, *26*, 1704-1710.
- (183) Wakim, S.; Blouin, N.; Gingras, E.; Tao, Y.; Leclerc, M. *Macromol. Rapid Commun.* **2007**, *28*, 1798-1803.
- (184) Li, J.; Dierschke, F.; Wu, J.; Grimsdale, A. C.; Müllen, K. *J. Mater. Chem.* **2006**, *16*, 96-100.
- (185) Zhang, Z.-B.; Fujiki, M.; Tang, H.-Z.; Motonaga, M.; Torimitsu, K. *Macromolecules* **2002**, *35*, 1988-1990.
- (186) Iovu, M. C.; Sheina, E. E.; Gil, R. R.; McCullough, R. D. *Macromolecules* **2005**, *38*, 8649-8656.
- (187) Ostrauskaite, J.; Stroehriegl, P. *Macromol. Chem. Phys.* **2003**, *204*, 1713-1718.
- (188) Yokozawa, T.; Adachi, I.; Miyakoshi, R.; Yokoyama, A. *High Perform. Polym.* **2007**, *19*, 684-699.
- (189) Perkampus, H.-H. *UV-VIS Atlas of Organic Compounds*. VCH: Weinheim, Germany, 1992. 532.
- (190) Belletête, M.; Bouchard, J.; Leclerc, M.; Durocher, G. *Macromolecules* **2005**, *38*, 880-887.
- (191) Strickler, S. J.; Berg, R. A. *J. Chem. Phys.* **1962**, *37*, 814-822.
- (192) Siebrand, W. *J. Chem. Phys.* **1967**, *46*, 440-447.

- (193) Iraqi, A.; Wataru, I. *J. Polym. Sci. A: Polym. Chem.* **2004**, *42*, 6041-6051.
- (194) Iraqi, A.; Wataru, I. *Synth. Met.* **2001**, *119*, 159-160.
- (195) Pommerehne, J.; Vestweber, H.; Guss, W.; Mahrt, R. F.; Bässler, H.; Porsch, M.; Daub, J. *Adv. Mater.* **1995**, *7*, 551-554.
- (196) Iraqi, A.; Pegington, R. C.; Simmance, T. G. *J. Polym. Sci. A: Polym. Chem.* **2006**, *44*, 3336-3342.
- (197) Iraqi, A.; Pickup, D. F.; Yi, H. *Chem. Mater.* **2006**, *18*, 1007-1015.
- (198) Liu, R.; Xiong, Y.; Zeng, W.; Wu, Z.; Du, B.; Yang, W.; Sun, M.; Cao, Y. *Macromol. Chem. Phys.* **2007**, *208*, 1503-1509.
- (199) http://en.wikipedia.org/wiki/CIE_1931_color_space.
- (200) Ajayaghosh, A. *Chem. Soc. Rev.* **2003**, *32*, 181-191.
- (201) Akoudad, S.; Roncali, J. *Chem. Commun.* **1998**, 2081-2082.
- (202) Zhou, E.; Wei, Q.; Yamakawa, S.; Zhang, Y.; Tajima, K.; Yang, C.; Hashimoto, K. *Macromolecules* **2010**, *43*, 821-826.
- (203) Heckmann, A. *diploma thesis 2004, University of Würzburg*.
- (204) Heckmann, A.; Lambert, C. *J. Am. Chem. Soc.* **2007**, *129*, 5515-5527.
- (205) Heckmann, A.; Lambert, C.; Goebel, M.; Wortmann, R. *Angew. Chem. Int. Ed.* **2004**, *43*, 5851-5856.
- (206) Domingo, V. M.; Castañer, J.; Riera, J.; Fajarí, L.; Labarta, A. *Chem. Mater.* **1995**, *7*, 314-323.
- (207) Maspoch, D.; Domingo, N.; Ruiz-Molina, D.; Wurst, K.; Tejada, J.; Rovira, C.; Veciana, J. *J. Am. Chem. Soc.* **2004**, *126*, 730-731.
- (208) Maspoch, D.; Domingo, N.; Ruiz-Molina, D.; Wurst, K.; Vaughan, G.; Tejada, J.; Rovira, C.; Veciana, J. *Angew. Chem. Int. Ed.* **2004**, *43*, 1828-1832.
- (209) Maspoch, D.; Ruiz-Molina, D.; Wurst, K.; Domingo, N.; Cavallini, M.; Biscarini, F.; Tejada, J.; Rovira, C.; Veciana, J. *Nat. Mater.* **2003**, *2*, 190-195.
- (210) Crivillers, N.; Mas-Torrent, M.; Perruchas, S.; Roques, N.; Vidal-Gancedo, J.; Veciana, J.; Rovira, C.; Basabe-Desmots, L.; Ravoo, B. J.; Crego-Calama, M.; Reinhoudt, D. N. *Angew. Chem. Int. Ed.* **2007**, *46*, 2215-2219.
- (211) Crivillers, N.; Mas-Torrent, M.; Vidal-Gancedo, J.; Veciana, J.; Rovira, C. *J. Am. Chem. Soc.* **2008**, *130*, 5499-5506.
- (212) Crivillers, N.; Munuera, C.; Mas-Torrent, M.; Simão, C.; Bromley, S. T.; Ocal, C.; Rovira, C.; Veciana, J. *Adv. Mater.* **2009**, *21*, 1177-1181.
- (213) Mas-Torrent, M.; Crivillers, N.; Mugnaini, V.; Ratera, I.; Rovira, C.; Veciana, J. *J. Mater. Chem.* **2009**, *19*, 1691-1695.
- (214) Amthor, S.; Lambert, C. *J. Phys. Chem. A* **2006**, *110*, 1177-1189.
- (215) Coropceanu, V.; Lambert, C.; Nöll, G.; Brédas, J.-L. *Chem. Phys. Lett.* **2003**, *373*, 153-160.
- (216) Lambert, C.; Amthor, S.; Schelter, J. *J. Phys. Chem. A* **2004**, *108*, 6474-6486.
- (217) Lambert, C.; Nöll, G. *J. Am. Chem. Soc.* **1999**, *121*, 8434-8442.
- (218) Lambert, C.; Nöll, G.; Hampel, F. *J. Phys. Chem. A* **2001**, *105*, 7751-7758.
- (219) Lambert, C.; Nöll, G.; Schelter, J. *Nat. Mater.* **2002**, *1*, 69-73.
- (220) Lambert, C.; Risko, C.; Coropceanu, V.; Schelter, J.; Amthor, S.; Gruhn, N. E.; Durivage, J. C.; Brédas, J.-L. *J. Am. Chem. Soc.* **2005**, *127*, 8508-8516.
- (221) Lloveras, V.; Vidal-Gancedo, J.; Ruiz-Molina, D.; Figueira-Duarte, T. M.; Nierengarten, J.-F.; Veciana, J.; Rovira, C. *Faraday Discuss.* **2006**, *131*, 291-305.
- (222) Nelsen, S. F.; Ismagilov, R. F. *J. Phys. Chem. A* **1999**, *103*, 5373-5378.
- (223) Nelsen, S. F.; Ismagilov, R. F.; Gentile, K. E.; Powell, D. R. *J. Am. Chem. Soc.* **1999**, *121*, 7108-7114.

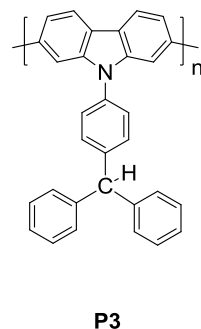
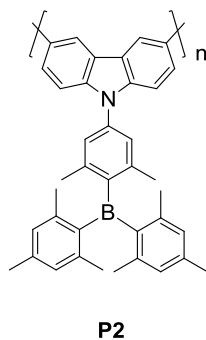
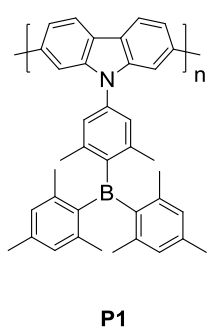
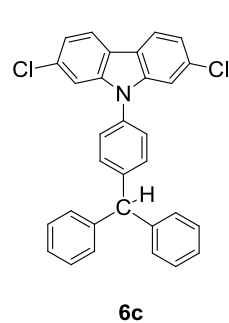
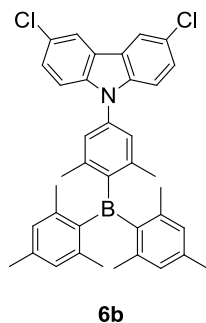
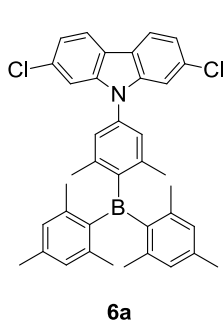
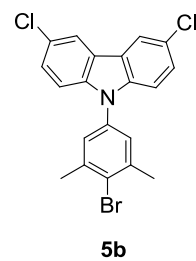
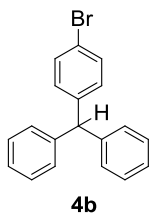
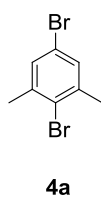
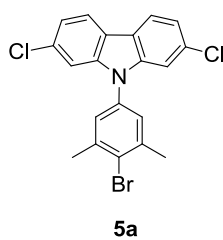
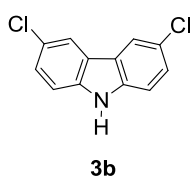
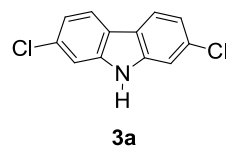
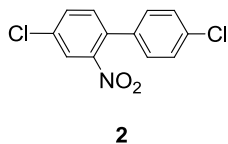
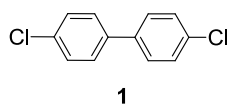
- (224) Nelsen, S. F.; Tran, H. Q. *J. Phys. Chem. A* **1999**, *103*, 8139-8144.
- (225) Nelsen, S. F.; Trieber, D. A.; Ismagilov, R. F.; Teki, Y. *J. Am. Chem. Soc.* **2001**, *123*, 5684-5694.
- (226) Rovira, C.; Ruiz-Molina, D.; Elsner, O.; Vidal-Gancedo, J.; Bonvoisin, J.; Launay, J.-P.; Veciana, J. *Chem. Eur. J.* **2001**, *7*, 240-250.
- (227) Sedó, J.; Ruiz, D.; Vidal-Gancedo, J.; Rovira, C.; Bonvoisin, J.; Launay, J.-P.; Veciana, J. *Adv. Mater.* **1996**, *8*, 748-752.
- (228) Nishikitani, Y.; Kobayashi, M.; Uchida, S.; Kubo, T. *Electrochim. Acta* **2001**, *46*, 2035-2040.
- (229) Hua, J.; Meng, F.; Li, J.; Ding, F.; Fan, X.; Tian, H. *Eur. Polym. J.* **2006**, *42*, 2686-2694.
- (230) Ballester, M.; Riera, J.; Castañer, J.; Badía, C.; Monsó, J. M. *J. Am. Chem. Soc.* **1971**, *93*, 2215-2225.
- (231) Kang, I.-N.; Hwang, D.-H.; Shim, H.-K.; Zyung, T.; Kim, J.-J. *Macromolecules* **1996**, *29*, 165-169.
- (232) Patil, N. M.; Kelkar, A. A.; Chaudhari, R. V. *J. Mol. Catal. A-Chem.* **2004**, *223*, 45-50.
- (233) Morin, J.-F.; Drolet, N.; Tao, Y.; Leclerc, M. *Chem. Mater.* **2004**, *16*, 4619-4626.
- (234) Amthor, S.; Noller, B.; Lambert, C. *Chem. Phys.* **2005**, *316*, 141-152.
- (235) Ballester, M. *Adv. Phys. Org. Chem.* **1989**, *25*, 267-445.
- (236) Heckmann, A.; Dümmler, S.; Pauli, J.; Margraf, M.; Köhler, J.; Stich, D.; Lambert, C.; Fischer, I.; Resch-Genger, U. *J. Phys. Chem. C* **2009**, *113*, 20958-20966.
- (237) Kasha, M. *Physical Processes in Radiation Biology*. Augenstein, L., Mason, R., and Rosenberg, B., Eds.; Academic Press: New York, 1964. 23-42.
- (238) Kietzke, T.; Hörhold, H.-H.; Neher, D. *Chem. Mater.* **2005**, *17*, 6532-6537.
- (239) Völker, S. F.; Uemura, S.; Limpinsel, M.; Mingebach, M.; Deibel, C.; Dyakonov, V.; Lambert, C. *Macromol. Chem. Phys.* **2010**, *211*, 1098-1108.
- (240) Bard, A. J.; Faulkner, L. R. *Electrochemical Methods*. 2nd ed.; John Wiley & Sons, Inc.: New York, 2001. 241.
- (241) Bard, A. J.; Faulkner, L. R. *Electrochemical Methods*. 2nd ed.; John Wiley & Sons, Inc.: New York, 2001. 456.
- (242) Brédas, J. L.; Silbey, R.; Boudreaux, D. S.; Chance, R. R. *J. Am. Chem. Soc.* **1983**, *105*, 6555-6559.
- (243) Schmidt, A.; Anderson, M. L.; Armstrong, N. R. *J. Appl. Phys.* **1995**, *78*, 5619-5625.
- (244) McNeill, C. R.; Abrusci, A.; Zaumseil, J.; Wilson, R.; McKiernan, M. J.; Burroughes, J. H.; Halls, J. J. M.; Greenham, N. C.; Friend, R. H. *Appl. Phys. Lett.* **2007**, *90*, 193506.
- (245) Gierschner, J.; Cornil, J.; Egelhaaf, H. J. *Adv. Mater.* **2007**, *19*, 173-191.
- (246) Sporer, C.; Ratera, I.; Ruiz-Molina, D.; Zhao, Y.; Vidal-Gancedo, J.; Wurst, K.; Jaitner, P.; Clays, K.; Persoons, A.; Rovira, C.; Veciana, J. *Angew. Chem. Int. Ed.* **2004**, *43*, 5266-5268.
- (247) Maksimenka, R.; Margraf, M.; Köhler, J.; Heckmann, A.; Lambert, C.; Fischer, I. *Chem. Phys.* **2008**, *347*, 436-445.
- (248) Mauser, H. *Formale Kinetik*. Bertelsmann Universitätsverlag: Düsseldorf, 1974. 74.
- (249) Bässler, H. *Phys. Status Solidi B* **1993**, *175*, 15-56.

- (250) Granström, M.; Petritsch, K.; Arias, A. C.; Lux, A.; Andersson, M. R.; Friend, R. H. *Nature* **1998**, 395, 257-260.
- (251) Holcombe, T. W.; Woo, C. H.; Kavulak, D. F. J.; Thompson, B. C.; Fréchet, J. M. J. *J. Am. Chem. Soc.* **2009**, 131, 14160-14161.
- (252) Koetse, M. M.; Sweelssen, J.; Hoekerd, K. T.; Schoo, H. F. M.; Veenstra, S. C.; Kroon, J. M.; Yang, X.; Loos, J. *Appl. Phys. Lett.* **2006**, 88, 083504.
- (253) Sang, G.; Zhou, E.; Huang, Y.; Zou, Y.; Zhao, G.; Li, Y. *J. Phys. Chem. C* **2009**, 113, 5879-5885.
- (254) Veenstra, S. C.; Verhees, W. J. H.; Kroon, J. M.; Koetse, M. M.; Sweelssen, J.; Bastiaansen, J. J. A. M.; Schoo, H. F. M.; Yang, X.; Alexeev, A.; Loos, J.; Schubert, U. S.; Wienk, M. M. *Chem. Mater.* **2004**, 16, 2503-2508.
- (255) Zhou, E.; Tajima, K.; Yang, C.; Hashimoto, K. *J. Mater. Chem.* **2010**, 20, 2362-2368.
- (256) Zoombelt, A. P.; Leenen, M. A. M.; Fonrodona, M.; Wienk, M. M.; Janssen, R. A. J. *Thin Solid Films* **2008**, 516, 7176-7180.
- (257) McNeill, C. R.; Greenham, N. C. *Appl. Phys. Lett.* **2008**, 93, 203310.
- (258) Melhuish, W. H. *J. Phys. Chem.* **1961**, 65, 229-235.
- (259) Connelly, N. G.; Geiger, W. E. *Chem. Rev.* **1996**, 96, 877-910.
- (260) Sawyer, D. T.; Roberts, J. L. *Experimental Electrochemistry for Chemists*. Wiley-Interscience: New York, 1974. 42.
- (261) Tsiplakides, D.; Archonta, D.; Vayenas, C. G. *Top. Catal.* **2007**, 44, 469-479.
- (262) Trebino, R.; DeLong, K. W.; Fittinghoff, D. N.; Sweetser, J. N.; Krumbügel, M. A.; Richman, B. A.; Kane, D. J. *Rev. Sci. Instrum.* **1997**, 68, 3277-3295.
- (263) Ekvall, K.; van der Meulen, P.; Dhollande, C.; Berg, L.-E.; Pommeret, S.; Naskrecki, R.; Mialocq, J.-C. *J. Appl. Phys.* **2000**, 87, 2340-2353.
- (264) http://www.gigahertz-optik.de/files/tutorials_doublesideprint.pdf.
- (265) Ballester, M.; Veciana, J.; Riera, J.; Castañer, J.; Rovira, C.; Armet, O. *J. Org. Chem.* **1986**, 51, 2472-2480.
- (266) *The signal is hidden below the THF signal as confirmed by comparison with the spectrum in CD₂Cl₂.*

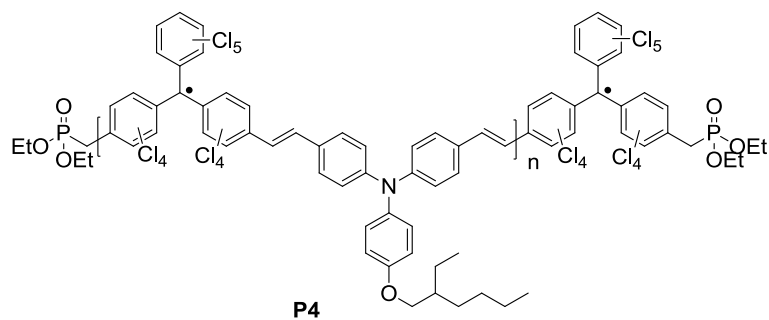
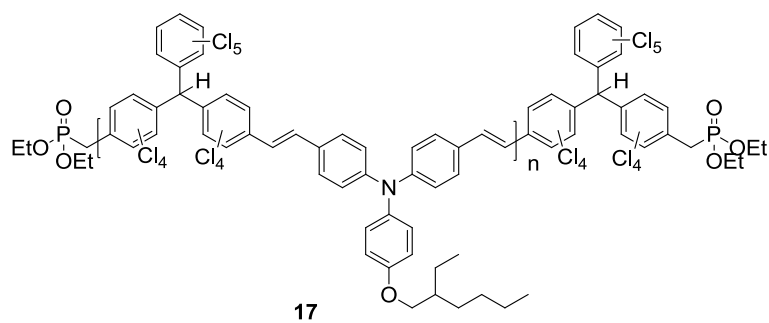
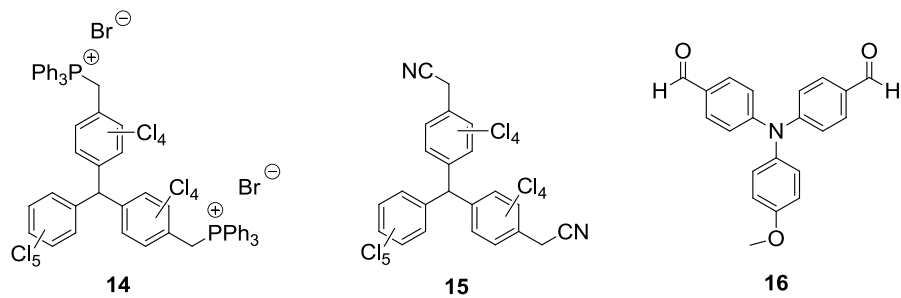
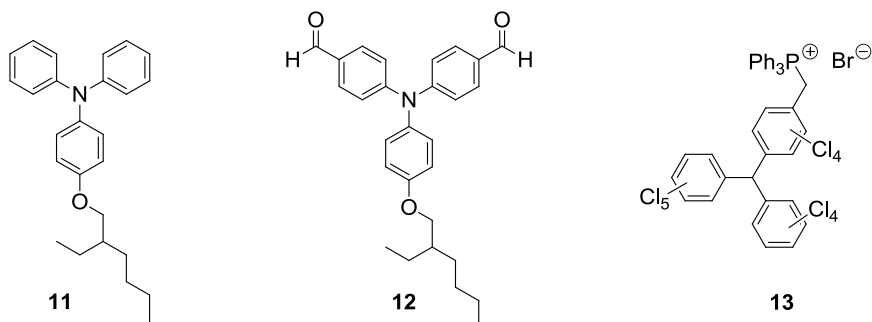
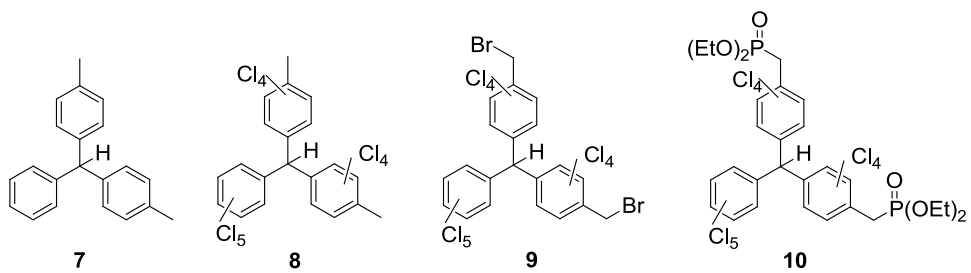
7 Appendix

7.1 Formeltafel

7.1.1 Polycarbazoles



7.1.2 Low Band Gap Polymer



7.2 Zusammenfassung

Im ersten Teil dieser Arbeit wurden die drei Polycarbazole Poly[*N*-((4-dimesitylboryl)-3,5-dimethylphenyl)-carbazol]-2,7-diyl **P1**, Poly[*N*-((4-dimesitylboryl)-3,5-dimethylphenyl)-carbazol]-3,6-diyl **P2** und Poly[*N*-(4-(diphenylmethylen)-phenyl)-carbazol]-2,7-diyl **P3** mittels Yamamoto Kupplung synthetisiert und ihre spektroskopischen und elektrochemischen Eigenschaften untersucht. Absorptions- und Fluoreszenzeigenschaften von **P1** und **P3** sind denen anderer 2,7-verknüpfter Polycarbazole ähnlich, wohingegen **P2** eine CT Absorptionsbande zeigt, die durch die Verschiebung von Elektronendichte vom Stickstoff des Carbazoldonors zum Triarylboranakzeptor verursacht wird. Daraus ergeben sich negativ solvatochromes Absorptions- und positiv solvatochromes Fluoreszenzverhalten und eine deutlich erhöhte Fluoreszenzquantenausbeute in Lösung und im Festkörper verglichen mit anderen 3,6-verknüpften Polycarbazolen. Das bedeutet, dass die spektroskopischen Eigenschaften durch die Art der C-C-Verknüpfung gesteuert werden können: das 2,7-verknüpfte Polycarbazol **P1** wird durch den Akzeptorsubstituenten aufgrund des starren Polymergerüsts, dem eine poly-*para*-phenylenartige und damit stärker delokalisierte Struktur zugrunde liegt, nicht beeinflusst. Im Gegensatz dazu treten beim 3,6-verknüpften Polycarbazol **P2** die Eigenschaften der Monomereinheit aufgrund der flexibleren 1,4-diaminobiphenyl Struktur in den Vordergrund.

Die Oxidationsprozesse von **P1-P3** wurden im Detail mittels Cyclovoltammetrie untersucht. Die Ergebnisse stimmen mit Literaturwerten überein. Außerdem wurde bei den Messungen von **P1** und **P2** ein reversibler Reduktionsprozess, der am Boranzentrum stattfindet, beobachtet. Eine Reduktion der Carbazoleinheit konnte hingegen nicht gefunden werden.

Mit der Herstellung von OLEDs der Struktur ITO/**P2**/Al konnte blaue Elektrolumineszenz mit den CIE Farbkoordinaten (0.17, 0.21) nachgewiesen werden.

Im zweiten Teil der Arbeit wurde das low band gap Polyradikal Poly{(((2,3,4,5,6-pentachlorphenyl)-bis(2,3,5,6-tetrachlorphenyl)methyl radical)-4,4'-diyl)-*alt*-4,4'-bis(vinylphenyl)-4-(2-ethylhexyloxy)phenylamin} **P4** mittels Horner-Emmons Reaktion synthetisiert. Im NIR beobachtet man eine IV-CT Absorptionsbande, die durch einen Elektronentransfer vom Triarylaminodonor zum PCTM-Radikalakzeptor hervorgerufen

wird. Dieser elektronische Übergang ist auf eine Monomereinheit begrenzt wie der Vergleich mit den Monomerabsorptionsspektren zeigt. HOMO und LUMO Energien von **P4**, die anhand der Cyclovoltammogramme bestimmt wurden, liegen bei -5.5 und -4.5 eV. Die im Vergleich zur optischen Energielücke (1.2 eV) kleinere elektrochemische Energielücke (1.9 eV) ist wahrscheinlich auf Ionenpaareffekte bei den elektrochemischen Messungen zurückzuführen, deutet aber auch auf eine geringe Excitonenbindungsenergie hin.

Transiente Absorptionsspektren zeigen die spektralen Charakteristika von oxidiertem Triarylaminendonator und reduziertem PCTM-Akzeptor vergleichbar mit den Spektren der spektroelektrochemischen Messungen, bei denen eine Lösung von **P4** jeweils nacheinander reduziert und oxidiert wurde. Dadurch konnte der Elektronentransferprozess, der zur Ausbildung der IV-CT Bande führt, zweifelsfrei nachgewiesen werden. Der IV-CT Zustand zerfällt biexponentiell. Der schnelle, lösungsmittelabhängige Zerfall beschreibt den direkten Übergang vom IV-CT Zustand in den elektronischen Grundzustand. Dagegen wird der langsame, lösungsmittelunabhängige Zerfall einer Gleichgewichtseinstellung zwischen IV-CT Zustand und vollständig ladungstrenntem Zustand, der durch Ladungswanderung entlang der Polymerkette erreicht wird, zugeschrieben.

In OFETs mit **P4** als Halbleiter und einer zusätzlich isolierenden, organischen PPcB Schicht wurde ein ausgeglichener, ambipolarer Ladungstransport mit Loch- und Elektronenbeweglichkeiten von ca. $3 \times 10^{-5} \text{ cm}^2 \text{ V}^{-1} \text{ s}^{-1}$ gefunden.

Polymer/Polymer BJJ Solarzellenmodule mit der Struktur Glas/ITO/PEDOT:PSS/(P3HT/**P4** 1:4)/Ca/Al hatten einen Wirkungsgrad von 0.0031 % bei einer Leerlaufspannung $V_{OC} = 0.38 \text{ V}$, einem Kurzschlussstrom $J_{SC} = 0.028 \text{ mA cm}^{-2}$ und einem Füllfaktor $FF = 0.29$.

Die ungeeignete Morphologie der **P4**- und P3HT/**P4**-Schichten als Ursache für die unbefriedigende Performance von OFETs und Solarzellen lässt solche Anwendungen für **P4** wenig sinnvoll erscheinen. Dagegen verdient die Hypothese der Ladungswanderung im angeregten Zustand eine vertiefte Untersuchung.

7.3 Danksagung

An dieser Stelle möchte ich mich bei allen bedanken, die zum Gelingen dieser Arbeit beigetragen haben. Mein besonderer Dank gilt dabei:

Herrn Dr. Matthias Grüne und Frau Elfriede Ruckdeschel für die Aufnahme der NMR Spektren.

Herrn Dr. Michael Büchner, Herrn Fritz Dadrich und Frau Antje Hautzinger für die Aufnahme der Massenspektren.

Herrn Michael Ramold für sämtliche Sonderanfertigungen für verschiedene Messungen.

Herrn Markus Braun für die gut gelaunte und jederzeit bereitwillige Unterstützung bei technischen Problemen.

Allen Angestellten des Instituts für Organische Chemie: *Herrn Dr. Christian Stadler, Frau Petra Leckert, Frau Anette Krug, Frau Angela Dreher, Frau Ursula Rüppel, Herrn Matthias Fromm, Herrn Manfred Ludwig, Herrn Frank Förtsch, Herrn Dipl.-Ing. Brunner.*

Frau Liselotte Michels für die Elementaranalysen und DSC Messungen.

Herrn Dr. Rüdiger Bertermann und Frau Marie-Luise Schäfer für die ^{31}P und phosphorentkoppelten ^{13}C NMR Messungen.

Den Würthner's:

Ana-Maria Krause, für den Erfahrungsaustausch in Sachen Cyclovoltammetrie und für die DSC Messungen.

Vladimir Stepanenko, für die AFM-Messungen, die Du trotz hoher Arbeitsbelastung noch zwischendurch für mich gemacht hast.

Matthias Stolte, für Dein offenes Ohr und deine Hilfestellung bei vielen mit der Forschung verbundenen Schwierigkeiten, für die Si-Wafer und für die Nutzung des spin coaters.

Hannah Bürckstümmer, für das zum Bau von Grätzelzellen zur Verfügung gestellte Material und die Einweisung in die Benutzung des Sonnensimulators.

Den Physikern:

Daniel Rauh und *Andreas Baumann*, für Bau/Messungen/Auswertungen von Solarzellen, die Hilfestellung beim Bau von OLEDs und die Hilfe bei allen anderen die Organic Electronics betreffenden Fragen. Vielen Dank!!

Maria Hammer, für Bau/Messungen/Auswertungen von OFETs und die allgemein gute Zusammenarbeit.

Den PC'lern:

Tatjana Quast und *Florian Kanal*, für Euer Engagement und Durchhaltevermögen bei den transienten Messungen!!

Sabine Keiber, für Dein Engagement beim Fitten der transienten Spektren und insbesondere für die postwendend gelieferten Fits!!

Martin Kullmann und *Stefan Rützel*, für Euren Einsatz bei den transienten Messungen auch zu später Stunde!!

Dr. Patrick Nürnberger, für die Diskussionen über die Interpretation der transienten Messergebnisse.

Vor allem möchte ich mich aber bei den Mitgliedern des Arbeitskreis Lambert für das angenehme Arbeitsklima, die schöne Zeit und die Hilfestellung bei der Bewältigung vieler mit dem Arbeitsalltag im Labor verbundener Probleme bedanken. Insbesondere bei:

Marco Holzapfel, für deine Unterstützung bei der Auseinandersetzung mit dem Fluoreszenz- und Lebensdauermeßgerät und für dein reges Interesse bei der Interpretation von Ergebnissen.

Barbara Geiß, für die wirklich gute Zusammenarbeit beim Bau der OLEDs, für die Organisation von AK-Feiern und für deine super gute Erdbeertorte.

Alexander Heckmann, für die Unterstützung bei den Syntheseprojekten zum Polyradikal und die damit verbundenen Diskussionen und für die Initiierung des Kochkreises.

Christian Müller, für die Organisation von AK-Feiern, Geschenken, Chem-Cup T-shirts etc. – kurz für die Organisation des Schönen Drumherum.

Conrad Kaiser, für deine schönen Geburtstagsfeiern.

Nina Dürrbeck, für deine Hilfe bei Computerproblemen und die schönen Gespräche.

Markus Steeger, für den abenteuerlichen Spaziergang auf der KOPO und die gute Zusammenarbeit im Messlabor.

Fabian Zieschang, für die gute Abzughbarschaft und deine Geduld wenn ich mal wieder vergessen hatte meinen Kolben vom Roti abzuhängen.

Sebastian Völker, für die super gute Musik im Labor. Das hat das Arbeiten im Labor definitiv noch schöner gemacht.

Johannes Klein, für deine unerschütterlich gute Laune.

Christian Rothgängel, für die Synthesearbeit während deines F-Praktikums.

Harald Ceymann, für das Grillen sämtlichen Grillguts.

Alexander Schmiedel, für die Unterstützung bei mathematisch-physikalischen Fragestellungen.

Christl Wendinger, für manche Synthesearbeit und insbesondere für die Synthese der Leitsalze.

Ganz besonders möchte ich mich auch bei meinen Eltern, meinen Schwiegereltern, meinen Schwestern und bei meinem Basti bedanken für die offenen Ohren, wenn's mal wieder gar nicht lief und die Nachsicht, wenn ich für nichts anderes Zeit hatte.